MIT-2344-10
MITNE-81

THE USE OF EXPERIMENTS ON A SINGLE FUEL ELEMENT TO DETERMINE THE NUCLEAR PARAMETERS OF REACTOR LATTICES

by

Edward E. Pilat, M. J. Driscoll,
I. Kaplan, T. J. Thompson

Contract AT(30-1)2344
U. S. ATOMIC ENERGY COMMISSION

February, 1967

AEC Research and Development Report
UC - 34 Physics

Department of Nuclear Engineering
Massachusetts Institute of Technology
Cambridge, Massachusetts

MASSACHUSETTS INSTITUTE OF TECHNOLOGY
DEPARTMENT OF NUCLEAR ENGINEERING
Cambridge, Massachusetts

THE USE OF EXPERIMENTS ON A SINGLE FUEL ELEMENT TO DETERMINE THE NUCLEAR PARAMETERS OF REACTOR LATTICES

by

Edward E. Pilat, M. J. Driscoll,
I. Kaplan, T. J. Thompson

February, 1967

MIT - 2344 - 10
MITNE - 81
AEC Research and Development Report
UC - 34 Physics

Contract AT(30-1)2344
U. S. Atomic Energy Commission

ABSTRACT

The nuclear parameters of a reactor lattice may be determined by critical experiments on that lattice, by theoretical calculations in which only cross sections are used as input, or by methods which combine theory and experiment. Of those methods which combine theory and experiment, the Single Element Method, abbreviated SEM, is shown to have great usefulness. As used here, the method combines experiments on the smallest meaningful unit of fuel – a single fuel element – with a theory which relates the behavior of a lattice of such elements to the experimentally determined behavior of the single element. This particular division of the problem into theory and experiment is useful for at least three reasons.

First, several parameters which characterize a reactor lattice – the thermal utilization and resonance escape probability, for example – often depend strongly and in a complicated manner on the properties of individual fuel elements, but only depend weakly or in a simple manner on interactions between the fuel elements. In the Single Element Method, the largest contribution to these parameters is determined by measurements on a single fuel element, and only a relatively small correction to account for the presence of the rest of the fuel elements need be estimated theoretically. Second, the determination of lattice parameters in this way represents a desirable saving of time, money, effort, and material over their determination in critical or exponential experiments. Third, it is shown that the method provides an excellent way of correlating the results of experimental measurements, since it shows what pertinent variables must be used to express the quantity of interest in a linear or nearly linear fashion.

Values obtained by the SEM for the thermal utilization of lattices of uranium rods in heavy water are accurate to about 0.3 percent (by comparison with THERMØS). Values of ρ_{28}, δ_{28}, and C^* are obtained by the SEM for the same lattices to an accuracy of between five and ten percent (by comparison with experiment). The same method yields values of δ_{28} with are equally accurate in lattices moderated by light water. In addition, the theoretical development of the SEM predicts that ρ_{28}, δ_{28}, C^*, and δ_{25} should vary nearly linearly with the inverse of the unit cell volume (for a fixed size of fuel element). This explains the experimentally observed behavior and provides an important tool for the rational correlation of experimental results.

ACKNOWLEDGMENTS

The success of the M. I. T. Heavy Water Lattice Project is due to the support of the U. S. Atomic Energy Commission and to the contributions of a number of individuals. The results of this report are due primarily to the work of the principal author, Edward E. Pilat, who has submitted substantially this same report in partial fulfillment of the requirements for the Ph. D. degree at M. I. T.

Overall direction of the project during this period of research was shared by Professors I. Kaplan, T. J. Thompson, D. D. Lanning, and M. Driscoll. Messrs. Joseph Barch, Albert Supple, and Norman Berube have provided great assistance in the experimental work. Helpful discussions have been held with Drs. H. Bliss, W. D'Ardenne, and E. Sefchovich.

The staffs of the M. I. T. Reactor, the Reactor Machine Shop, the Radiation Protection Office, and the Reactor Electronics Shop have provided advice and assistance throughout the experimental portion of this work. Mr. Thomas Green was of assistance in the fabrication of experimental equipment. Mrs. Mary Bosco has ably prepared the final manuscript.

All computer calculations were done at the M. I. T. Computation Center.

TABLE OF CONTENTS

LIST OF FIGURES

LIST OF TABLES

Chapter I

INTRODUCTION

1.1 THE M.I.T. HEAVY WATER LATTICE PROJECT

1.1.1 Purposes

The Nuclear Engineering Department at M.I.T., under the sponsorship of the United States Atomic Energy Commission, operates the Heavy Water Lattice Project for research on the physics of D_2O moderated reactors. Purposes of the Project are to obtain accurate measurements of important reactor parameters, to develop additional theoretical and experimental techniques for solving problems in reactor physics, and to use the measurements as benchmarks for testing the new techniques. Published reports which emphasize the careful measurement of standard reactor parameters are references B1, D1, P1, S1, W1 and W2; published reports which emphasize the development and testing of new techniques are references B2, H1, M1, P2, S2 and W3.

1.1.2 Scope of the Available Results

A large number of consistently measured data have been obtained on lattices of natural or slightly enriched uranium metal rods in heavy water. Table 1.1 gives the detailed specifications of these lattices. This large number of consistently measured data provides an ideal means for testing new analytical methods, which are desirable both for correlating the data more efficiently and for permitting accurate interpolation and extrapolation of the data to new lattice configurations. The search for better analytical techniques has led to the Single Element Method of interpreting lattice experiments. This interpretation has been found to provide a clarifying principle which not only facilitates interpolation and extrapolation but also suggests new experiments and new calculational techniques.

Table 1.1

Uranium Metal Lattices Studied in the
Heavy Water Exponential Assembly at M.I.T.

Concentration of U-235 in Fuel Rod (Wt. %)	Fuel Diameter (Inches)	Spacing (Inches)	Thickness of Al Clad (Inches)
0.711	0.998	4.50	0.028
		5.00	
		5.75	
1.027	0.250	1.25	0.028
		1.75	
		2.50	
1.143	0.250	1.25	0.028
		1.75	
		2.50	
0.947	0.750	2.50	0.028
		3.50	
		5.00	

1.2 THE SINGLE ELEMENT METHOD IN REACTOR PHYSICS

1.2.1 Theoretical Basis

The neutron balance in a system in steady state may be expressed in several different ways. These methods are equivalent in the sense that each one accounts for all the neutrons, but they differ in the particular manner by which the neutrons are enumerated. The balance is often made on the basis of where in space the neutrons are absorbed, or at what energy they are absorbed, or in what nuclide they are absorbed. The single element method enumerates neutrons according to their place of origin (in space).

In order to compute the neutron balance in this way, a "tool" is needed — the kernel that gives the flux or reaction rate as a function of position around a source localized in space. Since reactor lattices are assembled from fuel elements, it is convenient to use the complete single fuel element (rather than some small piece of it) as the basic localized source. The fuel elements used in the experiments reported here were cylindrical metal rods, but the principles enunciated here apply equally well to fuel elements of any shape or structure. This includes fuel elements which consist of individual, homogeneous fuel rods, fuel elements which consist of clusters of fuel rods surrounded by coolant or supporting structural material, and fuel elements which consist of successive annuli or layers of fuel with coolant in the intervening channels. Although the name, "Single Rod Method," might be more descriptive of the applications reported here, the name, "Single Element Method," abbreviated SEM, will be used to emphasize the generality of the method. When the SEM is used, the total flux or reaction rate at any point in a uniform lattice of such elements is then calculated by adding up the values of the kernels appropriate to each of the fuel elements in the system.

A remarkable property of this method, and the reason why the SEM is useful, is that for a uniform lattice, a detailed knowledge of the kernel is frequently unnecessary. It will be shown in Chapter II that in many cases of practical interest, those neutrons which originate "far enough" away from a particular unit cell result in a net flux (or reaction

rate) which may be regarded as constant across the cell. The profile of the total flux (or reaction rate) across the cell is then the sum of this constant "background" arising from these "distant" neutron sources, plus one or more rapidly varying terms which represent neutrons originating in nearby fuel elements. Sometimes the unit cell of interest is, itself, "far enough" away from other localized sources so that the total flux (or reaction rate) is essentially constant throughout the cell. A case frequently found is that in which all fuel elements outside the unit cell of interest are "far enough" away. In this case, the total flux (or reaction rate) consists of the "single element" component, whose magnitude varies throughout the unit cell, and the "lattice" component, which originates from all other fuel elements in the system and whose magnitude is essentially constant across the unit cell.

Chapter II will be devoted to a theoretical study showing under what conditions the flux (or reaction rate) is sufficiently uniform across a unit cell, as well as how the relationship between the magnitudes of the uniform background and the single element term may be quantitatively evaluated. Neither the total reaction rate nor its lattice component is ever exactly constant throughout a unit cell, so a means of estimating an upper bound on the deviation from absolute constancy will be given in Chapter II. It will be shown that in many practical cases this deviation is less than one percent. Chapter III will explain the experimental techniques used to measure single element kernels and related parameters. Chapters IV, V, and VI show how these theoretical and experimental techniques facilitate the study of reactor physics in the various regions of neutron energy, including the thermal, resonance, and fast energy regions. Chapter VII contains a summary of the results obtained thus far and a list of possible further applications.

1.2.2 Applicability to Various Kinds of Reactors

The theory which has been outlined here could reasonably be expected to apply to graphite or heavy water moderated lattices, for which kernels are easily defined because the volume fraction of fuel in such lattices is small and the reactor consists mostly of moderator. In lattices moderated by light water, one might expect difficulties

because the kernel is a strong function of the amount of fuel present. Nevertheless, the available experimental data indicate that the conceptual separation of effects into "single element" and "lattice" components appears to remain valid in most cases. Even though the Single Element Method may not be adequate for quantitative calculational purposes in these cases, the qualitative trends predicted by the theory are still observed. This property offers important aid in the interpretation and presentation of data, as will be shown in Chapter V.

1.2.3 Advantages of the Single Element Method

(1) The Single Element Method permits survey measurements on new types of fuel to be made with only one fuel element. This represents a desirable saving of money and material. Measurement of the kernel around the single fuel element provides a partial check on any purely theoretical computations which may have been made for the new element. In theory, at least, measurements using a single fuel element should be sufficient to establish its behavior in a lattice of any geometry and size.

(2) The Single Element Method provides an excellent way of correlating the results of experimental measurements. The method shows what pertinent variables must be used to express the quantity of interest as a linear or nearly linear function. Further, when the data are presented in an organized manner amenable to analytic representation, it should be possible to check their consistency and to reduce the error attributable to any point.

(3) The use of the Single Element Method results in a theory which enhances intuitive understanding. It is particularly valuable in studying the dependence of lattice parameters on the spacing between fuel elements and on the number of fuel elements in the system. These are just the areas where the conventional Wigner-Seitz formulation is least amenable to physical intuition, since few people have an intuitive "feel" for how the solution to a differential equation changes as the boundary conditions or domain of definition vary.

(4) The Single Element Method is applicable to lattices composed of clusters of fuel rods as well as to those consisting of individual fuel rods. If the kernel which characterizes each fuel element is determined experimentally, then the detailed structure of an element causes no concern. For theoretical purposes, the SEM can be used to establish the behavior of a single fuel element from the behavior of the individual fuel rods which comprise it. The behavior of a lattice of such clustered fuel elements can then be established by applying the SEM once more, using these composite fuel elements as the basic sources.

(5) The extent to which experimental results and results calculated by means of complicated theoretical models deviate from the simple trends predicted by the Single Element Method shows when more complex effects are important and when they can be ignored.

(6) The Single Element Method is applicable to nonuniform arrays of fuel elements. In this case, the addition of the kernels can be performed to find the total contribution from all fuel elements in the system. This is a case which is very difficult to handle using the Wigner-Seitz formalism.

1.2.4 Previous Work

Other investigators have published both theoretical and experimental studies of the relationships between single fuel elements and lattices. Where this work is directly pertinent, it is referenced specifically in the text and listed in Appendix G. A selected bibliography of other background material in this area is listed in Appendix I together with a short commentary.

Chapter II

DISCRETE SOURCE REPRESENTATION AND THE POISSON SUMMATION

2.1 INTRODUCTION

The transport of neutrons within a material medium may be calculated by either of two methods (W7). The method used more often is based on the treatment of problems in solid state physics by Wigner and Seitz (W17). The neutron distribution within a particular region is calculated by solving an appropriate equation within that region, with appropriate definition of the source within the region and with appropriate conditions on the neutron density at the boundaries of the region. In the alternative discrete source technique of Galanin (G2), the neutron distribution within a particular region is calculated as the sum of the appropriate neutron distributions in that region arising from each of the sources in the entire system. Both methods require some prior knowledge of neutron transport in the medium as a whole. The need for this information is implicit in the word "appropriate" which has been used in describing the two methods: the Wigner-Seitz technique requires that the boundary conditions at the edge of the region and the source distribution within the region be known; the discrete source technique requires that the kernels giving the neutron distribution from each of the individual sources be known.

The Wigner-Seitz technique has the advantage that in certain relatively simple cases, the source distribution and boundary conditions can be obtained from the principles of symmetry and neutron conservation without reference to the material properties of the medium. Conversely, its disadvantage lies in the difficulty of formulating correct source and boundary conditions for cases other than these simple ones.

The method of discrete source representation has the advantage of being applicable to arbitrarily spaced arrays of sources, and the disadvantage that kernels for finite, heterogeneous systems are not always

easy to define. In many problems of practical interest, these difficulties can be overcome by a reasonable approximation (G2) which will be explained in the next section. When this is so, the discrete source technique is applicable to a wider variety of problems than is the Wigner-Seitz technique, which is limited for practical purposes to large assemblies of identical fuel elements. A link between the Wigner-Seitz and discrete source methods is provided by the Poisson summation formula (M2). The use of this formula makes it possible to examine the adequacy of the usual Wigner-Seitz assumption of a uniform source throughout the unit cells in an infinite array. Such an investigation has been carried out previously (G2) for the particular case in which the age theory kernel describes the slowing-down process, but in the following analysis the exact form of the kernel will be left unspecified.

In this chapter, it will be shown with the aid of the Poisson summation formula that a sufficient condition for a reaction rate to be effectively constant across a unit cell (in a uniform, infinite array) is that the magnitude of the kernel which describes the reaction rate around a single fuel element must nowhere experience a large fractional change within a distance equal to the spacing between fuel rods. It will also be shown that even when this condition is not satisfied, the reaction rate of neutrons originating "far enough" away from the cell of interest is nevertheless nearly constant across this cell. These two conclusions will be the basis of the methods used in Chapters IV, V, and VI for the prediction of lattice parameters from measurements on a single fuel element, and will make it possible to present the results of measurements in lattices in a parametric form which is both convenient and heuristically useful.

2.2. THEORY

2.2.1 The Method of Discrete Source Representation

Consider a bare, finite reactor system (critical or subcritical) consisting of a uniform array of identical fuel elements distributed throughout an otherwise homogeneous medium. The reaction rate within a unit cell will be calculated from the relative macroscopic source

distribution, $S(\vec{r})$, in the fuel elements. Let $Q'(\vec{r}, \vec{r}_i, E)$ be the kernel giving the reaction rate at energy E and position $\vec{r}$ per source neutron at $\vec{r}_i$. This kernel depends on the vectors $\vec{r}$ and $\vec{r}_i$ as well as on the location of the extrapolated boundaries of the system, where both the flux and reaction rate are assumed to vanish. This dependence arises because the probability of a neutron leaking out of the medium before undergoing the desired reaction depends upon how close to the boundary the neutron originates and upon how close to the boundary it is expected to undergo the reaction. Not only is there a paucity of experimental information on such finite-medium kernels, but its vector dependence makes Q' difficult to handle mathematically. In order to obtain a more tractable form, we make a reasonable assumption.

> Assumption. The finite-medium kernel Q' may be replaced by the infinite-medium kernel $Q(|\vec{r} - \vec{r}_i|, E)$ if the summation over the sources is extended over all space by means of the analytic continuation of the source distribution existing within the actual system.

The infinite-medium kernel Q depends on the scalar distance between the source and field points because neither direction nor absolute location has any significance in a uniform, infinite medium. The infinite-medium kernel is, by definition, independent of the positions of any boundaries of the system. It is known (W7) that the assumption is rigorously correct if the equation describing the neutron transport is of the parabolic type as is the age equation. For other types of equations, such as the more rigorous Boltzmann equation, the use of the assumption is apparently (W7) an approximation but one which is, nevertheless, reasonable on physical grounds. The total reaction rate $R(\vec{r})$ at point $\vec{r}$ is:

$$R(\vec{r}) = \sum_{i=1}^{N} Q'(\vec{r}, \vec{r}_i, E)\, S(\vec{r}_i), \tag{2.1}$$

where N is the number of fuel elements in the system. By the assumption, this expression may be replaced by a sum over Q:

$$R(\vec{r}) = \sum_{i=1}^{\infty} Q(|\vec{r} - \vec{r}_i|, E)\, S(\vec{r}_i). \qquad (2.2)$$

Because the fuel elements are uniformly spaced and the array extends to infinity (through the assumption), Eq. 2.2 is most easily evaluated by means of Poisson's summation formula after the appropriate kernel Q has been determined.

2.2.2 Kernels for Use with the Method of Discrete Source Representation

The discrete source method, as presented in Eq. 2.1, may be applied to any problem in neutron transport, but only when kernels for the particular problem are known to sufficient accuracy can it be used for purposes of computation. A rigorous determination of the kernels demands, in effect, a solution to the whole problem: in calculating the kernels, one must be careful to exclude from the reaction rate at point j those neutrons which would have reached point j from point k, had they not already been removed at point k; thus, the true reaction rate at any point cannot be calculated until the reaction rate at neighboring points is known. This difficulty is not serious in problems where there are no strong, localized sinks of neutrons. Under these conditions, the corrections necessary to account for the removal of neutrons at neighboring points become small perturbations. These conditions are well satisfied in the high-energy and slowing-down regions of most reactors. The cross sections in these cases are small enough so that only a small fraction of the source neutrons is removed at any one position or energy. Furthermore, neutrons at energies far below the source energy will have made many collisions, so it is frequently adequate to homogenize the lattice when calculating the kernel. This does not imply that the neutron density is uniform, as it would be in an infinite, homogeneous medium, but only that the medium can be treated as homogeneous for the purpose of calculating the neutron distribution around a single, localized source.

When the problem does not involve strong, localized sinks of neutrons, most kernels have the general shape shown in Fig. 2.1.A. They decrease monotonically to zero. Such kernels include the first

collision kernel and those of age theory, one-group diffusion theory, and multigroup diffusion theory. If energy regions having strong, localized absorption were to be treated, the kernels would not have this property but would be more like the one in Fig. 2.1.B, which shows a possible kernel representing absorption at thermal energies around a single source rod. The nature of this kernel depends strongly on the positions of the neighboring fuel rods, since these determine the locations of the absorption peaks in the kernel.

This report will be concerned only with kernels which decrease monotonically and which describe a reaction or reactions undergone by all the neutrons, so that in an infinite system no neutrons are lost by other processes. Such reactions might be called removal reactions, in general. Besides actual removal or slowing down out of an energy group, they include absorption and first collision reactions. The application of the SEM to problems involving strong, localized absorption may be possible if these positions of strong absorption are thought of as negative sources. Thus, control rods might be treated by this method. Such problems will not be considered as within the scope of the present work.

2.2.3 Application of the Poisson Summation to the Method of Discrete Source Representation

Poisson's summation formula relates the sum of the values of a function at an infinite number of equally spaced arguments to a sum over the Fourier transform of the function. It will be used here to demonstrate that when the macroscopic source distribution S is the same in all fuel elements and is normalized to unity, the reaction rate of Eq. 2.2 may be expressed in the form:

$$R(\vec{r}) = \frac{1}{V_c}\{F + \text{correction terms}\}, \tag{2.3}$$

where F is the integral of the kernel over all space and V_c is the volume of a unit cell.

The basic formula expressing the Poisson summation, applied to a function of one variable, f(x), is (M2):

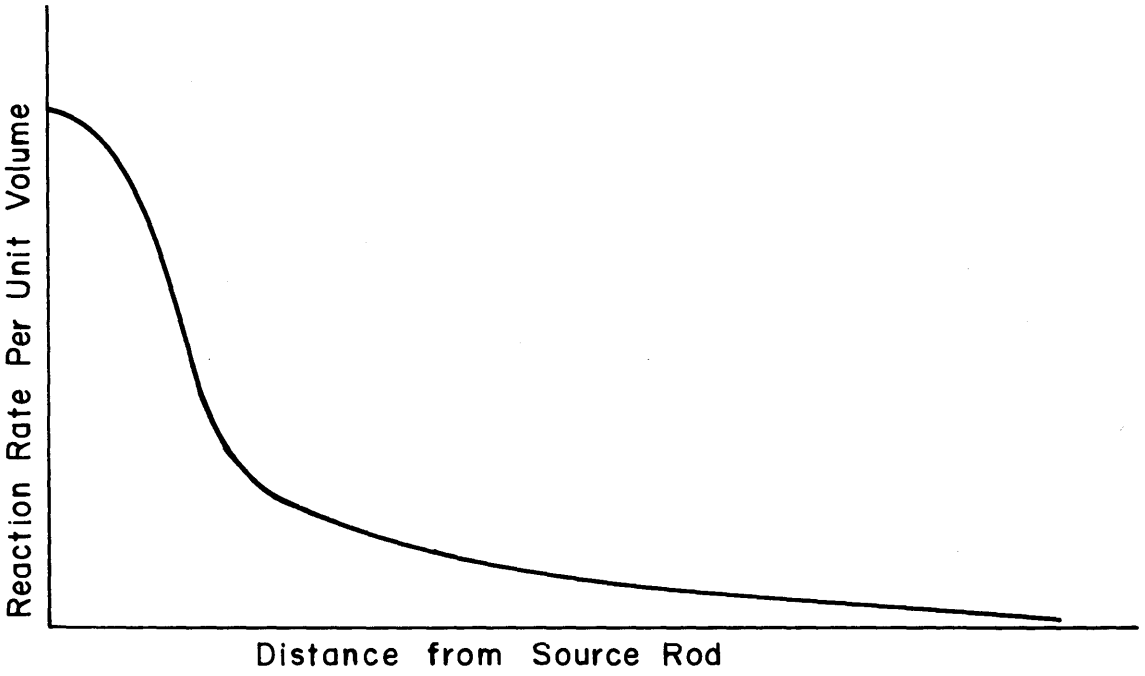

FIG. 2.1A REACTION RATE AROUND SINGLE SOURCE IN A MEDIUM NOT CONTAINING STRONG LOCAL NEUTRON SINKS

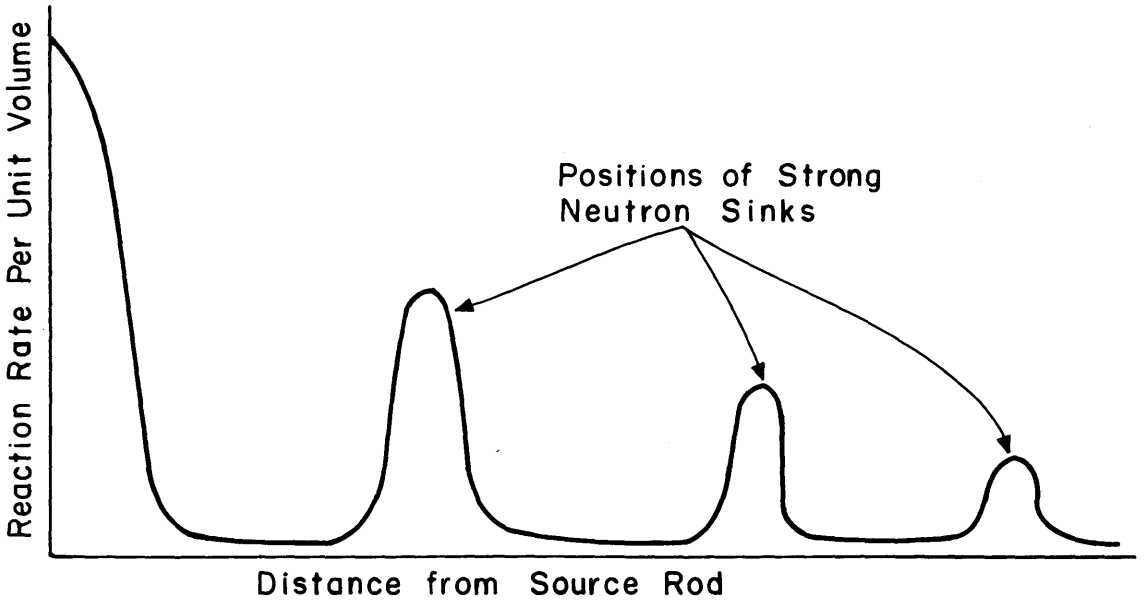

FIG. 2.1B REACTION RATE AROUND SINGLE SOURCE IN A MEDIUM CONTAINING STRONG LOCAL NEUTRON SINKS

$$\sum_{m=-\infty}^{\infty} f(\alpha m) = \frac{1}{\alpha} \sum_{\mu=-\infty}^{\infty} \int_{-\infty}^{\infty} dx\, e^{i\left(\frac{2\pi\mu}{\alpha}\right)x} f(x). \tag{2.4}$$

For a function of two variables, this becomes:

$$\sum_{m=-\infty}^{\infty} \sum_{n=-\infty}^{\infty} f(\alpha m, \beta n) = \frac{1}{\alpha\beta} \sum_{\mu=-\infty}^{\infty} \sum_{\nu=-\infty}^{\infty} \int_{-\infty}^{\infty} dx \int_{-\infty}^{\infty} dy\, e^{2\pi i\left(\frac{\mu x}{\alpha}+\frac{\nu y}{\beta}\right)} f(x, y). \tag{2.5}$$

In practice, f is the kernel K representing, in cylindrical geometry, the flux or reaction rate around a line or finite source in an infinite medium. Consider now the case in which the fuel elements are arranged in an array of parallelograms. This is only a slight restriction since it includes square, rectangular, and triangular spacings as special cases. Take coordinates x and y along two adjacent sides of the parallelogram as in Fig. 2.2. In an infinite medium, the total reaction rate R at the field point X, Y is:

$$R(X, Y) = \sum_m \sum_n K\left(\sqrt{(X-x_m)^2 + (Y-y_n)^2 - 2(X-x_m)(Y-y_n)\cos\theta}\right). \tag{2.6}$$

Equation 2.6 may be put into a form suitable for Poisson summation by writing for the source points:

$$x_m = am, \tag{2.7}$$

$$y_n = bn, \tag{2.8}$$

and for the field points:

$$X = aM, \tag{2.9}$$

$$Y = bN, \tag{2.10}$$

where m and n are integers because the source has the periodicity of the lattice, but M and N may be nonintegral. Here, a and b are the lengths of the two sides of the parallelogram (i.e., the lattice spacing in the two directions). In these terms:

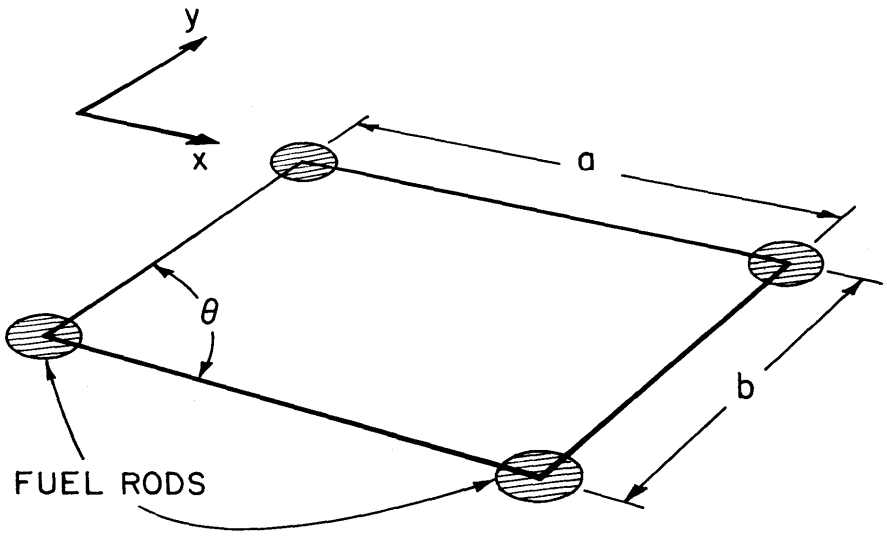

FIGURE 2.2
GEOMETRY OF UNIT CELL

$$R(X,Y) = \sum_{m=-\infty}^{\infty} \sum_{n=-\infty}^{\infty} K\left(\sqrt{a^2(M-m)^2 + b^2(N-n)^2 - 2ab(M-m)(N-n)\cos\theta}\right), \tag{2.11}$$

which becomes by means of Poisson summation:

$$R(X,Y) = \frac{1}{ab} \sum_{\mu=-\infty}^{\infty} \sum_{\nu=-\infty}^{\infty} \int_{-\infty}^{\infty} dx \int_{-\infty}^{\infty} dy\, e^{2\pi i\left(\frac{\mu x}{a} + \frac{\nu y}{b}\right)}$$

$$\cdot K\left(\sqrt{(X-x)^2 + (Y-y)^2 - 2(X-x)(Y-y)\cos\theta}\right). \tag{2.12}$$

The term with both indices equal to zero may be extracted from the summation, giving:

$$R(X,Y) = \frac{1}{ab}\left\{\int_{-\infty}^{\infty} dx \int_{-\infty}^{\infty} dy\, K\left(\sqrt{(X-x)^2 + (Y-y)^2 - 2(X-x)(Y-y)\cos\theta}\right)\right.$$

$$+ \sum_{\mu=-\infty}^{\infty'} \sum_{\nu=-\infty}^{\infty'} \int_{-\infty}^{\infty} dx \int_{-\infty}^{\infty} dy\, e^{2\pi i\left(\frac{\mu x}{a} + \frac{\nu y}{b}\right)}$$

$$\left.\cdot K\left(\sqrt{(X-x)^2 + (Y-y)^2 - 2(X-x)(Y-y)\cos\theta}\right)\right\}, \tag{2.13}$$

where primed summations omit the term with both indices zero.

The kernel is ordinarily normalized so that its integral over all space is a known number, F:

$$\int_{\substack{\text{all}\\ \text{space}}} dA K\left(\sqrt{(X-x)^2 + (Y-y)^2 - 2(X-x)(Y-y)\cos\theta}\right) = F. \tag{2.14}$$

The element of area in this coordinate system is (as may be seen from Fig. 2.2):

$$dA = dx\, dy \sin\theta, \tag{2.15}$$

where θ is a constant as far as the integrations are concerned. The kernel normalization integral may thus be rewritten as:

$$\int_{-\infty}^{\infty} dx \int_{-\infty}^{\infty} dy\, K\left(\sqrt{(X-x)^2 + (Y-y)^2 - 2(X-x)(Y-y)\cos\theta}\right) = \frac{F}{\sin\theta}, \tag{2.16}$$

which, upon substitution into Eq. 2.13, leads to:

$$R(X,Y) = \frac{1}{ab \sin\theta}\left\{ F + \sin\theta \sum_{\mu=-\infty}^{\infty\prime} \sum_{\nu=-\infty}^{\infty\prime} \int_{-\infty}^{\infty} dx \int_{-\infty}^{\infty} dy \right.$$

$$\left. e^{2\pi i\left(\frac{\mu x}{a}+\frac{\nu y}{b}\right)} K\left(\sqrt{(X-x)^2+(Y-y)^2 - 2(X-x)(Y-y)\cos\theta}\right)\right\} . \tag{2.17}$$

It is evident from Fig. 2.2 that ab sin θ is the area of the parallelogram which is also the area of a unit cell. In a three-dimensional system with no axial dependence, this is also the volume per unit height V_c of a unit cell, so that:

$$R = \frac{1}{V_c}\{F + \text{additional terms}\}. \tag{2.18}$$

To determine when the additional terms are important, one notes from Eq. 2.17 that each correction term consists of the integral of the product of a sinusoid (the exponential) with a positive, monotonically decreasing function (the kernel). The magnitude of the sinusoid is never greater than unity, so that the magnitude of each correction term cannot exceed that of the major term. Further, since the sinusoid is alternately positive and negative by equal amounts, the integral will tend to vanish unless the kernel changes magnitude significantly in one period of the sinusoid. But the periods are precisely fractions of the length of a unit cell. The largest periods occur when μ and ν are unity and are equal to a or b. Thus:

> If the kernel nowhere experiences a large fractional change in magnitude over a distance equal to the maximum dimension of a unit cell, the additional correction terms are negligible and the reaction rate is therefore effectively constant within each unit cell.

This generalizes the result of Galanin (G2), that the slowing-down density calculated from the age theory kernel is effectively constant within any unit cell in a lattice whose spacing is much smaller than 2π times the slowing-down length. The requirement that the slowing-down

length be much larger than the lattice spacing is a special case of our condition that the magnitude of the kernel experience only a small change within any unit cell. As long as the kernel satisfies this condition, the slowing-down density (or reaction rate) is not only effectively constant throughout any unit cell but is also independent of the shape of the kernel in space; the first term in Eq. 2.17 depends on the kernel through the term F which is the integral of the kernel over all space. When the condition on the kernel is not satisfied, higher terms in Eq. 2.17 become important and it is only in these higher terms that the shape of the kernel has any influence.

2.2.4 Estimation of the Error Incurred by Using Only the First Term in the Poisson Summation

Because the terms in the Poisson summation decrease in magnitude rapidly, the error incurred by using only the first (the constant) term of the summation may be estimated by evaluating the second term. For convenience, we shall use a one-dimensional lattice with spacing L. The integration over all space can be rigorously broken up into integrations over individual unit cells. The correction term C(X), which depends upon the field point X, is then, from Eq. 2.17:

$$C(X) = 2 \sum_{p=-\infty}^{\infty} \int_{pL/2}^{(p+1)L/2} \cos \frac{2\pi x}{L} K(x-X)\, dx. \tag{2.19}$$

Over each unit cell except the first, K(x-X) is a monotonically decreasing function and may be approximated by a straight line. Within the first unit cell, K(x-X) is not monotonic and must be approximated by two different straight lines, of the form $K(x-X) = cx+d$, as shown in Fig. 2.3.

But when c and d are constants:

$$\int_{pL/2}^{(p+1)L/2} \cos\left(\frac{2\pi x}{L}\right)[\, cx+d\,]\, dx \equiv 0, \tag{2.20}$$

and thus the sole contribution to the correction term arises from the integration over the first unit cell. Within this cell:

$$K(x-X) \approx K(X) + (x-X)\,|\langle K' \rangle|, \quad x \leq X, \tag{2.21}$$

$$K(x-X) \approx K(X) - (x-X)\,|\langle K' \rangle|, \quad x \geq X, \tag{2.22}$$

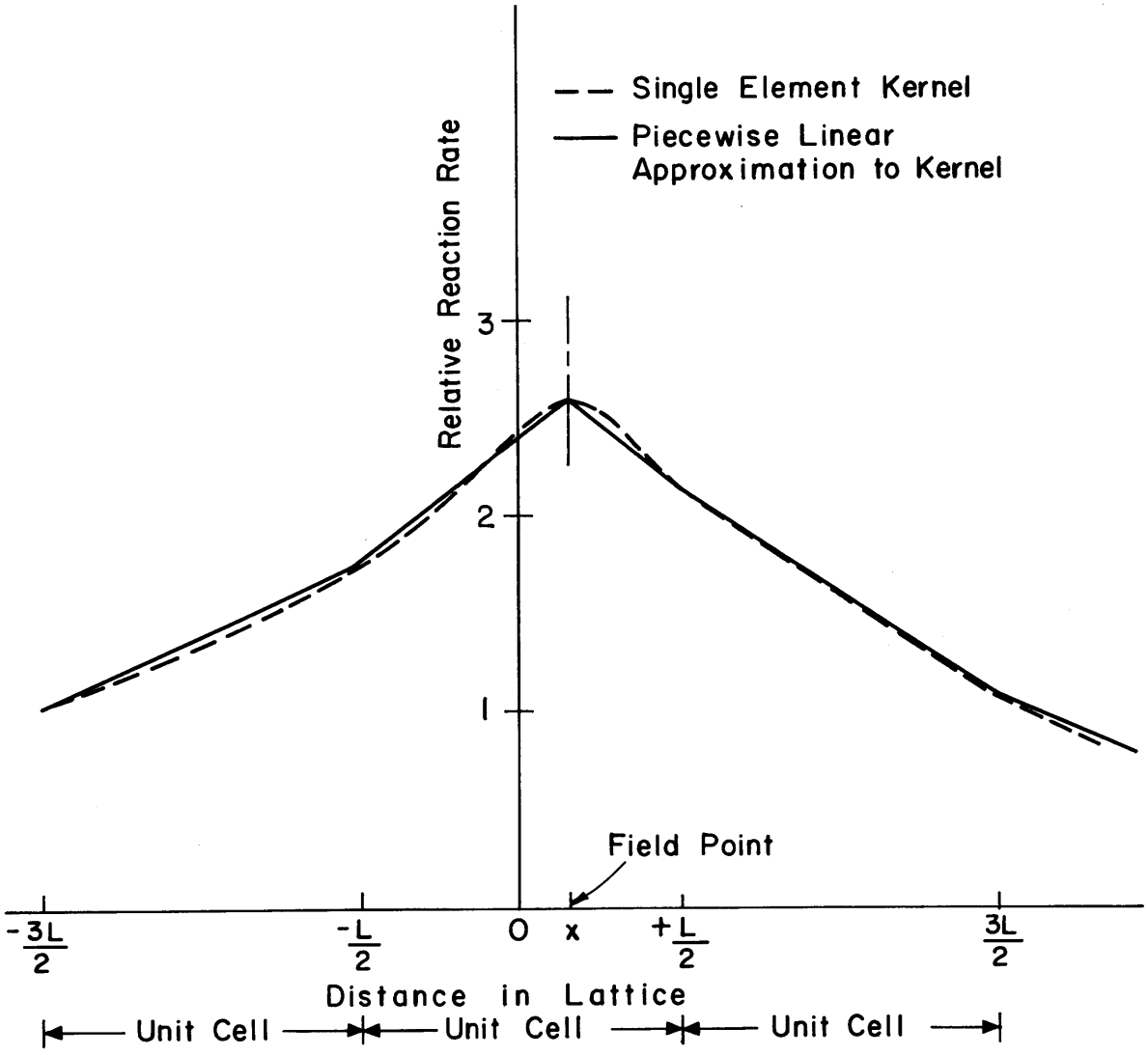

FIG. 2.3 THE SINGLE ELEMENT KERNEL, AND THE PIECEWISE LINEAR APPROXIMATION TO IT USED TO ESTIMATE THE ERROR IN THE TOTAL REACTION RATE AT THE POINT X.

where $\langle K' \rangle$ is the average value of the slope of the kernel K over half a cell's distance from its peak. Then:

$$C(X) = \int_{-L/2}^{X} [K(X)+(x-X)|\langle K' \rangle|] \cos \frac{2\pi x}{L} \, dx$$

$$+ \int_{X}^{L/2} [K(X)-(x-X)|\langle K' \rangle|] \cos \frac{2\pi x}{L} \, dx , \tag{2.23}$$

$$C(X) = |\langle K' \rangle| \int_{-L/2}^{X} dx \, (x-X) \cos \frac{2\pi x}{L} + |\langle K' \rangle| \int_{X}^{+L/2} dx (X-x) \cos \frac{2\pi x}{L} , \tag{2.24}$$

$$C(X) = \frac{L^2}{2\pi^2} \left[1 + \cos \frac{2\pi X}{L} \right] |\langle K' \rangle| , \tag{2.25}$$

$$C(X) \leq \left(\frac{L}{\pi} \right)^2 |\langle K' \rangle| . \tag{2.26}$$

The first (constant) term in the Poisson summation is given by:

$$\int_{-\infty}^{\infty} K(x-X) \, dx < \int_{-L/2}^{+L/2} K(x-X) \, dx = L\langle K \rangle , \tag{2.27}$$

where $\langle K \rangle$ is the average value of K over the first unit cell. Thus, the maximum fractional error incurred by using only the first term in the summation is:

$$\text{Maximum fractional error} \leq \left(\frac{L}{\pi} \right)^2 \frac{|\langle K' \rangle|}{L|\langle K \rangle|} , \tag{2.28}$$

$$\text{Maximum fractional error} \leq \frac{1}{\pi^2} \frac{\langle LK' \rangle}{\langle K \rangle} . \tag{2.29}$$

The ratio $\langle LK' \rangle / \langle K \rangle$ is the fractional change which occurs in K within the unit cell surrounding the origin. The error is then smaller than $1/\pi^2$ times this fractional change in the kernel.

2.2.5 The Use of a Modified Kernel in the Poisson Summation

In some kernels this fractional change is not small, so that a significant error may be incurred by using only the first, constant term in the Poisson summation. In particular, high energy neutrons are closer on the average to their place of origin than are low energy neutrons, so that kernels relating to high energy neutrons may exhibit sufficient peaking in space to cause a large error if only the first term in the Poisson summation is used. In many cases, however, a modified kernel can be defined which does satisfy the necessary conditions and which will be shown to have physical significance.

The crucial condition required for the success of this procedure is that the kernel should decrease monotonically to zero with increasing distance from the source. If this is true, its rate of change also decreases monotonically to zero. Consider, for simplicity, an infinite, one-dimensional, uniform lattice with fuel spacing L, and let Fig. 2.4 represent the kernel, K, which describes the reaction rate of neutrons originating in a single fuel slab in this system.

The total reaction rate at a point x_o, within the cell at the origin, is the sum of the reaction rates of neutrons which reach this position after originating in the fuel slabs at $x_o, L \pm x_o, 2L \pm x_o, \ldots$. To evaluate the total reaction rate at the point x_o, we add the values of the kernel at the points $x_o, L \pm x_o, 2L \pm x_o, \ldots$, as indicated in Fig. 2.4. Were Poisson summation used directly to evaluate this sum, more than one term in the Poisson summation would be needed, since K clearly exhibits a large fractional change in magnitude within the cell at the origin. The use of several terms is a valid procedure, but it is difficult to calculate higher terms analytically or to assign any physical significance to individual terms beyond the first.

These complications are avoided by defining, as shown in Fig. 2.5, a modified kernel K_1 which is identical with K everywhere outside the unit cell at the origin but is zero within this cell:

$$K_1(x) \equiv K(x), \quad |x| \geq L/2, \tag{2.30}$$

$$K_1(x) \equiv 0, \quad |x| < L/2 . \tag{2.31}$$

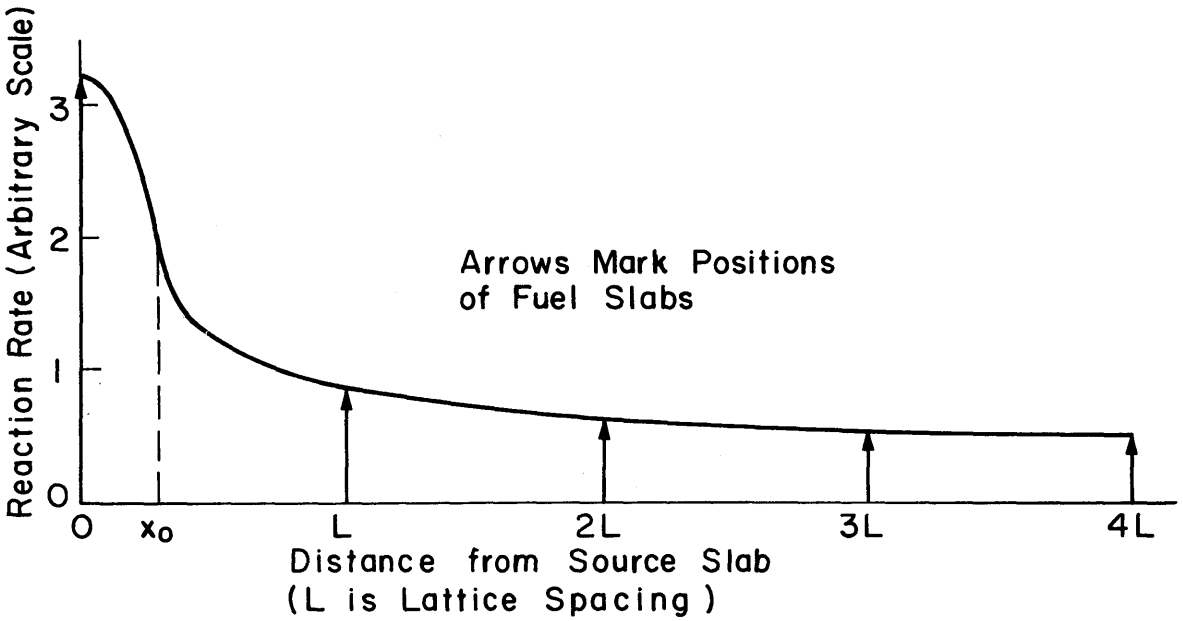

FIG. 2.4 THE ORIGINAL KERNEL, K

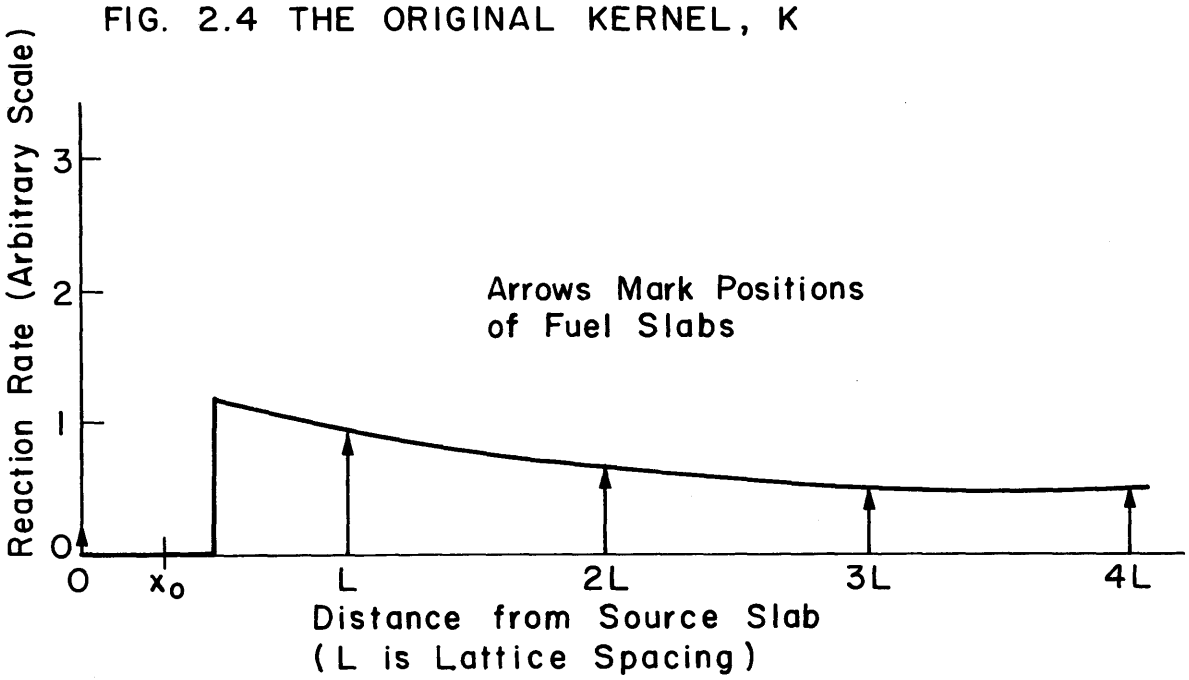

FIG. 2.5 THE MODIFIED KERNEL, K_1

Summing the values of K_1 at the same points as before, $(x_o, L \pm x_o, 2L \pm x_o, \ldots)$ is now equivalent to calculating the reaction rate at x_o, due to neutrons originating in all fuel elements except the one at the origin. The use of K_1 in Eq. 2.1 thus provides the contribution of all neutrons not produced in the closest fuel element. In particular, if x_o coincides with a fuel element position, K_1 gives the contribution from all fuel elements except that one. This contribution is sometimes known as the interaction contribution. Because K_1 is designed specifically to eliminate the rapidly changing part of the kernel, the sum over K_1 is adequately represented by the first term in the Poisson summation of K_1. (The abrupt change in K_1 where it drops to zero is permissible because it occurs exactly on the cell boundary.)

To obtain the total reaction rate at x_o, it is necessary to add to the interaction component the contribution arising from neutrons produced in the fuel element at the origin — that is, at the fuel element closest to x_o. This contribution was omitted from the sum when part of K was set equal to zero to obtain K_1. Thus, in general:

$$R(\vec{r}) = \text{single element contribution} + \text{interaction contribution}, \tag{2.32}$$

and by Poisson summation:

$$R(\vec{r}) = \text{single element contribution} + \frac{F_1}{V_c}, \tag{2.33}$$

where F_1 is the integral of the kernel K_1 over all space or, alternatively, the integral of K over all space outside the cell under consideration. Since

$$0 \leq K_1(x) \leq K(x), \tag{2.34}$$

for all x, it follows that:

$$F_1 \leq F. \tag{2.35}$$

The reaction rate, $R(\vec{r})$, defined by Eq. 2.33 is not constant throughout a unit cell because the single element contribution varies considerably within a cell, but the interaction contribution to $R(\vec{r})$ is constant over

any unit cell in an infinite system. If the system is finite, the single element contribution is unchanged; but the interaction contribution must be multiplied by P, the nonleakage probability between fission energies and the energy considered, for the macroscopic source mode used:

$$R(\vec{r}) = \text{single element contribution} + \frac{F_1 P}{V_c} . \tag{2.36}$$

Equation 2.33 may also be derived from heuristic considerations. Such a derivation has been carried out approximately in a study of the fast fission effect by Driscoll (D2). Driscoll divides the neutrons in a particular fuel element into those originating within that element and those originating elsewhere. Since the latter neutrons originate at so many different positions, it is not unreasonable to assume that variations in their density across the cell of interest average to zero, so that their density is constant over the cell. The reaction rate of these neutrons is thus proportional to $1/V_c$ per source neutron; the constant of proportionality can be determined from the requirement that, for an infinite lattice, the total reaction rate within the cell must equal the total source per fuel element. Thus:

$$\begin{bmatrix}\text{total source}\\ \text{per}\\ \text{fuel element}\end{bmatrix} = F_1 + \int_{\text{cell}} \begin{bmatrix}\text{reaction rate of neutrons}\\ \text{produced in the fuel}\\ \text{element in the cell}\end{bmatrix} , \tag{2.37}$$

But since there is no leakage, neutron conservation requires:

$$\begin{bmatrix}\text{total source}\\ \text{per}\\ \text{fuel element}\end{bmatrix} = \int_{\substack{\text{all}\\ \text{space}}} K , \tag{2.38}$$

and, by the definition of K:

$$\int_{\text{cell}} \begin{bmatrix}\text{reaction rate of neutrons}\\ \text{produced in the fuel}\\ \text{element in the cell}\end{bmatrix} = \int_{\text{cell}} K , \tag{2.39}$$

so that:

$$F_1 = \int_{\substack{\text{all}\\\text{space}}} K - \int_{\text{cell}} K = \int_{\substack{\text{all}\\\text{space}}} K_1, \tag{2.40}$$

which is identical with the definition of F_1 given previously.

The kernel K, although decreasing monotonically to zero, may in some cases exhibit large changes in magnitude within a region that includes not only the unit cell at the origin but also a number of surrounding unit cells. In these cases, K_1 should be defined by setting K to zero over all these unit cells. In effect, this may be considered a redefinition of the unit cell size in the lattice. The modified kernel represents the contribution of neutrons originating outside this region, just as the sum over the kernel shown in Fig. 2.5 represents the contribution made to the reaction rate in the fuel element at the origin by neutrons originating outside the unit cell at the origin.

2.3 GENERAL RESULTS

The results of this analysis and the conditions under which they are valid are collected here for convenience. Consider a system large enough so that the use of the infinite medium kernel is justified. Let K be the kernel describing the reaction rate of neutrons produced in a particular fuel element when the system is infinite. Let P be the nonleakage probability, from fission to the energy considered, for the actual system.

Theorem A: If the magnitude of K never experiences a large fractional change over a distance equal to the lattice spacing:

$$R(\vec{r}) = \frac{FP}{V_c}. \tag{2.41}$$

Theorem B: If K does experience a large fractional change within a distance equal to the lattice spacing but nevertheless decreases monotonically to zero, then:

$$R(\vec{r}) = \text{single element components} + \frac{F_1 P}{V_c}. \tag{2.42}$$

The quantities F and F_1 are the integrals of the kernel K, and the modified kernel K_1, over all space:

$$F = \int_{\substack{\text{all} \\ \text{space}}} K , \tag{2.43}$$

$$F_1 = \int_{\substack{\text{all} \\ \text{space}}} K_1 , \tag{2.44}$$

where K_1 is zero within those unit cells in which K experiences a large fractional change in magnitude and is identical to K in all other unit cells.

Chapter III

EXPERIMENTAL METHODS

3.1 THE M.I.T. LATTICE FACILITY

The M.I.T. Lattice Facility is a shielded, experimental exponential facility, funded by the Atomic Energy Commission and supplied neutrons by the M.I.T. Reactor. Only the main features will be explained here because the details of the assembly and of its supporting equipment have been amply described in several published reports (T1, M3, P1). The assembly consists of a cylindrical, aluminum tank which may be filled with heavy water and into which any number of fuel rods, up to a complete subcritical reactor lattice, may be inserted (Fig. 3.1). Two such tanks, three and four feet in diameter, are presently available. The exponential assembly is fed from the bottom by neutrons which originate in the M.I.T. Reactor, pass through its horizontal thermal column, and thence into a graphite-lined cavity or "hohlraum" beneath the exponential tank, as shown in Fig. 3.2. The cavity serves both to direct the horizontal current of neutrons upward into the exponential tank and to assure that the energy spectrum of the source neutrons is highly thermal. In the hohlraum, the measured cadmium ratio of gold is between 3,000 and 4,000 (P1). The sides of the exponential tank are covered with cadmium, 0.020 inch thick, in order to bring the thermal flux to zero at the edge as quickly and reproducibly as possible.

The techniques used for a direct measurement of lattice parameters in the exponential assembly have been adopted from other laboratories or developed at M.I.T., with the details evolving in response to the needs and experience of workers on the project (B1, W1, W2, S1, D1).

The experiments reported here were made around a single fuel element situated vertically along the central axis of the tank. All measurements were made at a height chosen so that the axial dependence of the flux was, indeed, exponential.

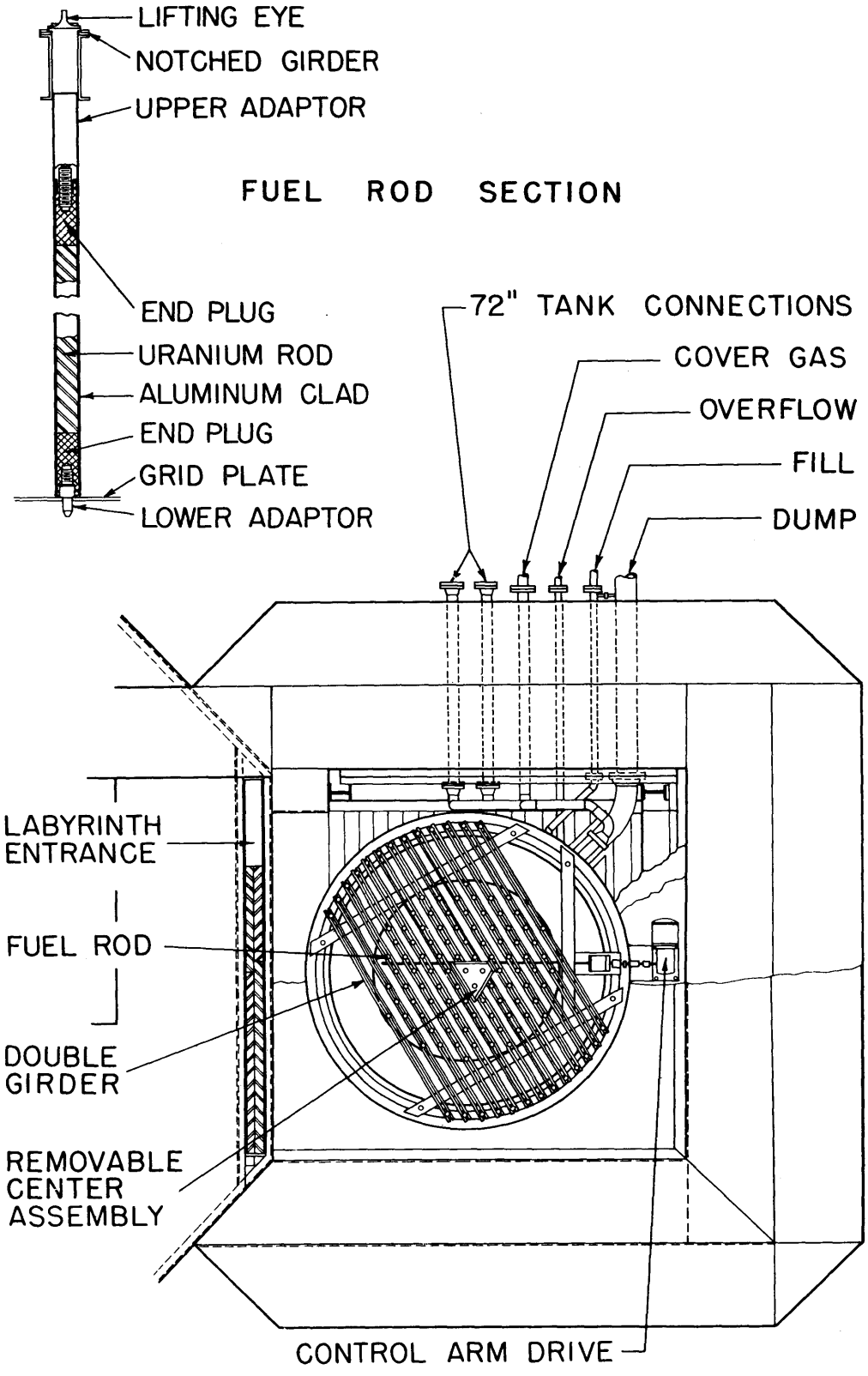

FIG. 3.1 PLAN VIEW OF THE SUBCRITICAL ASSEMBLY

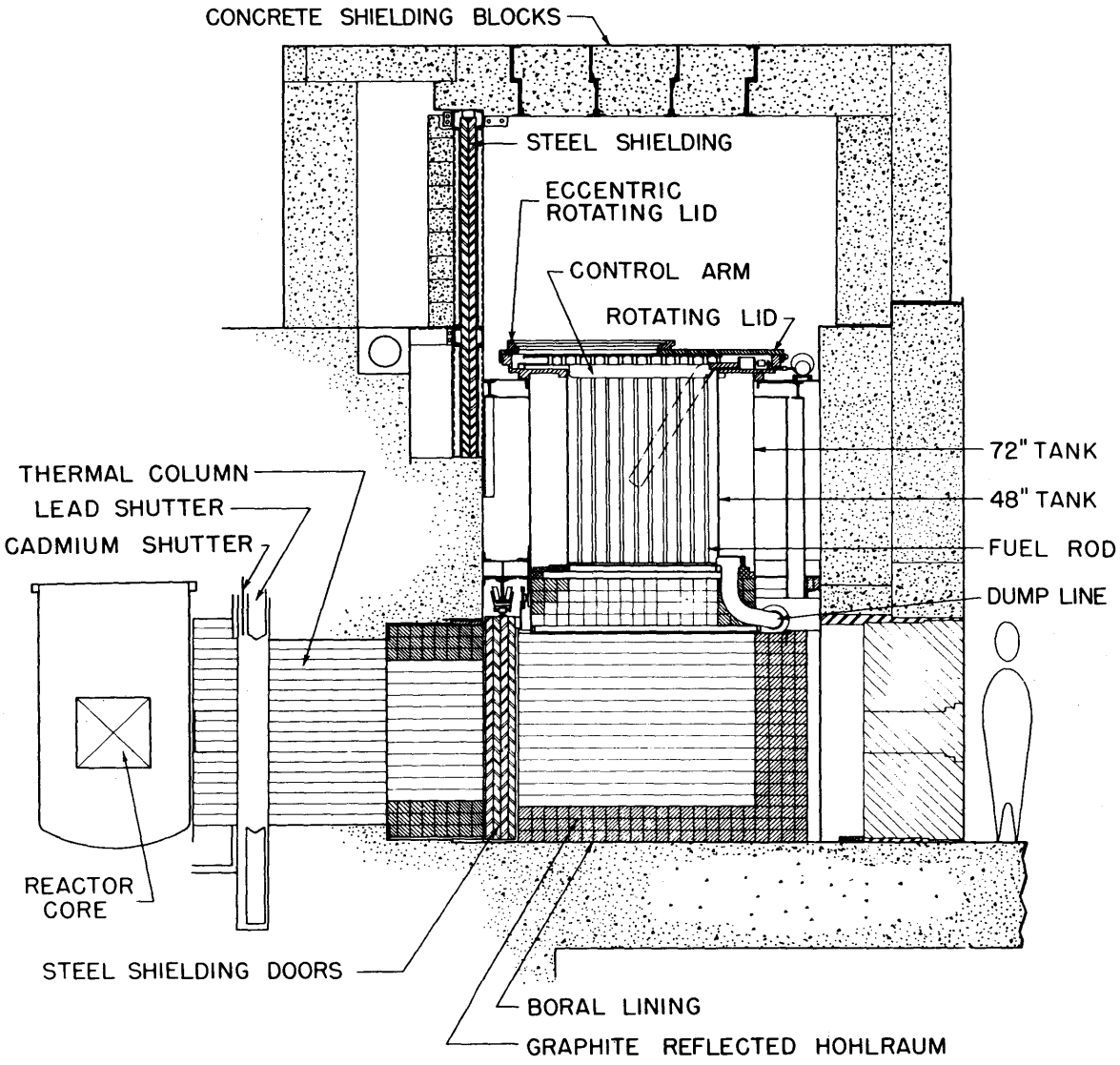

FIG. 3.2 VERTICAL SECTION OF THE SUBCRITICAL ASSEMBLY

3.2 MEASUREMENTS IN THE THERMAL ENERGY REGION

3.2.1 Foils and Cadmium Covers

Gold foils were used to measure the relative activities induced by neutrons of epicadmium and subcadmium energies. For this purpose, gold sheet of at least 99.95 percent purity was punched into circular foils. Measurements as a function of radial position at a fixed height were made with foils of 0.010-inch thickness and one-quarter-inch diameter, and measurements as a function of height at a fixed radius were made with foils of 0.010-inch thickness and one-eighth-inch diameter. Foils were weighed to an accuracy of about 0.02 percent on a microgram balance.

Cadmium covers for radial traverses were made from cadmium sheets of 0.020 ± 0.001-inch thickness. The covers consisted of two parts. A bottom part, 0.625 inch in diameter, was preformed into a cup of inside diameter 0.325 inch. The gold foil was placed in the cup and a top plate, 0.325 inch in diameter, was then pressed-fit above it into the cup by means of a punch press. The arrangement is shown in Fig. 3.3. The resulting cadmium covers were adequately shockproof and leaktight. They could be dropped onto a wooden table from a height of one foot without opening, and they endured immersions in heavy water for up to twelve hours with only a negligible fraction showing any signs of water leakage.

Cadmium covers used in axial traverses were of the type designed by Simms (S1) and shown in Fig. 3.4.

3.2.2 Foil Holders

Foil holders were fabricated of Type 1100 aluminum. Typical holders for use in axial and radial traverses are shown in Fig. 3.5. In each holder, depressions of 0.010-inch depth were milled out at fixed intervals in order to position bare foils accurately. Slightly wider but shallower depressions were milled out above them for positioning cadmium-covered foils. Both bare foils and cadmium pillboxes were affixed to the holders by using two layers of 0.001-inch-thick Mylar tape. Before the foils were removed at the end of each irradiation, the

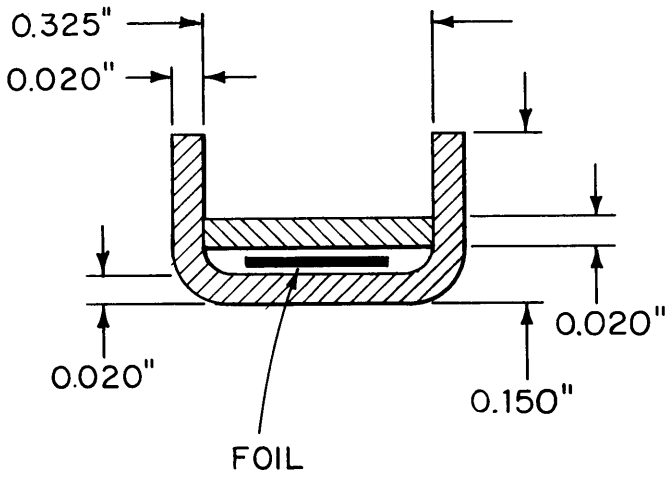

FIGURE 3.3
CADMIUM COVERS FOR ONE-QUARTER INCH DIAMETER FOILS

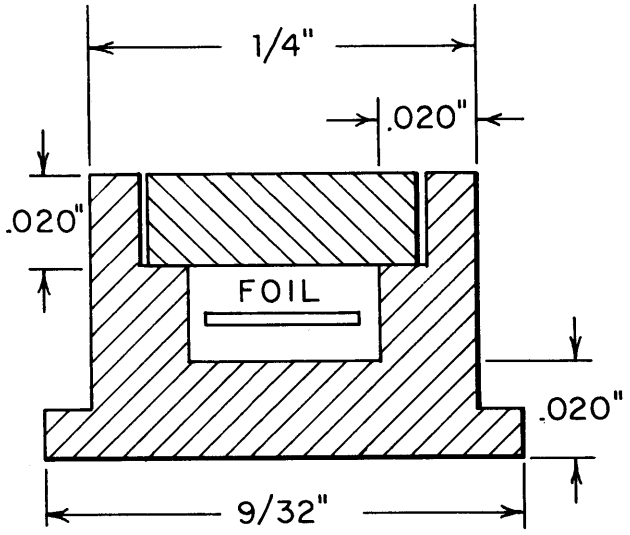

FIG. 3.4 CADMIUM PILLBOX USED FOR ONE EIGHTH INCH DIAMETER GOLD FOILS

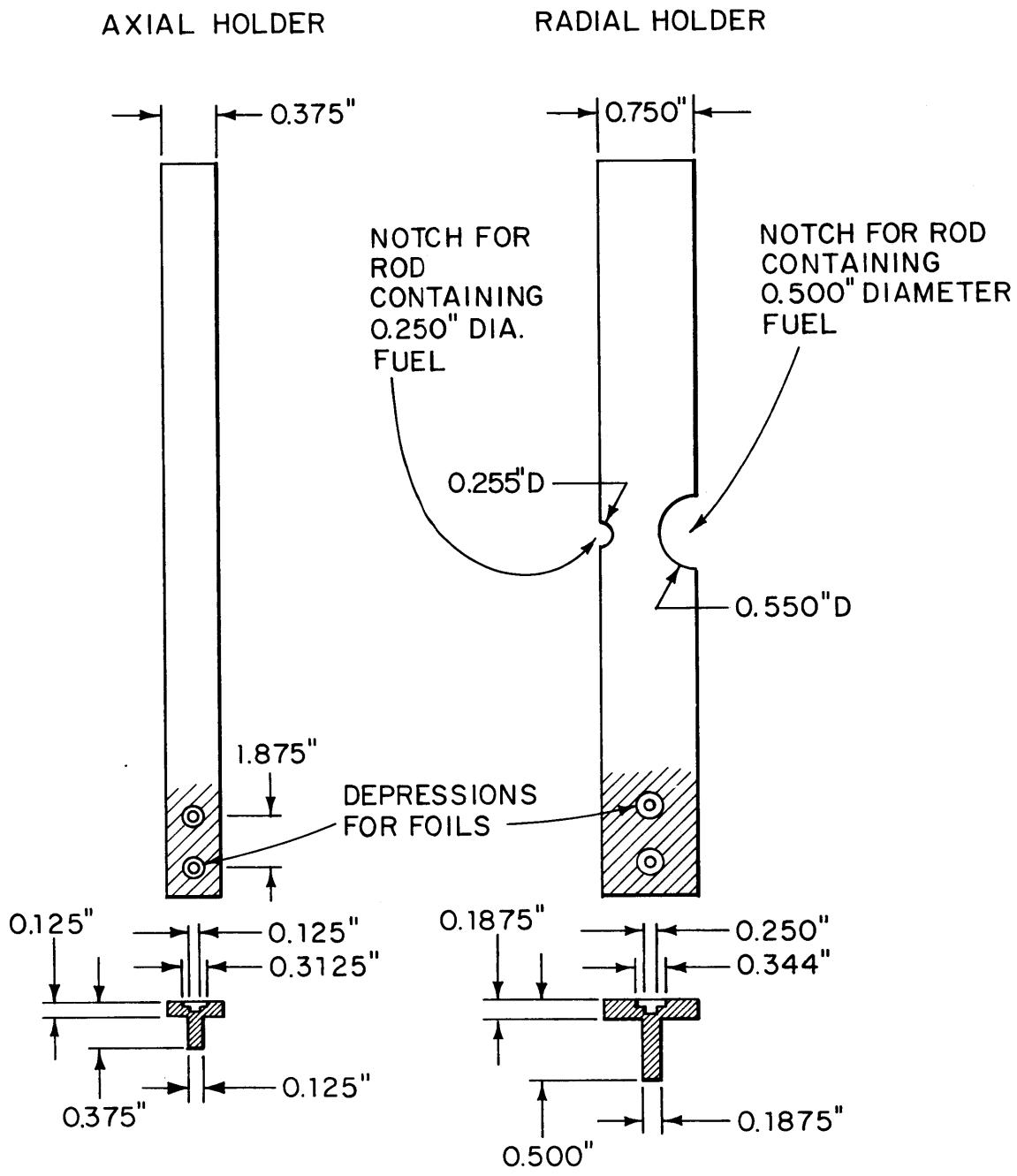

FIGURE 3.5
FOIL HOLDERS FOR AXIAL AND RADIAL TRAVERSES AROUND A SINGLE FUEL ELEMENT

arrangement was examined visually to insure that no movement of the foils had occurred, either by relaxation of the Mylar tape or by bumping of the holder during placement and removal.

The length of each radial foil holder was about one inch less than the diameter of the tank in which it was used, to facilitate placement and removal of the holder. A semicircular notch, whose radius was slightly larger than that of the fuel rod with which the holder was to be used, was milled out of the side of each radial foil holder. During the experiments, the single fuel rod was inserted into this notch so that its position relative to the foil holder was well determined. Notches of different size were made on opposite sides of each holder so that each radial foil holder could be used (at different times) with fuel rods of two different sizes.

3.2.3 Experimental Procedure

The single fuel element used in any experiment was suspended by means of a pin which was fixed through its top adapter and was locked into position on the girder atop the tank. To ensure that it was vertical, the fuel element was allowed to hang freely without hitting the bottom of the tank. Proper placement of the fuel element in the center of the tank was thus assured as long as the girder was properly aligned.

The axial foil holder was attached to an aluminum rod suspended from a small, movable, aluminum plate on the girder. Since the single fuel element used in the experiments was suspended from the center of the same girder, it was possible to position the foil holder accurately with respect to the element by simply moving the plate to locations which were marked in advance on the girder.

The radial foil holder was suspended horizontally by two chains made of aluminum beads. Each chain was attached one-third of the way from one end of the holder. The upper ends of the chains terminated in aluminum blocks which rested on the overhead girder at positions that were marked beforehand. The chains were checked before each experiment to make sure that both were of the same desired length.

To maintain the purity of the heavy water, all experiments were inserted and removed from the exponential tank through the glove box

at its top. In making a typical run, the fuel element was first inserted into the tank and was hung in position from the girder. The aluminum block on one end of the radial holder was positioned on the girder, and the second aluminum block was maneuvered to the other side of the girder. After the second aluminum block was fixed in position, the first one was rechecked to be sure it had not moved. The holder was inspected visually to ascertain that it was hanging horizontally, was not entangled with the chain, and that the fuel element was fitted into the notch on the side of the holder. (See Fig. 3.6.) Irradiations lasted up to twelve hours for cadmium-covered foils, and from one-half to two hours for bare foils, depending on the reactor power.

3.2.4 Counting Procedure

The activity of the gold foils was recorded by one of the three automatic counting and sample changing systems in use on the Lattice Project. They all employed thalium-activated, sodium iodide crystals for counting the 411-kev photopeak of Au^{198}. Figure 3.7 shows block diagrams of the electronics in these systems. A single-channel analyzer was used to straddle the peak, with the baseline set at the lowest point in the spectrum below the peak. The system was calibrated before and after each set of runs. Additionally, the ACTIVE (S1) code, which was used to reduce the raw counting data, uses the known half-life of gold, so that counter drift would have appeared as a large spread in the values of the corrected activities of a foil as computed from the individual passes.

Each foil was counted in at least two passes, and the accumulated counts were at least 40,000 for each bare foil and 20,000 for each cadmium-covered foil. This ensured an inherent counting uncertainty of less than 0.5 percent for the bare foils and 0.75 percent for the cadmium-covered foils.

The ACTIVE code (S1) was used to correct the raw counts for background and deadtime and to reduce the results to relative activity per milligram of foil at end of irradiation.

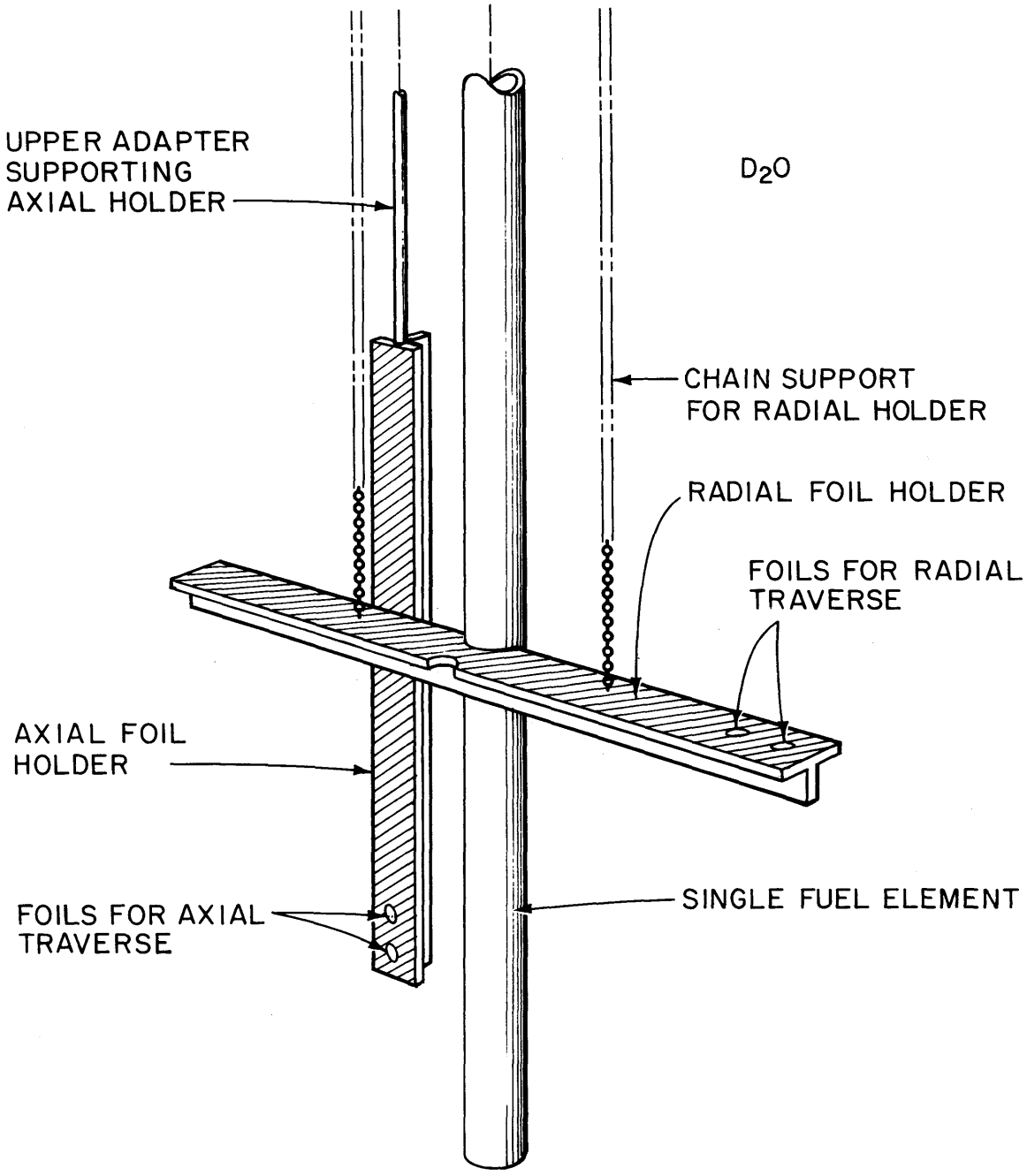

FIGURE 3.6
EXPERIMENTAL ARRANGEMENT FOR TRAVERSES AROUND A SINGLE FUEL ELEMENT

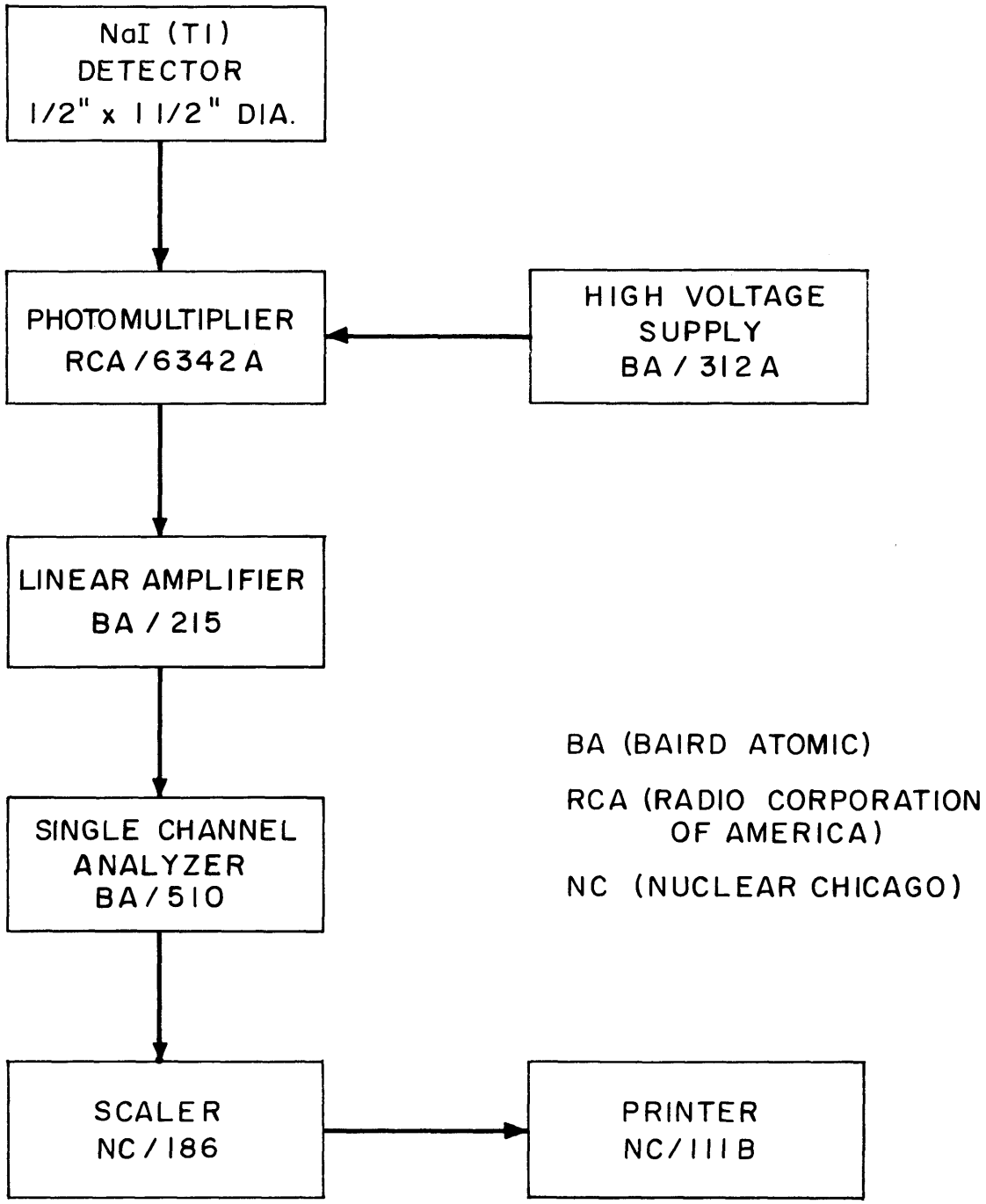

FIG. 3.7 BLOCK DIAGRAM OF GAMMA - COUNTING SYSTEM USED FOR Au^{198}

3.2.5 Uncertainties in the Experiment

Uncertainties in the resulting curve of activity as a function of radius arise from uncertainties in the positioning and in the counting of the foils. These are independent uncertainties, so at a particular radius r the uncertainty of the activity A(r) measured at r is:

$$\sigma^2_{A(r)} = A^2\sigma^2_N + \left(\frac{\partial A}{\partial r}\right)^2 \sigma^2_r + \left(\frac{\partial A}{\partial z}\right)^2 \sigma^2_z , \tag{3.1}$$

where σ_N is the inherent uncertainty in N counts.

For bare foils, the expected errors in position, σ_r and σ_z, are small because the foils fit into depressions on the holder. The maximum possible uncertainty in either direction is about 0.3 cm, and an average positioning uncertainty of 0.15 cm is estimated, due both to foil misplacement on the holder and to holder misalignment relative to the source rod.

The order of magnitude of the expected value of σ_A may then be calculated from this by making reasonable assumptions about the flux distribution. For example, one can use the flux distribution characteristic of a homogeneous exponential and evaluate the radial derivative halfway between the center and edge of the tank. Then, for a three-foot-diameter, exponential tank with a typical axial relaxation length of 20 cms, the result is:

$$\frac{\sigma_{A(r)}}{A(r)} \approx 0.01 . \tag{3.2}$$

Thus, the average expected error in each individual point is about one percent. This result is consistent with the observed variations in activity between corresponding foils on opposite sides of the fuel element.

3.3 MEASUREMENTS IN THE RESONANCE REGION

3.3.1 Foils Used

Activity resulting from epicadmium absorptions in uranium was measured by irradiating foils of natural and depleted uranium. These foils were the standard set used on the Lattice Project and, as such, they had been carefully punched to avoid burrs or chips at the edges

(D1, H3). The foils were 0.005 inch thick and were either 0.250 or 0.750 inch in diameter. All foils were of high purity uranium obtained from Oak Ridge National Laboratory. The depleted uranium foils of one-quarter-inch diameter had a measured concentration of eighteen atoms of U^{235} per million atoms of uranium (W1). For each experiment, the foils were weighed with an accuracy of about 0.02 percent on a microgram balance. Because some oxidation of the surfaces of the foils could occur without being visible to the naked eye, the overall accuracy of the weights was estimated to be about 0.05 percent, entirely adequate for these experiments.

3.3.2 Experimental Procedure

The object of these experiments was to measure an activity proportional to the rate of absorption of epicadmium neutrons in a fuel rod. It was desired to make the measurement as a function of the distance separating the fuel rod from the source of fission neutrons.

Foils having the diameter of the fuel rod of interest were inserted between two fuel buttons of the same diameter and one-quarter inch high, and the whole assembly was covered with cadmium. The fuel buttons caused the foils to have the same effective disadvantage factor as a fuel rod but were small enough to contribute only a negligible neutron source from epicadmium fissions. The buttons were necessary because the spectrum of neutrons around the source rod was space-dependent, causing the disadvantage factor also to be space-dependent. Were it independent of position, the disadvantage factor would have been unimportant in obtaining the relative values of the activity needed here. In practice, catcher foils of depleted uranium were inserted around the depleted foil to be counted, so that it was not contaminated with fission products from the neighboring fuel buttons.

The experimental arrangement of such a foil packet is shown in Fig. 3.8. Cadmium plates were placed above and below the fuel buttons to prevent neutrons of subcadmium energies from entering the packet, and after the whole packet was inserted in an aluminum tube, cadmium sheet was positioned around the tube, at the height of the packet, for the same purpose. The cadmium was 0.020 inch thick. Aluminum rods were

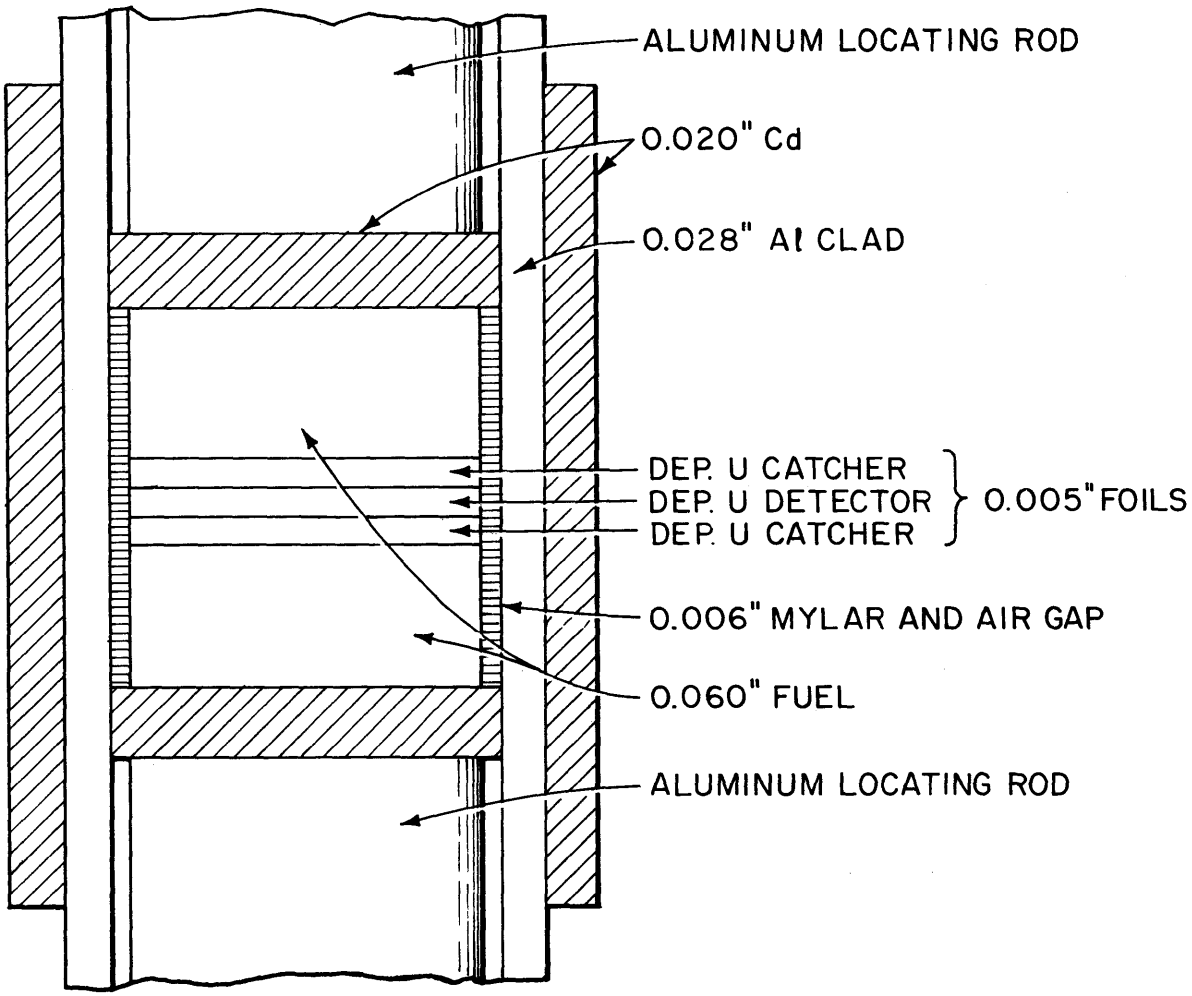

FIGURE 3.8
ARRANGEMENT USED TO DETERMINE RELATIVE CAPTURE IN U^{238} IN RODS AROUND A SINGLE SOURCE ELEMENT.

placed in the tube, above and below the packet, so that it was situated a suitable distance from the bottom. The distance of the foil packet from the top of the tube was measured. The tubing was made of Type 1100 aluminum and was 0.028 inch thick. Foil packets were placed sixteen inches above the bottom of the tube. This ensured that the packets were situated in a region where the axial dependence of the flux was exponential. It was shown experimentally (Chapter IV) that the axial relaxation length in the single element experiment is independent of the radius at which foils are exposed in those regions where the axial dependence is, in fact, exponential. Locating the packet in such a region thus resulted in an axial leakage that was proportional to the flux, with a constant of proportionality that was independent of radius.

For each experiment, a fuel rod was inserted into the tank and was hung vertically at the center, from the girder overhead. The aluminum tubes were then inserted into the tank and hung from the girder at the proper distances from the central fuel rod. These distances were determined by measuring the center-to-center spacing between the fuel element and each aluminum tube.

Irradiation times lasted from twelve to one hundred hours. The longer times were preferred because the central fuel rod provided the only source of neutrons of epicadmium energies and long irradiation times were needed to achieve countable activities in the foils.

At the end of each irradiation, the aluminum tubes were removed from the exponential tank and the foil packets were unloaded. At this time, the cadmium sheet wrapped around the tube was examined to ascertain that it had not slipped.

3.3.3 Counting Procedure

The depleted uranium foils were gamma-counted for Np^{239} activity. Counting was begun about twelve hours after the end of the irradiation, so that the U^{239} had sufficient time to decay to Np^{239} and in order to allow for the decay of short-lived, highly active fission products which would have provided a time-dependent background. A thalium-activated, sodium iodide crystal, one-half inch thick by one and one-half inches in diameter, was used to detect the 103-kev peak

in the spectrum of Np^{239}. A single-channel analyzer was calibrated to straddle this peak, using the 84-kev photopeak of Tm^{170} and the 123-kev photopeak of Co^{57}. A block diagram of the counting system is shown in Fig. 3.9.

All foils were counted at least three times. All count rates were low enough so that dead-time corrections were negligible.

3.3.4 Data Analysis

Raw counting data were reduced by hand. Corrections were made for background activity, variations in foil weight and measured variations in the height of the foils when they were irradiated. The height correction was based on the measured value of the axial relaxation length.

The activity of each foil in a pass was corrected to the time at which the first foil in that pass was counted. The value of the total activity of each foil was established by adding together the values of its corrected activity on each pass. This was permissible because only the relative activities were of interest, and the correction factor for decay from pass to pass was common to all foils.

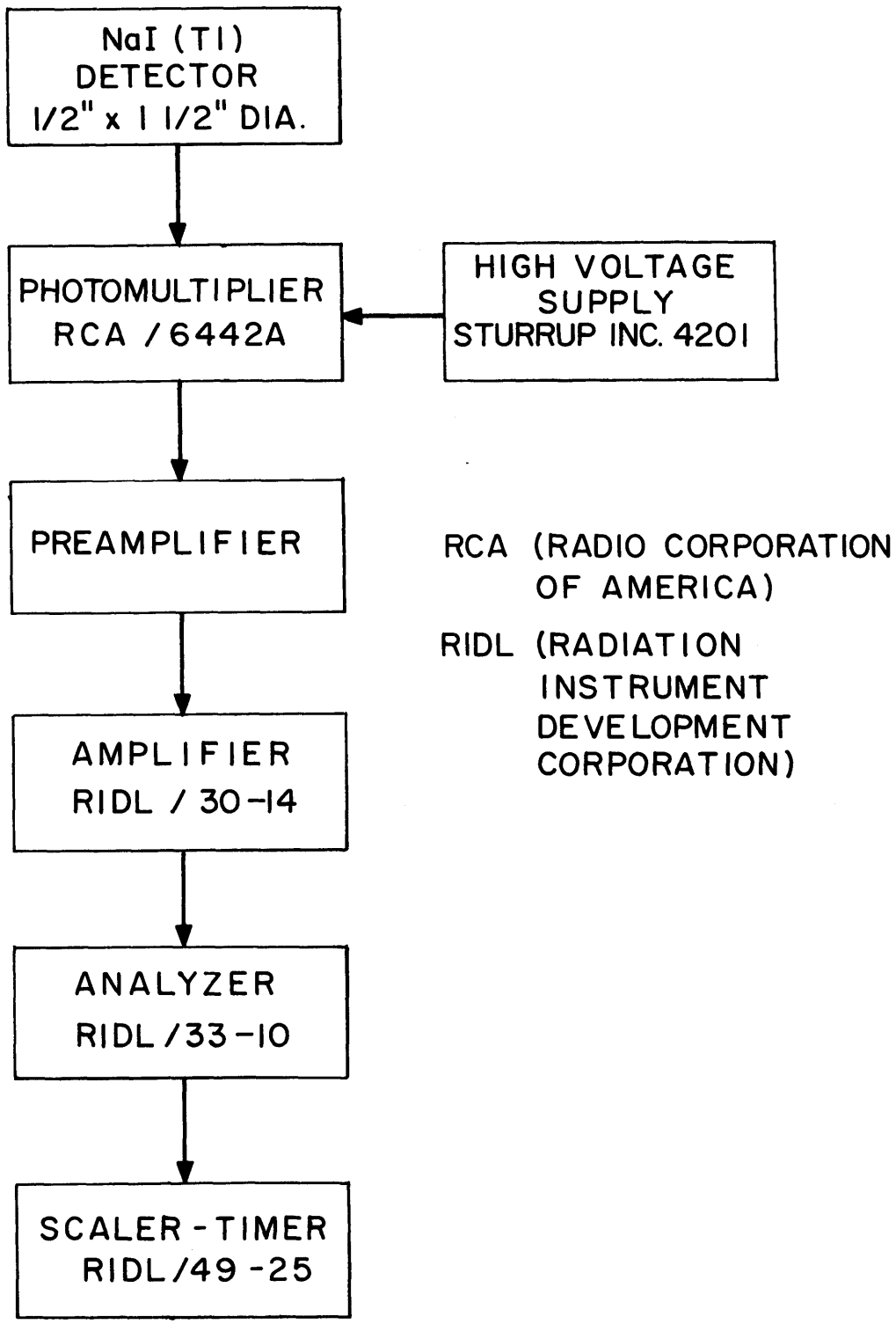

FIG. 3.9 COUNTING SYSTEM USED TO MEASURE THE Np^{239} ACTIVITY OF THE DEPLETED URANIUM FOILS

Chapter IV

THE USE OF EXPERIMENTS ON A SINGLE FUEL ELEMENT TO INFER THE VALUE OF THE THERMAL UTILIZATION IN A LATTICE

4.1 INTRODUCTION

4.1.1 Purpose of the Investigation

This part of the investigation is meant to provide a technique for determining the value of the thermal utilization in a uniform lattice by means of measurements made around a single fuel element. Such a technique is expected to be useful because the complicating factors which make it difficult to calculate the thermal utilization by any simple method are mainly peculiar to an individual fuel element and are insensitive to the presence or absence of neighboring elements. For example, the transport effects attendant upon the strong absorption in even a simple, cylindrical rod of uranium cause diffusion theory to give values of the thermal utilization which are low by as much as two percent (M4). Similarly, in the A. E. C. superheat critical experiments (P4) undertaken by General Electric, the presence of light water within an individual fuel element causes such a large change in the thermal neutron spectrum that an ordinary diffusion theory calculation is not valid.

When the distribution of fuel within the element is a function of only one spatial variable, these problems can be solved (if the necessary basic data are available) by the use of transport theory codes, such as THERMØS (H4), although the extensive machine time required by such codes frequently makes them unsuitable for survey computations. If the fuel distribution within the element is a function of two variables (as in an element consisting of a fuel bundle), then the efficacy of the present transport theory codes is doubtful. Thus, it was stated in May, 1965 at Argonne National Laboratory during the Conference (B2) on the Application of Computing Methods to Reactor Problems that a two-dimensional THERMØS was considered too unwieldy for production

purposes. If the problem is somehow reduced to an "equivalent" one-dimensional problem, one loses the main advantage of a transport theory calculation – a reasonable assurance that, if the input nuclear data are correct, the results are correct. In this case, it is difficult to decide what quantitative error is incurred through the use of the "equivalent" geometry (U1). Thus, for elements consisting of 19-rod uranium oxide clusters in heavy water, calculated and measured values of the thermal utilization differed by as much as 3 percent (H5). This discrepancy was attributed to inadequacies in the scattering kernel used for heavy water. In graphite, where the scattering kernel is presumably much more accurate, the disagreement was 0.3 percent (H5). It is clear that the high accuracy, which is often thought to invariably result from transport theory calculations of the value of the thermal utilization, is presently unattainable in many practical applications, either because of computational limitations, geometric complexity, or the lack of basic nuclear data.

Problems such as these illustrate the need for a method combining an experimental treatment of these "single rod" complications with a theoretical treatment of the interaction effects between fuel elements.

The method explained here accomplishes this by characterizing each element by a single parameter, related to an extrapolation length. The feasibility of the method is demonstrated by showing that this parameter can be determined from experiments on a single fuel element and that its use gives accurate values of the thermal utilization in lattices containing heavy water as the moderator. The individual fuel rods available at M. I. T. have been used as the fuel elements in this investigation. Lattices of these rods in heavy water have been studied extensively in the exponential assembly at M. I. T. and the values of the thermal utilizations in them are known accurately.

4.1.2 Methods Used

Galanin (G2) has expressed the thermal utilization in an infinite, uniform lattice in terms of the ratio Γ' of the thermal flux at the rod surface to the net thermal neutron current at the rod surface. Klahr (K2)

subsequently noted that the use of this definition involves both an approximation and a computational difficulty. The approximation arises because the ratio Γ' is defined in terms of quantities at the surface of the fuel rod, but it is used with a theory of neutron diffusion which treats the fuel elements as line sources and sinks. The resulting error might be expected to be small whenever the effective extrapolation length is large compared to the radius of the fuel element. Nevertheless, it is desirable to eliminate this approximation.

The computational difficulty arises because the relation between the thermal utilization and the ratio Γ' depends upon the theory used to calculate thermal neutron transport in the lattice. If the correct value of the thermal utilization is to be obtained, then the ratio Γ' must be defined consistently with the method of calculating thermal neutron transport. If Γ' is defined in terms of the actual flux at the rod surface, the method of calculating the neutron transport must predict this flux accurately. This requires the use of a high-order approximation to the Boltzmann equation, with all its computational difficulties. Klahr (K2) observed that both the approximation and the computational difficulties can be avoided if Γ' is defined as the ratio of an effective thermal flux at the center of the fuel element to the net current of thermal neutrons into the fuel element. The ratio so defined will be denoted by Γ (without the prime). The effective thermal flux is that flux which would exist if all fast neutron sources in the system remained unchanged in all respects but if, in the calculation of the thermal neutron transport, the fuel elements were replaced by moderator. Since this definition eliminates the strong absorption in the fuel elements, diffusion theory is now adequate to determine this effective thermal flux at the center of the element. Although it will be demonstrated in section 4.2.2 that the thermal utilization of a lattice may be expressed theoretically in terms of the effective thermal flux by using diffusion theory, the concept of the effective flux is of practical use only to the extent that its value can be inferred from measurements in or around real fuel elements. A procedure for determining the value of the effective thermal flux from measurements around a single fuel element immersed in moderator will be given in section 4.2.1.

The effective thermal flux as defined here is computationally and conceptually useful, but no claim is made that in itself it is physically measurable — nor is it. The sole justification for its use is that it provides a helpful intermediate between the real flux distribution measured around a single rod immersed in moderator and the real thermal utilization in a lattice. It is analogous in its function to an output or input impedance in electronics. Thus, "the output impedance of this amplifier is $Z = R + j\omega/C$" does not mean that if the cover is removed, the amplifier will be found to consist of a resistance R in series with a capacitor C. The statement means only that the relation between current and voltage at the output terminals of the amplifier is expressible in terms of a quantity Z. Similarly, the statement, "the effective flux at the center of this fuel element is ϕ_o," should be interpreted as meaning only that the relation between the absorption in the element and the thermal utilization in a lattice of such elements is expressible in terms of the quantity ϕ_o. Just as Z can be calculated from a knowledge of electrical circuit theory plus a knowledge of the values of the actual, physical elements used in the amplifier circuit, so ϕ_o can be calculated from a knowledge of diffusion theory and nuclear constants. Just as Z may be a good representation of the amplifier's output impedance only over a restricted range of frequencies, beyond which such things as stray capacitances will introduce further terms, so Γ is a good representation of the fuel element's behavior in a thermal neutron spectrum similar to that in which the experimental determination of Γ is made.

When a single fuel element is immersed in moderator, the net thermal neutron current into the element is related to the thermal flux around the element by the neutron conservation equation. In the work reported here, measurement of the relative thermal flux has been used with the conservation equation to deduce the relative net current of thermal neutrons into the element. The magnitude of the relative flux which would exist at the center of the element, were the latter replaced by moderator, is obtained by properly extrapolating the values of the moderator flux back into the element. Thus, the parameter characterizing each kind of fuel element in a particular moderator is obtainable

from experiments on just one such element immersed in moderator. It will be shown that the values of the thermal utilization calculated from such experiments are in good agreement with those obtained from more complicated calculational models.

4.2 THEORY

4.2.1 The Determination of the Single Rod Parameter Γ from Experiments on a Single Fuel Rod Immersed in Moderator

The following definitions will be needed:

$J_{rod} \equiv$ the number of thermal neutrons absorbed by the fuel element per unit time and per unit length of element; these are neutrons whose energies lie below the cadmium cut-off energy;

$\phi_o \equiv$ the subcadmium flux which would exist at the center of the fuel element if all the fuel elements in the system could be replaced by moderator without in any way changing the magnitude or spatial distribution of the slowing-down density into the energy region of subcadmium energies;

$$\Gamma \equiv \frac{\phi_o}{J_{rod}}.$$

The effective flux is the solution to a diffusion equation describing the thermal (subcadmium) flux. This equation differs from the usual diffusion equation applicable in a lattice in that all fuel elements are replaced by moderator, but the terms representing the slowing-down source are left unchanged. The elimination of the fuel elements suppresses the flux dip which would otherwise result from neutron absorption in the fuel elements. The medium is thus homogeneous; if the slowing-down source into the subcadmium region is constant in space, so will the effective flux be constant in space. In this lattice, the subcadmium disadvantage factor is unity. For such a lattice, the effective flux at the center of an element, ϕ_o, may alternatively be defined as the value attained by the moderator flux far from the element when it is

extrapolated to the center of the fuel element position. Since the thermal flux far from the element is insensitive to the presence or absence of thermal absorption in the element, this latter definition of ϕ_o may be used to obtain a value of ϕ_o from measurements of the real subcadmium flux around a real fuel element. It has, so far, proved impossible to verify by theoretical calculations that the result of this procedure of extrapolation is, in fact, the exactly correct value of ϕ_o. Nevertheless, its usefulness is demonstrated by the agreement between values of the thermal utilization obtained from values of ϕ_o deduced by extrapolation and values of the thermal utilization obtained from THERMØS.

Consider a single vertical fuel element immersed in moderator at the center of an exponential assembly fed by a source beneath the assembly. The radial dependence, $\phi(r)$, of the thermal flux will be investigated at a height where the axial flux dependence has its asymptotic form, $\sinh \gamma(H-z)$. The equation describing the radial flux dependence in the moderator, under the assumption that diffusion theory applies there, is:

$$\nabla_R^2 \phi(r) + (\gamma^2 - \kappa^2)\phi(r) + \frac{\eta \epsilon P J_{rod}}{D} G(r) \equiv 0, \qquad (4.1)$$

where:

ϕ represents the radial dependence of the thermal flux (n/cm^2-sec).

∇_R^2 represents the radial Laplacian operator, $\frac{1}{r}\frac{1}{dr}\left(r \frac{d}{dr}\right)$.

$\kappa^2 = \frac{1}{L^2}$; L is the thermal diffusion length in the moderator alone (cm^{-2}).

D is the diffusion coefficient of the moderator alone (cm).

ϵ is the fast fission factor for the single fuel element.

η is the total number of fast neutrons produced in the rod by fission in U^{235} per subcadmium absorption in the fuel element.

P is the net probability that a fast neutron born in the fuel element will slow down to subcadmium energies without leaking out of the exponential assembly or being absorbed in the region of resonance energies. The explicit value of P will not be needed in what follows, so methods of evaluating P need not be considered.

G(r) is the kernel which gives the slowing-down density (cm^{-2}) to subcadmium energies per unit of horizontal (radial) area at the radius r. The kernel is normalized so that:

$$\int_A dA\ G(r) = 1, \tag{4.2}$$

where A is the cross-sectional area of the exponential assembly.

The inverse diffusion area, κ^2, of the moderator is a known quantity, and γ^2 is obtained from measurements of the relative axial dependence of the flux. As used here, the axial relaxation length is assumed to be independent of radius. This assumption was verified in several cases by making axial traverses at various radii, as shown in Fig. 4.1.

Gold foils were used to measure the relative thermal flux, ϕ, around the single fuel element. Details of the experimental procedure are given in section 3.2.2. The value of $(\eta\epsilon P)\frac{J_{rod}}{D}$ could have been obtained by fitting Eq. 4.1 to these data. However, the direct use of Eq. 4.1 is inadvisable because of the need to differentiate the experimental data in making the fit, a procedure which is likely to introduce serious uncertainties. The derivatives were removed from Eq. 4.1 by integrating as follows:

Replace r by the dummy variable u, multiply by the element of area $2\pi u\ du$, and integrate Eq. 4.1 from zero to w:

$$\int_0^w du\ 2\pi u \frac{1}{u}\frac{d}{du}\left(u\frac{d\phi}{du}\right) + (\gamma^2-\kappa^2)\int_0^w du\ 2\pi u\ \phi(u)$$

$$+ \eta\epsilon P \frac{J_{rod}}{D}\int_0^u du\ 2\pi u\ G(u) = 0. \tag{4.3}$$

The use of zero as a lower limit of integration is justified if the fuel element is a line source and sink of neutrons. The parameters which result from fitting this equation to the experimentally measured flux will then be parameters appropriate to that line source and sink which produces the same subcadmium flux distribution as the real fuel element.

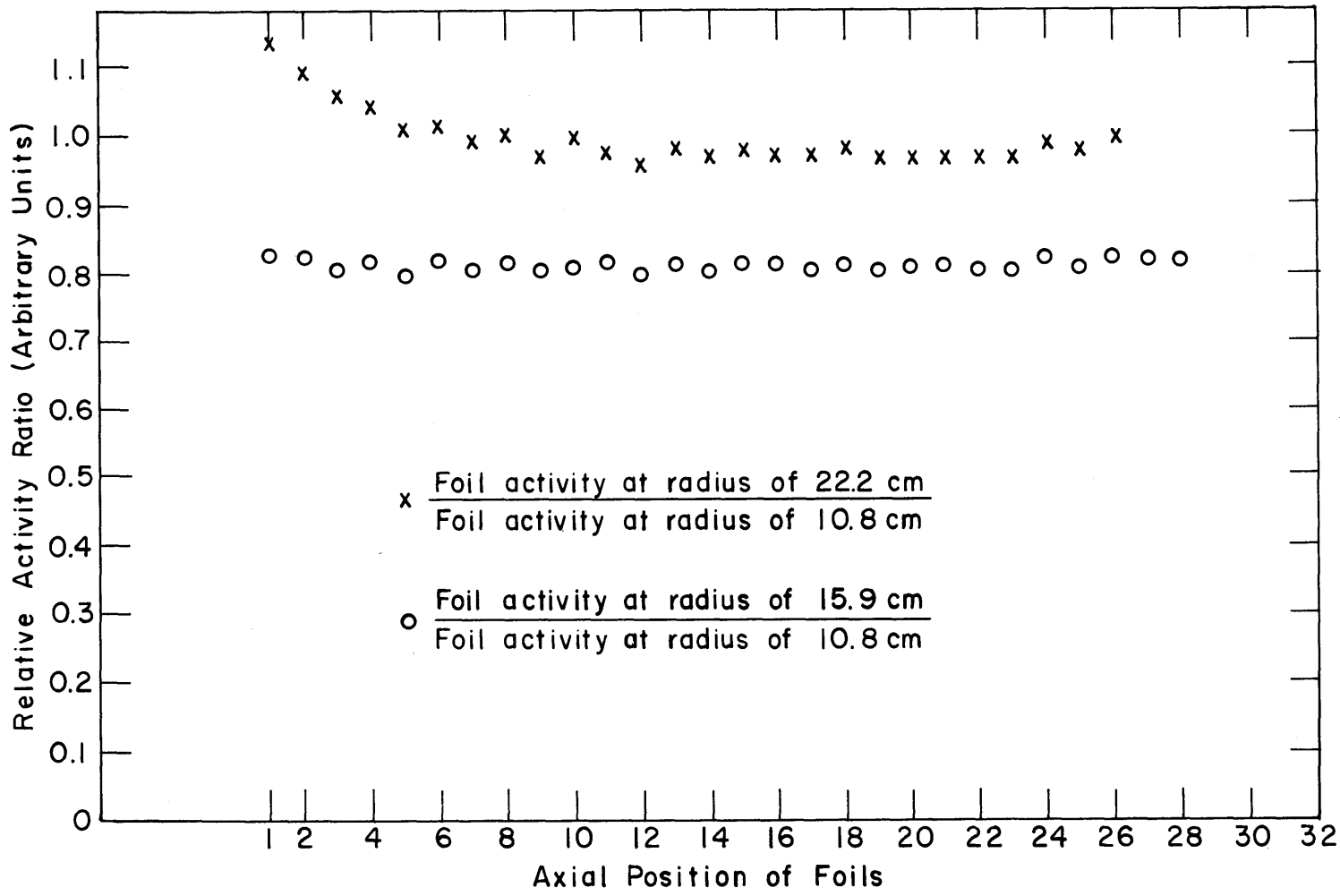

FIG. 4.1 RATIOS OF CORRESPONDING (SAME HEIGHT) FOIL ACTIVITIES FROM 3 AXIAL TRAVERSES AT DIFFERENT RADII AROUND A ONE INCH DIAMETER, NATURAL URANIUM ROD IN HEAVY WATER

These are the parameters needed to produce a consistent theory, as discussed in section 4.1.2.

Using the boundary condition that the net current into the fuel element should equal the number of neutrons absorbed there:

$$\lim_{u\to 0} 2\pi u \frac{d\phi}{du} = \frac{J_{rod}}{D} , \tag{4.4}$$

Eq. 4.3 may be integrated from zero to r to get:

$$-r\left(\frac{J_{rod}}{D}\right) + \left(\eta\epsilon P \frac{J_{rod}}{D}\right) \int_0^r dw \int_0^w 2\pi u\, G(u)\, du$$

$$= 2\pi \int_0^r \phi(w)\, dw - 2\pi r\phi(r) - 2\pi(\gamma^2-\kappa^2) \int_0^r dw \int_0^w u\phi(u)\, du . \tag{4.5}$$

Equation 4.5, with r set equal to the values of the radii at which the various measurements were made, is used to obtain $\frac{J_{rod}}{D}$ and $(\eta\epsilon P)\frac{J_{rod}}{D}$ by means of a least-squares fit to the data at the various radii. For this purpose, a computer program, ØNE-RØD, has been written for the IBM 7094 at the M.I.T. Computation Center. The code calculates the right-hand side of Eq. 4.5 from the experimental data and uses the age theory line source kernel to evaluate the double integral on the left-hand side. The inexactness of the age theory kernel appears as a variation in the values of $\eta\epsilon P$ and J_{rod}/D, depending upon the number and position of the data points used in the fit. Figure 4.2 shows the typical variation of the output values of these quantities as the outermost radial data points are successively dropped. If the kernel were correct, the values of $\eta\epsilon P$ and J_{rod}/D would be independent of the number of points used in the fit. The large values of $\eta\epsilon P$ result from using in the fit only a few data points near the rod. These large values are found because the age theory kernel for a line source is a poor representation of the slowing-down density in the immediate vicinity of a real fuel rod of finite radius. It may be seen from Fig. 4.2 that the values of J_{rod}/D are less sensitive to inaccuracies in the kernel than are the values of $\eta\epsilon P$. Values of J_{rod}/D needed for the calculation of the value of the single element parameter Γ were obtained as an average of the values

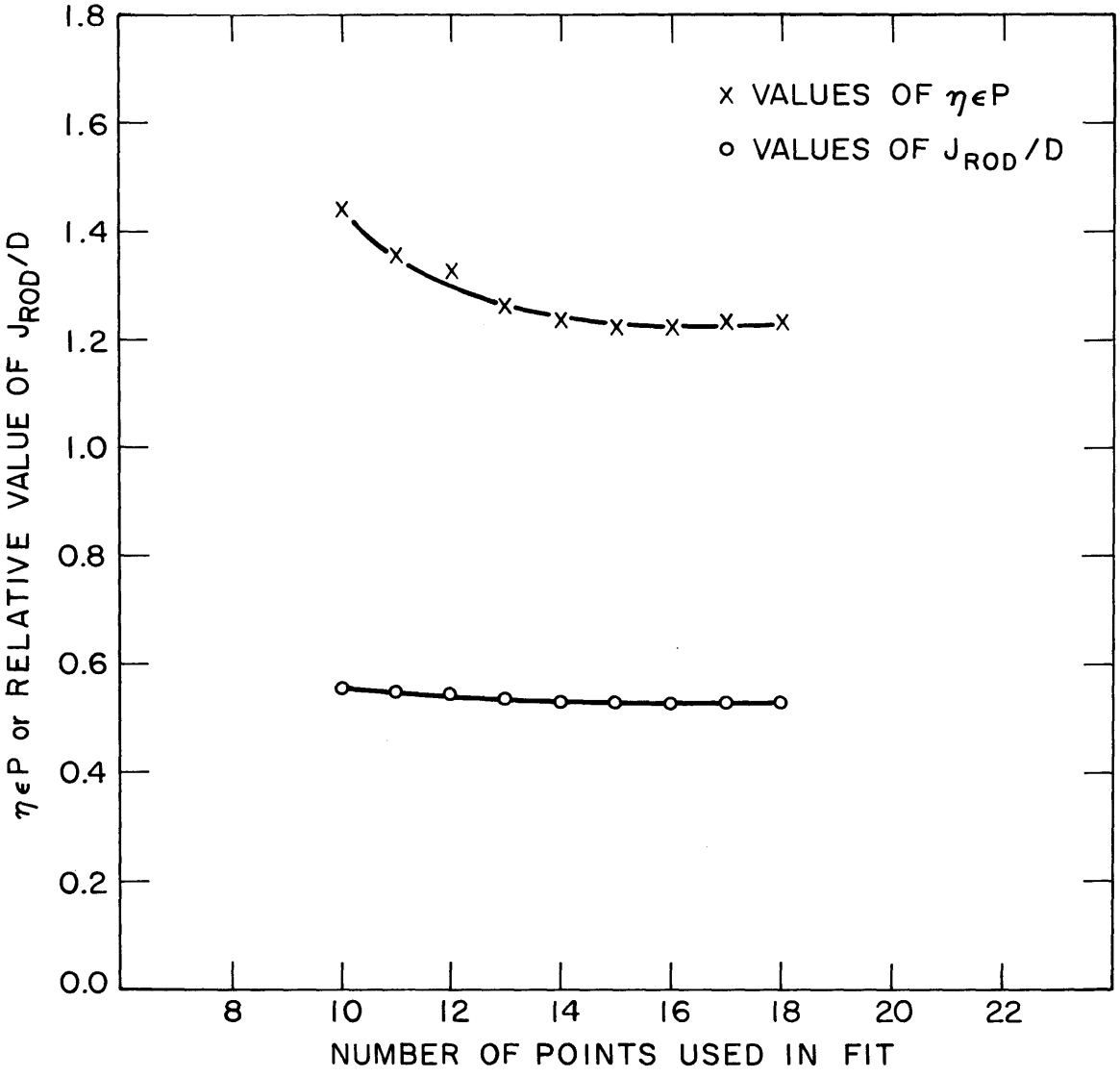

FIG. 42 VALUES OF $\eta\epsilon P$ AND J_{ROD}/D AS FUNCTIONS OF THE NUMBER OF POINTS USED IN FITTING THE DATA (1.010 INCH DIAMETER NATURAL URANIUM ROD IN D_2O)

of J_{rod}/D resulting from using ten through eighteen points in the fit.

The same data used to obtain the current, J_{rod}, into the rod are also used to obtain ϕ_o, the effective flux at the rod center. For this purpose, the flux around the rod must be presented in a manner which facilitates its extrapolation back to the center of the rod. The shape of the flux in space is complicated not only by the absorption in the rod but also by radial leakage from the side of the exponential assembly. The latter complication is easily avoided by dividing the relative values of the flux by $J_o(ar)$, the asymptotic flux shape far from the rod in the presence of radial leakage. This procedure effectively removes the complications caused by the leakage, and the result is found to be a straight line over a large fraction of the radial extent. Figure 4.3 shows a typical example of this behavior. Absorption in the rod causes the values to fall below the straight line near $r = 0$. Edge effects at the side of the exponential tank cause the measured values to rise above the straight line at large radii. The nonzero slope of the straight line is caused by the spatial nonuniformity of the slowing-down source into the subcadmium energy region. The value of the slope is related to strength of the fast neutron source in the single fuel rod, but no quantitative relation between the two has been developed.

It is now easy to avoid the flux dip at the rod and to obtain the value of ϕ_o by extrapolating the straight line back to $r = 0$. This has been done by fitting a straight line by a least-squares procedure to the points resulting when the measured subcadmium activities are divided by $J_o(ar)$:

$$\frac{A(r)}{J_o(ar)} = c_o + c_1 r . \tag{4.6}$$

To eliminate the flux dip around the rod, points near the rod are dropped until the resulting straight line exhibits minimum variance of fit. The constant term in the resulting equation of the form of Eq. 4.6 is then identified as the relative value of ϕ_o, since it is the value the activity would have at the center in the absence of the flux dip:

$$\phi_o = [A(0)]_{\substack{no \\ flux\ dip}} = J_o(0)c_o = c_o . \tag{4.7}$$

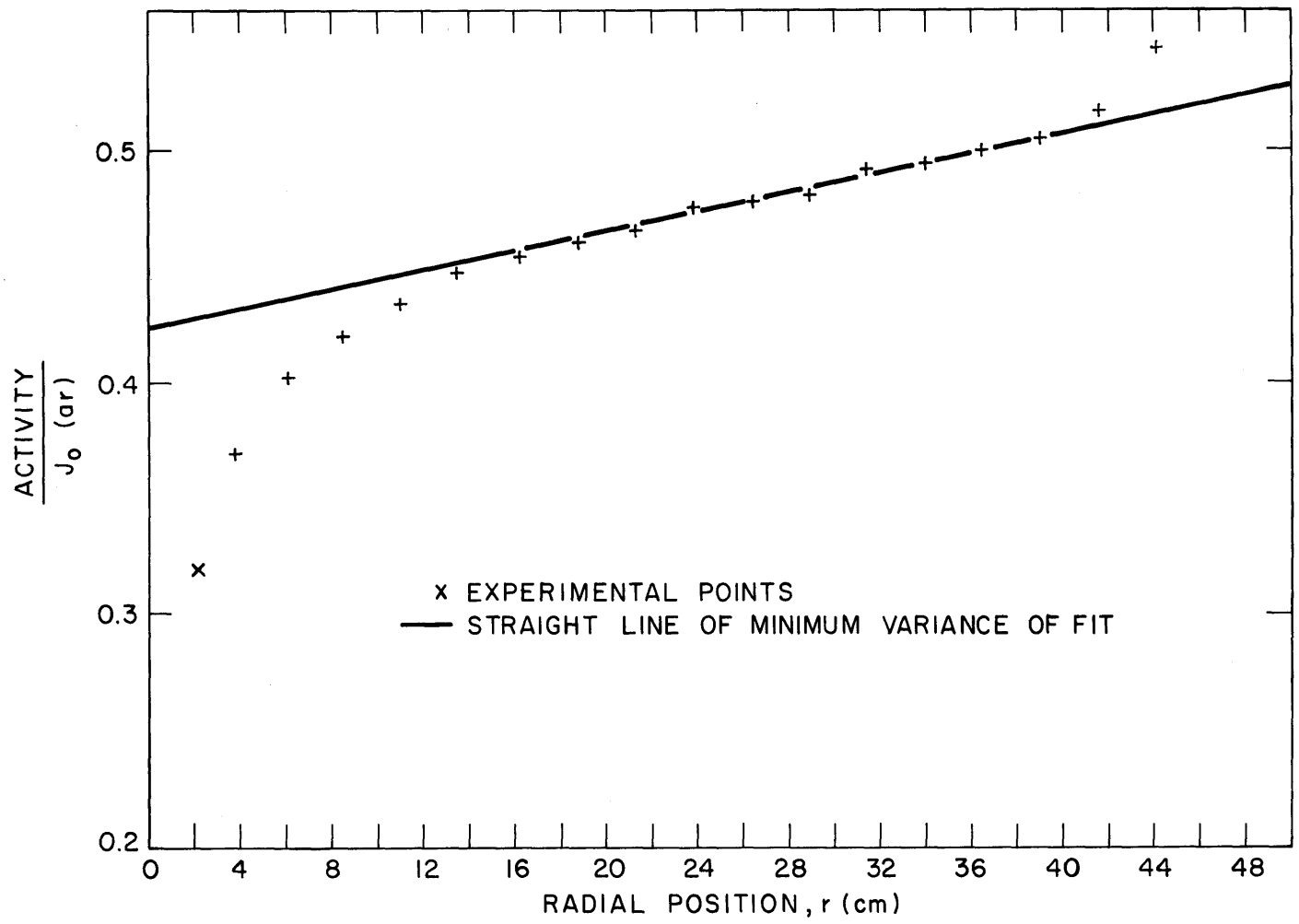

FIG. 4.3 RELATIVE VALUES OF Au^{198} ACTIVITY DIVIDED BY $J_0(ar)$ AS A FUNCTION OF RADIAL POSITION (1.010 INCH DIAMETER NATURAL URANIUM ROD IN D_2O)

Because the relative values of J_{rod} and ϕ_o are both determined from the same set of data, the constant of proportionality is the same in both, and their quotient yields the absolute value of Γ.

4.2.2 The Relationship Between the Thermal Utilization, f, and the Single Rod Parameter, Γ

Consider a line source of fast neutrons, normalized to one fast neutron per unit length, in an infinite sea of moderator. The equation describing the thermal flux, ϕ, is:

$$D\nabla^2\phi - \Sigma_{aM}\phi + G = 0, \tag{4.8}$$

where Σ_{aM} and D refer to the moderator. Since this equation describes the "effective" flux which would exist if there were no fuel rod sinks in the system, all the neutrons will eventually be absorbed in the moderator. Let Γ have the definition used in this work, the ratio of "effective thermal flux" at the center of an element to the net current of thermal neutrons into the element. The net current is identical to the absorption rate of thermal neutrons in the element. Then the thermal utilization of a lattice of fuel elements in this moderator is:

$$f = \frac{\text{absorptions in all fuel elements}}{\text{absorptions in all fuel elements + absorptions in moderator}}. \tag{4.9}$$

The flux is calculated from Eq. 4.8, which describes the case in which no fuel elements are present in the infinite sea of moderator. All the neutrons supplied by the source G are therefore absorbed in the moderator, so if G is normalized to one source neutron per second, the moderator absorption is unity. The parameter Γ is the ratio of the thermal flux existing at the center of the element to the thermal absorption rate in the element. This flux is exactly that given by Eq. 4.8, so the expression for the thermal utilization, Eq. 4.9, becomes:

$$f = \frac{\frac{1}{\Gamma}\sum_i \phi(r_i)}{1 + \frac{1}{\Gamma}\sum_i \phi(r_i)}, \tag{4.10}$$

(since the source is normalized to unity). Here, ϕ_i is defined as the value of the flux at the center of the i^{th} fuel element. Equation 4.10 provides the relationship between f and Γ when the summations are evaluated using Eq. 4.8 to determine the various $\phi(r_i)$. The sums are evaluated with the aid of the Poisson summation formula given in Chapter II:

$$\sum_n \sum_m \phi(an, bm) = \frac{1}{A_c} \sum_p \sum_q \bar{\phi}\left(\frac{2\pi p}{a}, \frac{2\pi q}{b}\right), \tag{4.11}$$

where a and b are the dimensions of the unit cell, $\bar{\phi}$ is the two-dimensional Fourier transform of ϕ with transform variables $2\pi p/a$ and $2\pi q/b$, and A_c is the area of a unit cell. $\bar{\phi}$ is easily calculated by taking the transform of Eq. 4.8. Using the age theory kernel for G, one obtains:

$$\sum_n \sum_m \phi(an, bm) = \frac{1}{A_c} \sum_p \sum_q \frac{\exp\left\{4\pi^2\left(\frac{p^2}{a^2} + \frac{q^2}{b^2}\right)\tau\right\}}{4\pi^2\left(\frac{p^2}{a^2} + \frac{q^2}{b^2}\right) + \Sigma_{aM}} . \tag{4.12}$$

In most reactor lattices:

$$2\pi\sqrt{\tau} \geq a \text{ or } b, \tag{4.13}$$

so that only the p=q=0 term is significant. The result of the summation is:

$$\sum_n \sum_m \phi(an, bm) = \frac{1}{\Sigma_{aM} A_c} . \tag{4.14}$$

The relationship given by Eq. 4.10 between f and Γ now becomes:

$$f = \frac{\frac{1}{\Gamma A_c \Sigma_{aM}}}{1 + \frac{1}{\Gamma A_c \Sigma_{aM}}}, \tag{4.15}$$

$$\frac{1}{f} = 1 + \Gamma A_c \Sigma_{aM} . \tag{4.16}$$

This is the desired relation between Γ and f. It differs from that derived by Feinberg and Galanin in having Γ where their relation has $(\Gamma'+C_1)$, C_1 being a number dependent upon the fuel to cell volume ratio. Equation 4.16 has been derived here by using the Poisson summation, but it can equally well be derived by using the Wigner-Seitz formalism. It is only necessary to make the same assumption used in reducing the Poisson summation to a tractable form — that both dimensions of the cell are much smaller than 2π times the slowing-down length, so that the slowing-down density is essentially constant across any unit cell. The slope of the thermal flux is zero at the cell boundary and, since ϕ is computed as before with no sink rod present in the cell, it follows that ϕ is constant:

$$\phi = \frac{\text{slowing-down density}}{\Sigma_{aM}} = \frac{1}{A_c \Sigma_{aM}} . \tag{4.17}$$

The thermal utilization is defined as before:

$$f = \frac{\text{fuel absorption}}{\text{fuel absorption + moderator absorption}} , \tag{4.18}$$

except that now the definition is on the basis of a unit cell. The result is:

$$f = \frac{\frac{\phi}{\Gamma}}{1 + \frac{\phi}{\Gamma}} , \tag{4.19}$$

or:

$$\frac{1}{f} = 1 + \Gamma \Sigma_{aM} A_c . \tag{4.20}$$

The result is the same as was obtained before, but this derivation gives some clue to why the formula for f differs from that of Feinberg and Galanin. Their parameter Γ' accounts for the thermal flux dip at the fuel element, so that their formula for f must somewhere include an effective disadvantage factor, which depends on the volume fraction of fuel. In the present formulation, however, an effective flux is used which is constant throughout the cell, and so the disadvantage factor exhibits no dependence on the volume fractions. It was pointed out in

section 4.1.2 that either formulation is correct, provided the equation used to relate f and Γ is consistent with the definition of Γ.

4.3 EXPERIMENTAL RESULTS – VALUES OF Γ

Values of the single rod parameter Γ are given in Table 4.1 for the fuel elements investigated in this work. The values have been obtained by means of the procedures of section 4.2. The uncertainties given in parentheses are the observed standard deviations of the mean of several independent determinations.

Table 4.1

Values of the Parameter Γ
for Slightly Enriched Uranium Rods in Heavy Water

Rod Diameter (Inches)	Rod Enrichment (Wt. %)	Γ (cm^{-1})	Number of Determinations
0.25	1.14	8.15 ± 1.21	4
0.25	1.03	7.73 ± 0.87	2
0.75	0.947	1.85 ± 0.04	2
1.00	0.711	1.25 ± 0.12	4

Each value of Γ presented here is peculiar not only to the fuel element used, but also to the moderator used. The latter dependence arises because of the definition of Γ. In Feinberg's original formulation, Γ' was defined as the ratio of the actual thermal flux at the rod surface to the net current into the rod. As long as diffusion theory was used, this Γ' could be calculated in terms of only the properties of the fuel element because the diffusion equation describing the conservation of neutrons within the rod is a second-order differential equation whose solution involves two constants. These are determined by the conditions that the total absorption in the rod be equal to the net current into the rod and that the flux at the surface be ϕ_o.

The parameter Γ defined by Klahr (and used here) refers explicitly to events occurring in the moderator, and thus its value depends upon the particular moderator used. One of the compensations for this choice is that there is no longer any need to decide just what constitutes the "surface" of a fuel element, a question that is both important and difficult to answer for elements having a complex geometric shape or containing moderator internally. Even if the surface of the fuel element is well defined, measurements of the flux at the surface are difficult to make because of the large flux gradient at the surface of the element.

If higher-order approximations than diffusion theory were used, Feinberg and Galanin's original definition would also depend on the properties of the moderator. This comes about because more boundary conditions would be needed to determine the flux distribution within the fuel element, and these are equivalent to specifying the details of the angular dependence of the flux at the surface of the fuel element. This angular dependence is a function of the moderator used.

4.4 INFERRED VALUES OF THE THERMAL UTILIZATION AND DISCUSSION

Equation 4.16 has been used to compute thermal utilizations from the values of Γ in Table 4.1.

Values of the macroscopic absorption cross section of the moderator have been obtained from the THERMØS code (H4) and are listed in Table 4.2. These values are smaller than the values computed for a Maxwellian spectrum at the temperature of the moderator (20°C to 25°C). In Table 4.3, the values of the thermal utilization obtained by the present method are compared with values obtained from THERMØS. The THERMØS values are taken as standard because the subcadmium flux profiles obtained from THERMØS are in excellent agreement with the experimental results. It is evident that the method presented here is adequate to determine the thermal utilization to at least 0.5 percent for uniform lattices consisting of single rods in heavy water.

The present method, like all techniques for determining values of the thermal utilization, requires that the absorption cross section of the moderator be known. In contrast to other techniques, however, it does

Table 4.2

Geometric and Nuclear Parameters Used in Calculation of the Thermal Utilization

Concentration of U-235 in the Rod (Wt. %)	Diameter of Rods (Inches)	Lattice Spacing (Inches)	Volume Fraction of Fuel	Macroscopic Absorption Cross Section of Moderator* Σ_{aM}	Volume of Unit Cell Per Unit Height (cm^2)
1.14	0.25	1.25	0.03628	0.914×10^{-4}	8.729
		1.75	0.01851	0.971	17.11
		2.50	0.009069	1.082	34.92
1.03	0.25	1.25	0.03628	0.917	8.729
		1.75	0.01851	0.975	17.11
		2.50	0.009069	1.007	34.92
0.947	0.75	2.50	0.0816	1.016	34.92
		3.50	0.0416	1.108	68.42
		5.00	0.0204	1.162	139.64
0.711	1.00	4.50	0.04571	0.642	113.13
		5.00	0.03702	0.654	139.68
		5.75	0.02799	0.667	184.73

*From THERMØS

Table 4.3

Values of the Thermal Utilization† for Lattices of Slightly Enriched Uranium Rods in Heavy Water

Concentration of U-235 in Rod (Wt. %)	Rod Diameter (Inches)	Lattice Spacing (Inches)	Value of the Thermal Utilization†		Percentage Difference**	
			From Eq. 4.17*	From THERMØS	In f	In (1-f)
1.14	0.25	1.25	0.9935	0.9927	0.08	11
		1.75	0.9866	0.9852	0.14	9
		2.50	0.9701	0.9673	0.29	9
1.03	0.25	1.25	0.9939	0.9923	0.16	21
		1.75	0.9873	0.9844	0.29	19
		2.50	0.9735	0.9678	0.59	18
0.947	0.75	2.50	0.9935	0.9947	0.13	23
		3.50	0.9861	0.9884	0.23	20
		5.00	0.9708	0.9748	0.41	16
0.711	1.00	4.50	0.9910	0.9911	0.01	1
		5.00	0.9887	0.9890	0.03	3
		5.75	0.9848	0.9847	0.01	1

* Obtained from Eq. 4.16 with the values of Γ from Table 4.1 and cross sections from Table 4.2.

** From the THERMØS values.

† Including the cladding with the fuel.

not require that the absorption cross section of the fuel be known, since this absorption rate is contained implicitly in Γ. This circumstance lessens the need for an accurate calculation of hardened thermal group cross sections, since the spectrum is usually much less hardened in the moderator than in the fuel. This is illustrated by Table 4.4 which lists some values of the effective temperature increase (obtained from THERMØS calculations) for the lattices studied here. The effective temperature is defined here as the temperature of that Maxwellian distribution which yields the same thermal absorption cross section as that obtained from THERMØS. Because the values of the thermal utilization in heavy water lattices are near unity, an error of x percent in the moderator absorption, 1 - f, becomes an error of about x(1-f) percent in f. For these reasons, a simple estimate of the spectral hardening in the moderator should be sufficiently accurate in calculating f by

Table 4.4
Comparison of Average Neutron Temperature* Increases in Fuel and Moderator

Concentration of U-235 in Fuel Rod (Wt. %)	Lattice Spacing (Inches)	Moderator ΔT (°C)	Fuel ΔT (°C)
0.947	2.50	128	208
	3.50	61	132
	5.00	26	93
1.143	1.25	88	119
	1.75	44	73
	2.50	21	49
1.027	1.25	85	114
	1.75	42	69
	2.50	21	46

*Temperature differences are relative to physical temperature of moderator and were obtained from THERMØS.

this technique. For example, an error of 10 percent in the moderator absorption cross section leads to an error of only 0.2 percent in thermal utilization when f is about 0.98 .

4.5 APPLICABILITY TO OTHER MODERATORS

The conceptual basis of the method presented here can be applied to other moderators as well as to heavy water. Its practical value depends upon the extent to which errors in the measurement of Γ are affected by the properties of the moderator and upon the extent to which errors in Γ will affect the values of the thermal utilization in various moderators.

Table 4.1 shows that Γ has been determined to better than about 12 percent in most cases. As the thermal utilization decreases, Γ must be known with increasing accuracy in order to retain a given accuracy in f. Table 4.5 shows the standard deviation in Γ which will yield 0.5 percent standard deviation in f (assuming no other uncertainties). It is evident that the observed values of the standard deviations in the Γ's reported here are consistent with the observed inaccuracies in the values of the thermal utilization derived therefrom and shown in Table 4.3. If the uncertainty in Γ can be reduced by a factor of five (to about 2.5 percent), then it should be possible to obtain the thermal utilization to within 0.5 percent for many lattices in graphite and most lattices of fuel clusters in heavy water.

Table 4.5

Accuracy Required in the Parameter Γ to Attain a Given Accuracy in the Value of the Thermal Utilization

Thermal Utilization, f	Standard Deviation of Γ for 0.5% Accuracy in f	Standard Deviation of Γ for 0.25% Accuracy in f
0.98	25%	12%
0.90	4.5	2.3
0.85	2.8	1.4
0.80	2.0	1.0
0.75	1.5	0.7

Because the determination of Γ requires considerable analysis of the raw data, the uncertainty in its final value reflects not only experimental but also theoretical uncertainties. Most of these uncertainties appear in J_{rod} which is evaluated (from Eq. 4.4) as the small difference between two large numbers.

The experimental contributions to this uncertainty arise from uncertainties in the activities of the foils (because of the statistical nature of radioactive decay), from inaccuracies in the positioning of the foils on the holder, and from inaccuracies in the positioning of the holder relative to the fuel element. Their effects are difficult to assess analytically because of the complicated relation between J_{rod} and the observed activities. All foils gave at least 40,000 counts and corrections for epicadmium activation were only a few percent of the total activity, so that the standard deviation of the net count for each foil was, at most, 0.5 percent, and usually less. If necessary, it can be further reduced by accumulating a larger number of total counts for each foil. Such uncertainties, therefore, are not a limiting factor in the determination of Γ. Errors in positioning can be minimized by careful design and experimental procedures. It is particularly important to keep the foil holder horizontal, since a tilted holder introduces spurious flux gradients which affect the calculation of J_{rod}. It should be possible to position the foils more accurately and more reproducibly in a solid moderator than in water, thus reducing the experimental contribution to the uncertainty in Γ.

The theoretical uncertainty arises in the choice of a slowing-down kernel, G, for use in Eq. 4.4. The age theory kernel used in this report provides only a fair representation of the spatial distribution of the slowing-down density in heavy water, whereas in graphite, it is a good approximation. The error in Γ incurred by the use of age theory should thus be much smaller for graphite than for heavy water.

On the basis of this discussion, it is concluded that the method discussed here has a high probability of being useful in graphite as well as in heavy water. The use of graphite requires greater accuracy in the determination of Γ, but in graphite, both the experimental and theoretical situations are conducive to attaining the increased accuracy.

It is not clear whether the method presented here will yield good results in light water. The small values of the slowing-down and diffusion lengths in light water will increase the experimental difficulties. The question can only be settled by an actual experiment.

The method presented here is expected to apply equally well to fuel elements consisting of clusters of individual fuel rods. The flux distribution in the moderator around such an element depends on the azimuthal angle considered, but this azimuthal dependence should be negligible at distances beyond a scattering mean-free path (about one inch in D_2O and C) from the element. Since the present method employs the flux in the moderator at distances beyond a mean-free path, the use of clustered fuel elements requires no new techniques. The impedance analogy from electronics is again applicable here. Just as a complex circuit, when viewed from a particular set of terminals, may be representable by a single impedance, so a complex, clustered fuel element, when viewed from the moderator, may be represented by a single parameter Γ.

Chapter V

THE USE OF EXPERIMENTS ON A SINGLE FUEL ELEMENT TO INFER CADMIUM RATIOS IN LATTICES

5.1 INTRODUCTION

5.1.1 Purpose and Importance of This Section of the Investigation

The values of the ratios of epicadmium to subcadmium reaction rates in a reactor lattice are of interest for at least two reasons. First, quantities of practical importance, such as the multiplication factor for an infinite lattice and the initial conversion ratio, may be expressed in terms of these ratios (W12). Second, the values of the ratios depend on the flux spectrum in the reactor, and the ability of a theoretical model to predict such ratios is a measure of the adequacy of the model for treating other similar problems. The method explained here makes it possible to obtain values of the ratios by making a theoretical interpretation of the results of an experiment on a single fuel element. The method is of particular interest because it not only produces accurate values of the ratios but also shows how they depend in a simple way on the various parameters of the lattice. The latter property of the method facilitates the interpolation and extrapolation of measured values of the ratios.

The ratios of interest, ρ_{28}, δ_{25}, and C^*, are:

$$\rho_{28} \equiv \frac{\text{average epicadmium } U^{238} \text{ capture rate in fuel}}{\text{average subcadmium } U^{238} \text{ capture rate in fuel}},$$

$$\delta_{25} \equiv \frac{\text{average epicadmium } U^{235} \text{ fission rate in fuel}}{\text{average subcadmium } U^{235} \text{ fission rate in fuel}},$$

$$C^* \equiv \frac{\text{average total } U^{238} \text{ capture rate in fuel}}{\text{average total } U^{235} \text{ fission rate in fuel}}.$$

5.1.2 Methods Used

The techniques of Chapter II are used to evaluate the ratios by choosing an appropriate kernel and summing the fluxes originating from all fuel elements in the system. Since epithermal events, such as resonance capture or fission, typically involve neutrons of several different energies, and since the proportion of neutrons involved at each energy depends on the particular process considered, it is desirable to determine the kernel experimentally. This is the principal purpose of the single element experiment, in which the relative activity resulting from a particular absorption process is measured at various distances from the single element. The kernel so obtained may be applied to lattices insofar as the slowing-down properties of the moderator are unaffected by the presence of the additional fuel rods comprising the lattice. This is an excellent approximation in the heavy water lattices studied at M. I. T. because the volume fraction of fuel is usually less than five percent in these lattices, and above 100 kev the slowing-down properties of uranium are quite similar to those of heavy water. Because the volume fraction of fuel is usually small in graphite-moderated reactors, the same method is expected to give good results in graphite-moderated reactors, too. Furthermore, it was shown in Chapter II that, under certain conditions, the slowing-down density in a large uniform reactor is independent of the particular kernel describing the slowing-down process. Thus, it should be possible to apply the same technique to many uniform reactors moderated by light water, even though the kernel may be known only approximately because it depends upon the lattice spacing.

5.2 THEORY

5.2.1 Assumptions

(1) It is assumed that throughout the intermediate energy region the flux per unit energy, $\phi(E)$, and the slowing-down density, $q(E)$, are related by:

$$\phi(E) = \frac{q(E)}{\xi \Sigma_s E} . \qquad (5.1)$$

This assumption is used to normalize the relative absorption rates around the single element in order to obtain the absorption rate per source neutron. The normalization requirement is that the integral over all space of the slowing-down density around the single element must equal the number of source neutrons produced in the element.

(2) It is assumed that the kernel measured around the single element is a good approximation to the infinite medium kernel. This is true if the measurement is made in a system much larger than the characteristic dimension of the slowing-down kernel.

5.2.2 Derivation of the Formulas for the Ratios

These assumptions will now be used in a detailed derivation of the formula for ρ_{28} in a large, uniform lattice. The derivations of formulas for δ_{25} and C^* are similar and will be discussed only insofar as they differ from the development of the formula for ρ_{28}.

Nomenclature

$T(\vec{r}_i)$ ≡ subcadmium absorption rate per unit length in a fuel element at $\vec{r}_i$ normalized to unity at the fuel element of interest.

$Q'(\vec{r}, \vec{r}_i, E)$ ≡ the slowing-down density past energy E at position $\vec{r}$ per unit fission neutron created at $\vec{r}_i$; this is the finite medium kernel, which is a function of the vectors $\vec{r}$ and $\vec{r}_i$.

$Q(|\vec{r} - \vec{r}_i|, E)$ ≡ the slowing-down density past energy E at position $\vec{r}$ per unit fission neutron created at $\vec{r}_i$ when the medium is extended to infinity; this is the infinite medium kernel, which is a function of the scalar distance $|\vec{r} - \vec{r}_i|$.

A_{epi} ≡ epicadmium absorption rate in U^{238} per unit length in the fuel element of interest.

N_{28} ≡ number density of U^{238} atoms in the fuel elements.

$\eta\epsilon(\vec{r}_i)$ ≡ net number of fast neutrons produced per subcadmium absorption in the fuel element at $\vec{r}_i$.

$V_F \equiv$ volume of a fuel element per unit length.

$V_c \equiv$ volume of a unit cell per unit length.

$q(\vec{r}, E) \equiv$ slowing-down density at $\vec{r}$ past energy E.

$E_c \equiv$ cadmium cutoff energy.

$\sigma^{28}_{1/v}(E) \equiv$ 1/v component of the microscopic U^{238} absorption cross section.

$\sigma^{28}_{Res}(E) \equiv$ resonance component of microscopic U^{238} absorption cross section.

$\sigma^{28}_{o} \equiv$ 2200 m/sec value of $\sigma^{28}_{1/v}(E)$.

$A_{sub} \equiv$ subcadmium absorption rate in U^{238} per unit length in the fuel rod of interest.

The slowing-down density at $\vec{r}$ is the sum of the slowing-down densities from all the fission sources (i.e., all the fuel elements) in the system:

$$q(\vec{r}, E) = \sum_{i=1}^{\text{number of elements in system}} Q'(\vec{r}, \vec{r}_i E)\, \eta\epsilon(\vec{r}_i)\, T(\vec{r}_i)\,. \tag{5.2}$$

As shown in Chapter II, the finite medium kernel Q' may be replaced by the infinite medium kernel Q if the sum is extended over an infinite system:

$$q(\vec{r}, E) = \sum_{i=1}^{\infty} Q(|\vec{r} - \vec{r}_i|, E)\, T(\vec{r}_i)\, \eta\epsilon(\vec{r}_i)\,. \tag{5.3}$$

The U^{238} activity resulting from epicadmium absorptions is:

$$A_{epi}(\vec{r}) = \int_{E_c}^{\infty} \phi(\vec{r}, E)\, N_{28} V_F \{\sigma^{28}_{1/v}(E) + \sigma^{28}_{Res}(E)\}\, dE, \tag{5.4}$$

which may be related to the slowing-down density by assumption (1), with the result:

$$A_{epi}(\vec{r}) = N_{28} V_F \eta\epsilon \int_{E_c}^{\infty} \sum_{i=1}^{\infty} \frac{Q(|\vec{r} - \vec{r}_i|, E)\, T(\vec{r}_i)}{\xi \Sigma_s E} \left\{\sigma_{1/v}^{28}(E) + \sigma_{Res}^{28}(E)\right\} dE. \tag{5.5}$$

It has been assumed that the lattice is uniform, so that $\eta\epsilon$ is not a function of position and may therefore be removed from the summation.

It was shown in Chapter II that if the spacing between fuel rods is small enough so that the fractional change in Q over the length of one unit cell is always small, then:

$$\sum_{i=1}^{\infty} Q(|\vec{r} - \vec{r}_i|, E)\, T(\vec{r}_i) \approx \frac{P}{V_c}, \tag{5.6}$$

where P is the nonleakage probability from fission to energy E. Then if an average value of P is used:

$$A_{epi} = \eta\epsilon \frac{N_{28} V_F P}{V_c} \int_{E_c}^{\infty} \frac{\left\{\sigma_{1/v}^{28}(E) + \sigma_{Res}^{28}(E)\right\}}{\xi \Sigma_s E} dE. \tag{5.7}$$

For most moderators, $(\xi\Sigma_s)$ in the resonance region is independent of energy, so:

$$A_{epi} = \frac{\eta\epsilon N_{28} V_F P}{\xi \Sigma_s V_c} \int_{E_c}^{\infty} \left\{\sigma_{1/v}^{28}(E) + \sigma_{Res}^{28}(E)\right\} \frac{dE}{E}. \tag{5.8}$$

The integral in Eq. 5.8 has been evaluated by Weitzberg (W10) with $E_c = 0.4$ ev:

$$\int_{E_c}^{\infty} \left\{\sigma_{1/v}^{28}(E) + \sigma_{Res}^{28}(E)\right\} \frac{dE}{E} = 0.5\, \sigma_o^{28} + ERI^{28}. \tag{5.9}$$

In order to determine ρ_{28}, it is also necessary to calculate the subcadmium absorption in the fuel rod at $\vec{r}$. This is:

$$A_{sub} = \left(\frac{\Sigma_a^{28}}{\Sigma_a^{28} + \Sigma_a^{25}} \right)_{SC}, \tag{5.10}$$

where:

$$\left(\frac{\Sigma_a^{28}}{\Sigma_a^{28} + \Sigma_a^{25}}\right)_{SC}$$

is the ratio of the values of the cross sections averaged over the subcadmium spectrum in the fuel element. For simple types of fuel rods, it is adequate to average the cross sections over a Maxwellian distribution. Because the quantity of interest is a ratio, errors due to spectrum changes will tend to cancel. It follows that:

$$\rho_{28} \equiv \frac{A_{epi}}{A_{sub}} = \frac{\eta\epsilon P N_{28} V_F \{0.5\ \sigma_o^{28} + ERI^{28}\}}{\xi \Sigma_s V_c \left(\frac{\Sigma_a^{28}}{\Sigma_a^{25} + \Sigma_a^{28}}\right)_{SC}} . \qquad (5.11)$$

This must be modified slightly, as discussed below, to account for the competing effects of the various processes occurring.

The term representing 1/v absorption was derived under the assumption that the epithermal spectrum is P/E per fast source neutron. The 1/E dependence is a good approximation in a thermal reactor, but the magnitude must be multiplied by a correction factor to account for flux depletion due to resonance absorption in the U^{238}. In a 1/E spectrum, about 75 percent of the epicadmium 1/v absorption occurs between the cadmium cutoff (about 0.4 ev) and 6 ev, whereas the lowest resonance in U^{238} lies at 6.7 ev. It is therefore reasonable to assume that although the flux seen by the 1/v cross section is 1/E, its magnitude is reduced by a factor of p, the U^{238} resonance escape probability. To a first approximation, the magnitude of the correction factor is therefore assumed to equal p. The 1/v absorption in U^{238} is typically only a few percent of the resonance capture. This is evident if the magnitudes of the 0.5 σ_o^{28} and the ERI^{28} terms in Eq. 5.11 are compared. For rods of one-quarter-inch diameter, the 1/v capture in U^{238} is about eight percent of the resonance capture, so that this approximate correction should be adequate for most purposes.

It must also be recognized that neutrons absorbed in resonances have a nonleakage probability different from that of neutrons absorbed

in 1/v captures because these two events occur largely at different energies. Thus, the single nonleakage probability, P, should be replaced by a P_{Res} and a $P_{1/v}$. With these corrections, the formula for ρ_{28} becomes:

$$\rho_{28} = \frac{\eta\epsilon \frac{N_{28}V_F}{\xi\Sigma_s V_c}\{0.5\,\sigma_o^{28} P_{1/v} p + P_{Res} ERI^{28}\}}{\left(\frac{\Sigma_a^{28}}{\Sigma_a^{28} + \Sigma_a^{25}}\right)_{SC}} . \qquad (5.12)$$

A similar expression will now be derived for δ_{25}. In the same way that Eq. 5.8 was derived, the number of epicadmium fissions in U^{235} per subcadmium capture in the fuel element is

$$\frac{\eta\epsilon p N_{25} V_F P_{25}}{\xi\Sigma_s V_c} ;$$

the number of subcadmium fissions in U^{235} per subcadmium absorption in the fuel element is

$$\left(\frac{\Sigma_f^{25}}{\Sigma_a^{25} + \Sigma_a^{28}}\right)_{SC} .$$

The ratio of these two terms gives the formula for δ_{25}:

$$\delta_{25} = \frac{\eta\epsilon p \frac{N_{25}V_F P_{25}}{\xi\Sigma_s V_c} ERI^{25}}{\left(\frac{\Sigma_f^{25}}{\Sigma_a^{25} + \Sigma_a^{28}}\right)_{SC}} . \qquad (5.13)$$

Here, ERI^{25} is the resonance integral for fission in U^{235} and is defined to include both the smooth and resonance components of the fission cross section above the cadmium cutoff. The nonleakage probability for neutrons which cause epicadmium fission is denoted by P_{25}. As always, p denotes the probability of a neutron escaping resonance capture in

U^{238}. The use of p here is based on the assumption that most of the epicadmium fission in U^{235} occurs at energies below that of the lowest resonance in U^{238}. This is a reasonable assumption because the smoothly varying cross section for fission in U^{235} has a significant magnitude at energies just above the cadmium cutoff (about 0.4 ev) and so makes a large contribution to the fission resonance integral. As more data become available on the distribution in energy of the various contributions to ERI^{25}, it will become possible to develop more accurate expressions to use here in place of p.

The quantity C^* is defined as the ratio of the absorption in U^{238} to the fission in U^{235}. The epicadmium absorption in the U^{238} of the fuel rod per subcadmium absorption in the fuel rod is given by Eq. 5.8. The subcadmium absorption in the U^{238} of the fuel rod per subcadmium absorption in the fuel rod is

$$\left(\frac{\Sigma_a^{28}}{\Sigma_a^{28}+\Sigma_a^{25}}\right)_{SC}.$$

The fission in the U^{235} of the fuel rod per subcadmium absorption in the fuel rod is

$$\left(\frac{\Sigma_f^{25}}{\Sigma_a^{28}+\Sigma_a^{25}}\right)_{SC}(1+\delta_{25}).$$

In terms of these expressions, the ratio C^* is:

$$C^* = \frac{\left(\frac{\Sigma_a^{28}}{\Sigma_a^{28}+\Sigma_a^{25}}\right)_{SC} + \frac{\eta\epsilon V_F N_{28}}{\xi\Sigma_s V_c}\left[0.5\,\sigma_o p P_{1/v} + P_{Res}\,ERI^{28}\right]}{\left(\frac{\Sigma_f^{25}}{\Sigma_a^{28}+\Sigma_a^{25}}\right)_{SC}(1+\delta_{25})}. \qquad (5.14)$$

5.2.3 The Functional Dependencies of ρ_{28}, δ_{25}, and C^*

Equations 5.12 through 5.14 show that, for a fuel rod of fixed size, ρ_{28}, δ_{25}, and C^* vary linearly with the volume fraction of fuel in the cell. Strictly speaking, η, ϵ, and the cross-section ratios are also functions of the fuel rod spacing; ϵ because of the interaction contribution to fast fission in a lattice, and η and the cross-section ratios because the subcadmium spectrum depends on the fuel rod spacing. These variations are second-order effects in comparison with the change in volume fraction. The linear relationships have been noted in measurements of ρ_{28}, C^*, and δ_{25} at M. I. T. (M5) and in measurements of ρ_{28} at the Argonne National Laboratory (A4).

The linear relationships are important because they facilitate interpolation and because they provide a simple way of checking the consistency of experimental data. Figures 5.1 to 5.4 show that this linearity is found in many different kinds of lattices. This result is to be expected, since it was shown in Chapter II that, regardless of the particular kernel used, the $1/V_c$ term arises whenever the slowing-down density is essentially uniform across a unit cell. For uranium metal lattices in light water, the metal (fuel) to water ratio, V_F/V_{H_2O}, rather than V_F/V_c has been used as the abscissa. This accounts approximately for the variation of $\xi\Sigma_s$ with lattice spacing, a large effect in H_2O lattices. Since the fuel has no significant elastic slowing-down power, $\xi\Sigma_s$ of a unit cell is proportional to the volume fraction of moderator in the cell, V_{H_2O}/V_c. Thus, the term, $\frac{1}{\xi\Sigma_s}\frac{V_F}{V_c}$, in Eqs. 5.12 through 5.14 is proportional to V_F/V_{H_2O}. The data for Figs. 5.1 to 5.4 were taken from the references listed therein and were plotted in the linear form by the present author. The straight lines may be interpreted directly in terms of the quantities discussed in Chapter II. The intercept represents the value of the ratio of interest in a cell of infinite size; it is thus the "single element" component mentioned in Chapter II. The increase in the value of the ratio as the size of a unit cell is decreased results from the increased "lattice contribution" to the reaction rate. The near-linearity of the curves shown here illustrates the usefulness of the SEM treatment for obtaining experimentally

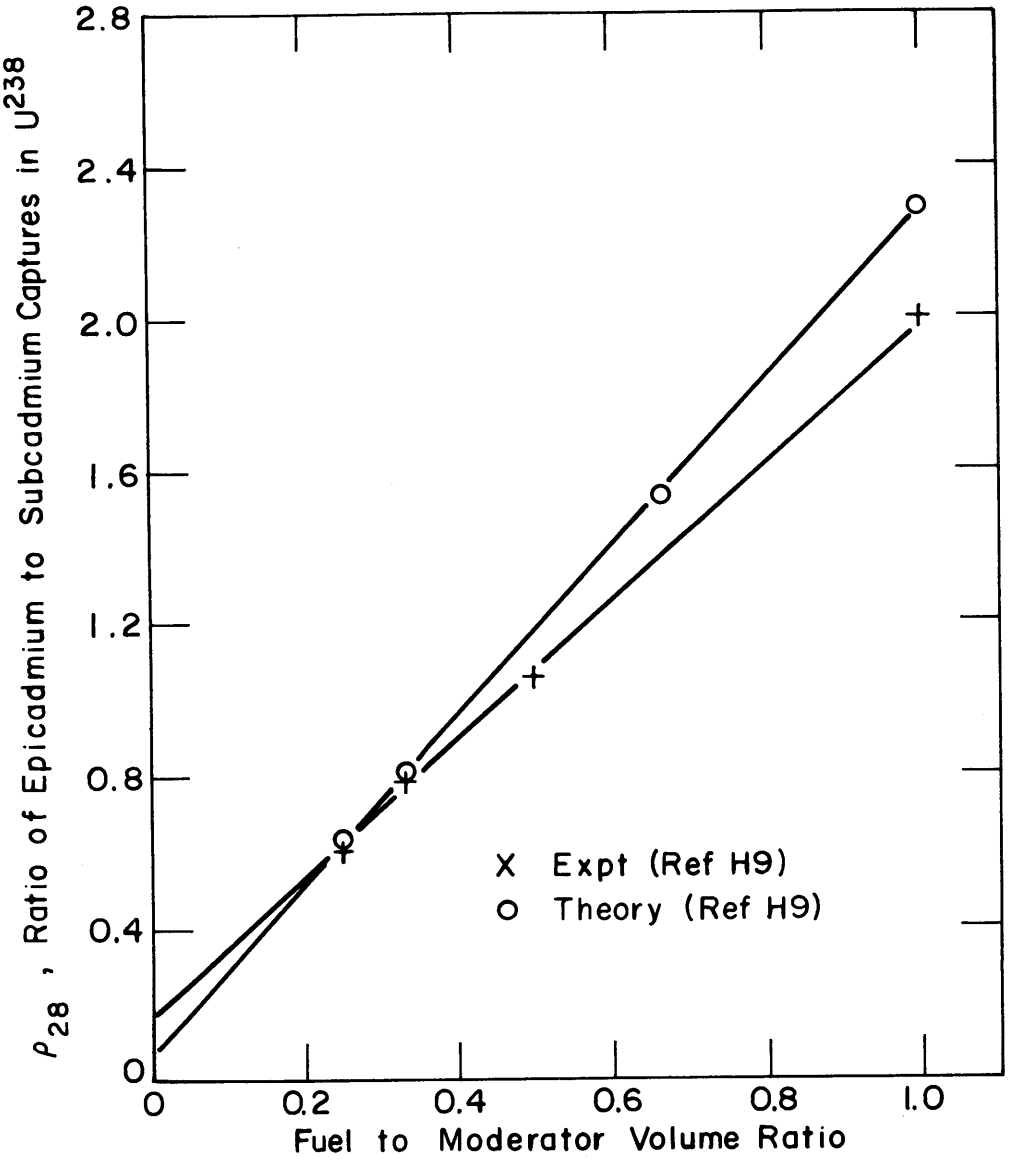

FIG. 5.1 THE RATIO, ρ_{28}, OF EPICADMIUM TO SUBCADMIUM CAPTURES IN U^{238} VS. FUEL TO MODERATOR VOLUME RATIO FOR 1.0% ENRICHED, 0.600" DIAM URANIUM RODS IN H_2O.

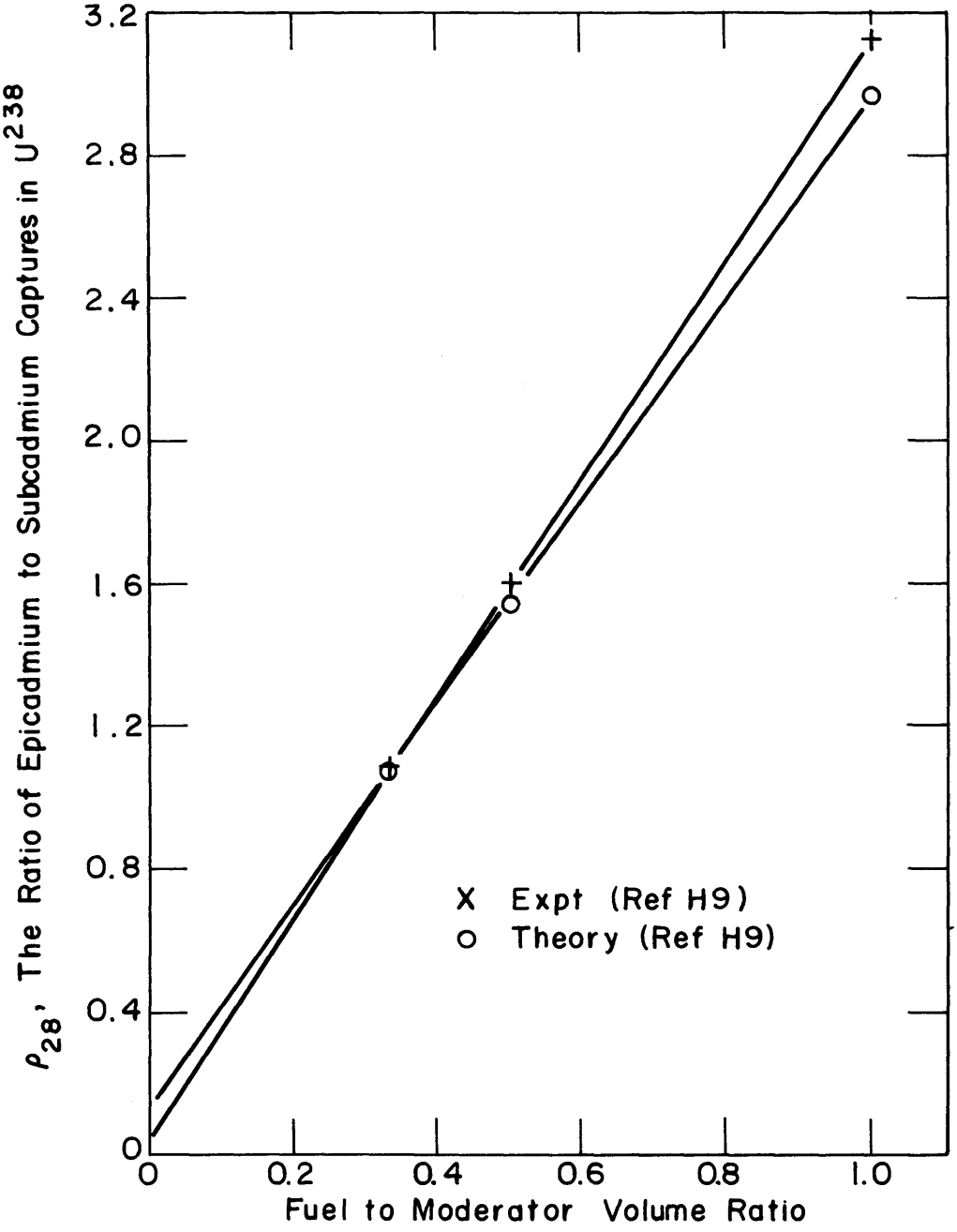

FIG. 5.2 THE RATIO, ρ_{28}, OF EPICADMIUM TO SUBCADMIUM CAPTURES IN U^{238} VS. FUEL TO MODERATOR VOLUME RATIO FOR 1.3% ENRICHED, 0.387" DIAM. URANIUM ROD IN H_2O

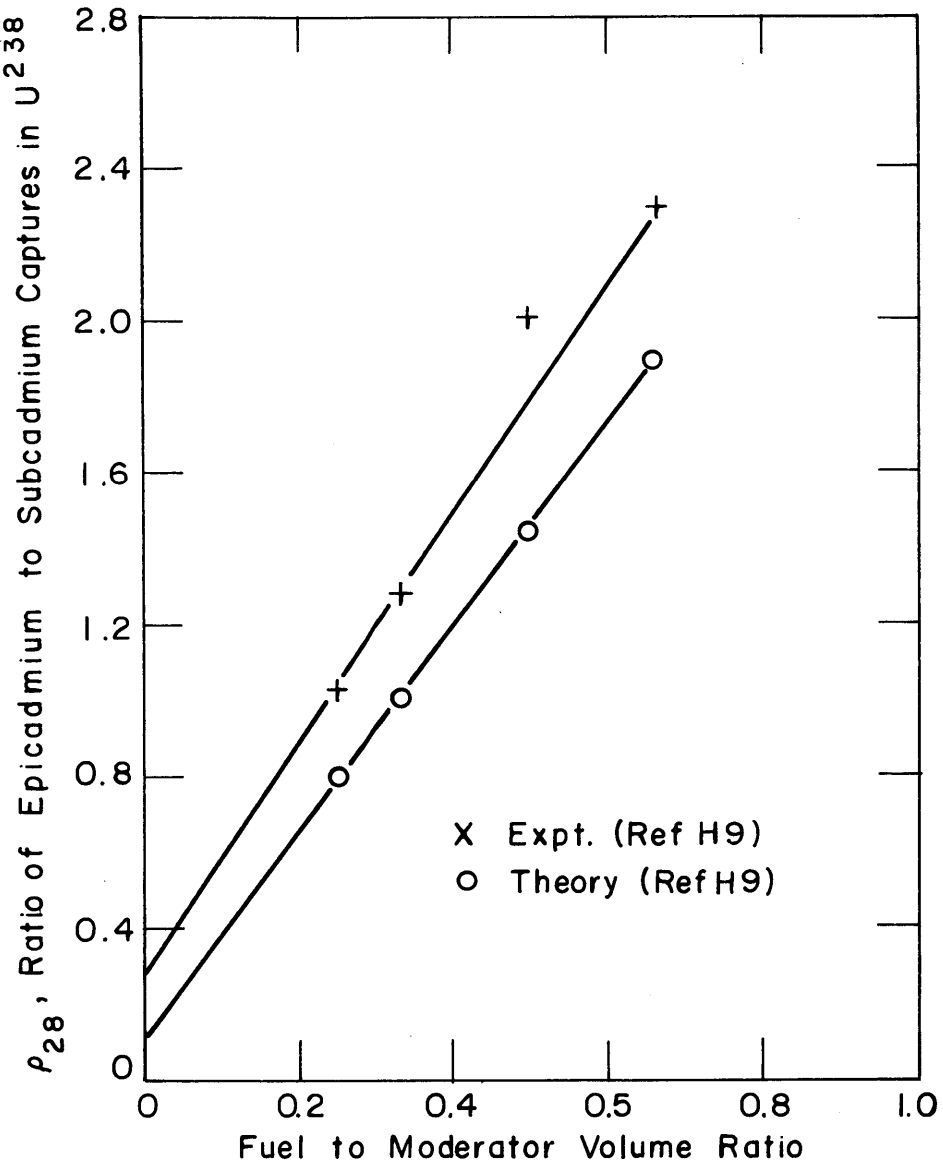

FIG. 5.3 THE RATIO, ρ_{28}, OF EPICADMIUM TO SUBCADMIUM CAPTURES IN U^{238} VS. FUEL TO MODERATOR VOLUME RATIO FOR 1.0 % ENRICHED, 0.250 INCH DIAM. URANIUM RODS IN H_2O. FROM REF. K 5

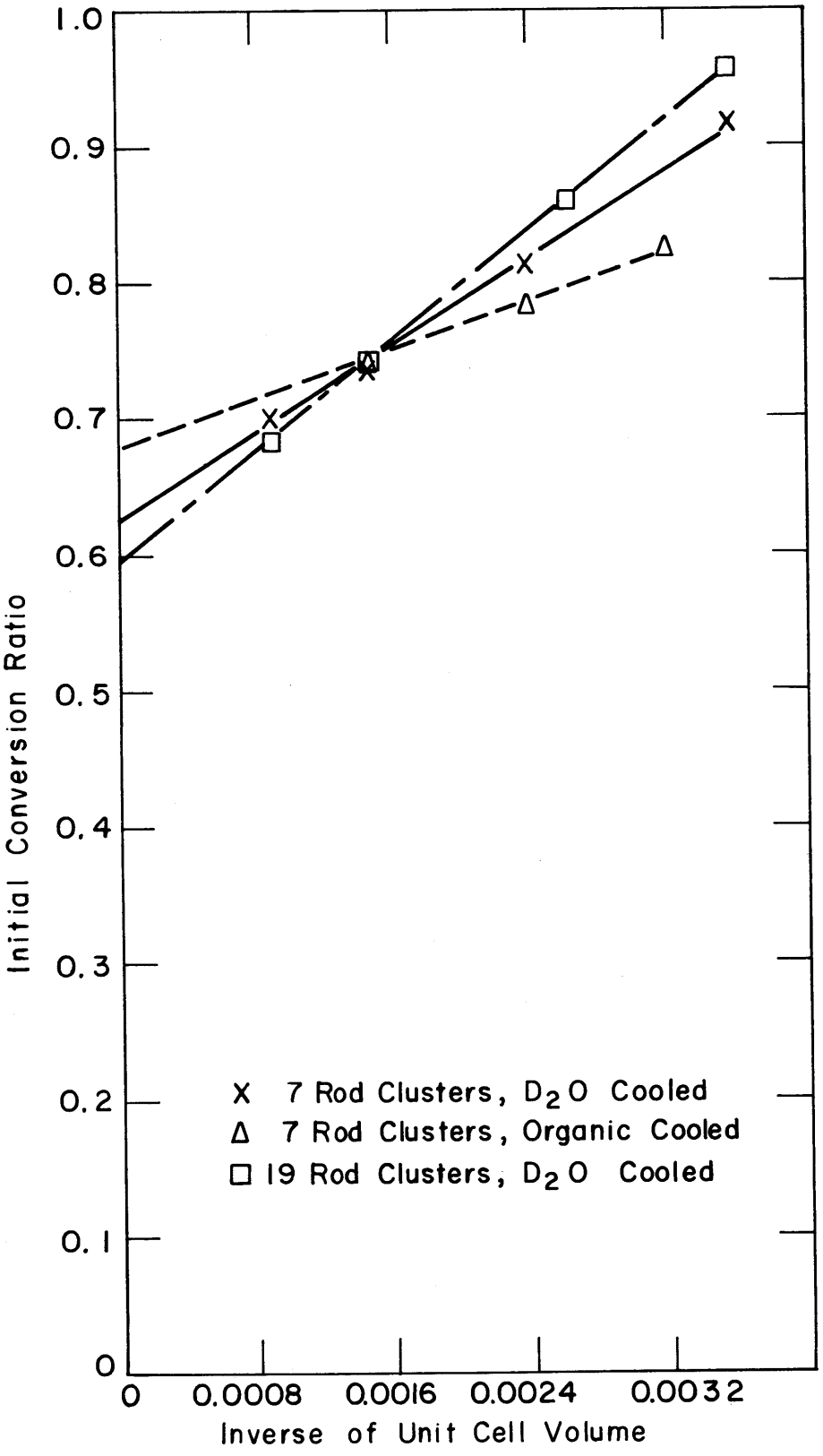

FIG. 5.4 INITIAL CONVERSION RATIO FOR THREE KINDS OF ROD-CLUSTER LATTICES IN D_2O MODERATOR FROM REF. 61

based values of the ratios with a minimum of effort. When the curves can be assumed to be exactly linear, experimental measurements on lattices at two different spacings completely determine the position of the line and therefore the values of the ratio for all other lattice spacings. One such experimental measurement can even be on the "lattice" whose spacing is infinite – that is, on a single fuel element immersed in a large sea of moderator. It will be shown in Chapter VI that the fast fission ratio exhibits a similar linearity. At least four important reactor parameters may thus be determined for any lattice spacing of a particular kind of fuel element by means of an experiment on a single such fuel element and an experiment on just one lattice of this kind of fuel element.

5.2.4 Use of the Resonance Escape Probability in the Expressions for ρ_{28} and C^*

Equations 5.12 and 5.14 can be put into more general form because a term in each of them is directly related to the resonance escape probability, p. The expression, $\frac{N_{28}V_F}{\xi\Sigma_s V_c} ERI^{28}$, in these equations represents the resonance capture rate per fast source neutron (in a uniform, infinite system). This is equal to 1 - p, so that Eqs. 5.12 and 5.14 may be rewritten as:

$$\rho_{28} = \frac{\eta\epsilon\left\{0.5\,\sigma_o P_{1/v} p \frac{N_{28}V_F}{\xi\Sigma_s V_c} + P_{Res}(1-p)\right\}}{\left(\frac{\Sigma_a^{28}}{\Sigma_a^{25}+\Sigma_a^{28}}\right)_{SC}}, \tag{5.15}$$

$$C^* = \frac{\left(\frac{\Sigma_a^{28}}{\Sigma_a^{25}+\Sigma_a^{28}}\right)_{SC} + \eta\epsilon(1-p)P_{Res} + 0.5\,\sigma_o\eta\epsilon p P_{1/v}\frac{N_{28}V_F}{\xi\Sigma_s V_c}}{\left(\frac{\Sigma_f^{25}}{\Sigma_a^{25}+\Sigma_a^{28}}\right)_{SC}(1+\delta_{25})}. \tag{5.16}$$

This change in the form of Eqs. 5.12 and 5.14 is advantageous because the ERI^{28} used in them is difficult to calculate. The flux spectrum in a lattice is not exactly a 1/E spectrum, both because of the Dancoff effect and because the capture in each resonance depletes the spectrum found at lower resonances. Equations 5.12 and 5.14 remain correct if the ERI^{28} used in them is calculated or measured for the spectrum of interest rather than for a 1/E spectrum. The Dancoff effect causes a reduction in the resonance integral and the magnitude of this reduction can be calculated from theory (A5, S5). The change in the ERI caused by depletion of the spectrum relative to a 1/E spectrum because of the resonance absorption itself cannot be found without a detailed calculation of the neutron spectrum in the lattice of interest. Such a calculation requires a large digital computer (K3). In lieu of such a detailed calculation, a good approximation to the value of the resonance escape probability may be calculated using the resonance integral appropriate to a 1/E spectrum in the formula (B5, W13):

$$p = e^{-\frac{N_{28} V_F}{\xi \Sigma_s V_c} (ERI)^{28}_{1/E}} . \qquad (5.17)$$

In this report, the resonance escape probability will be evaluated with Eq. 5.17. However, Eqs. 5.13, 5.15, and 5.16 for δ_{25}, ρ_{28}, and C^* are expressed in general terms and do not presuppose the use of any particular formula to find the value of the resonance escape probability, p. In using these formulas, the reader is therefore free to evaluate p by whatever means is felt to be most accurate for the particular problem under consideration.

5.3 EXPERIMENTAL RESULTS

The formulas derived in section 5.2 showed that knowledge of the slowing-down kernel is frequently unnecessary in computing the slowing-down density in uniform lattices. Nevertheless, the kernel must be known in order to calculate nonleakage probabilities and for use in situations not covered by the simple approximations used in section 5.2. The results of this section show that in heavy water the slowing-down

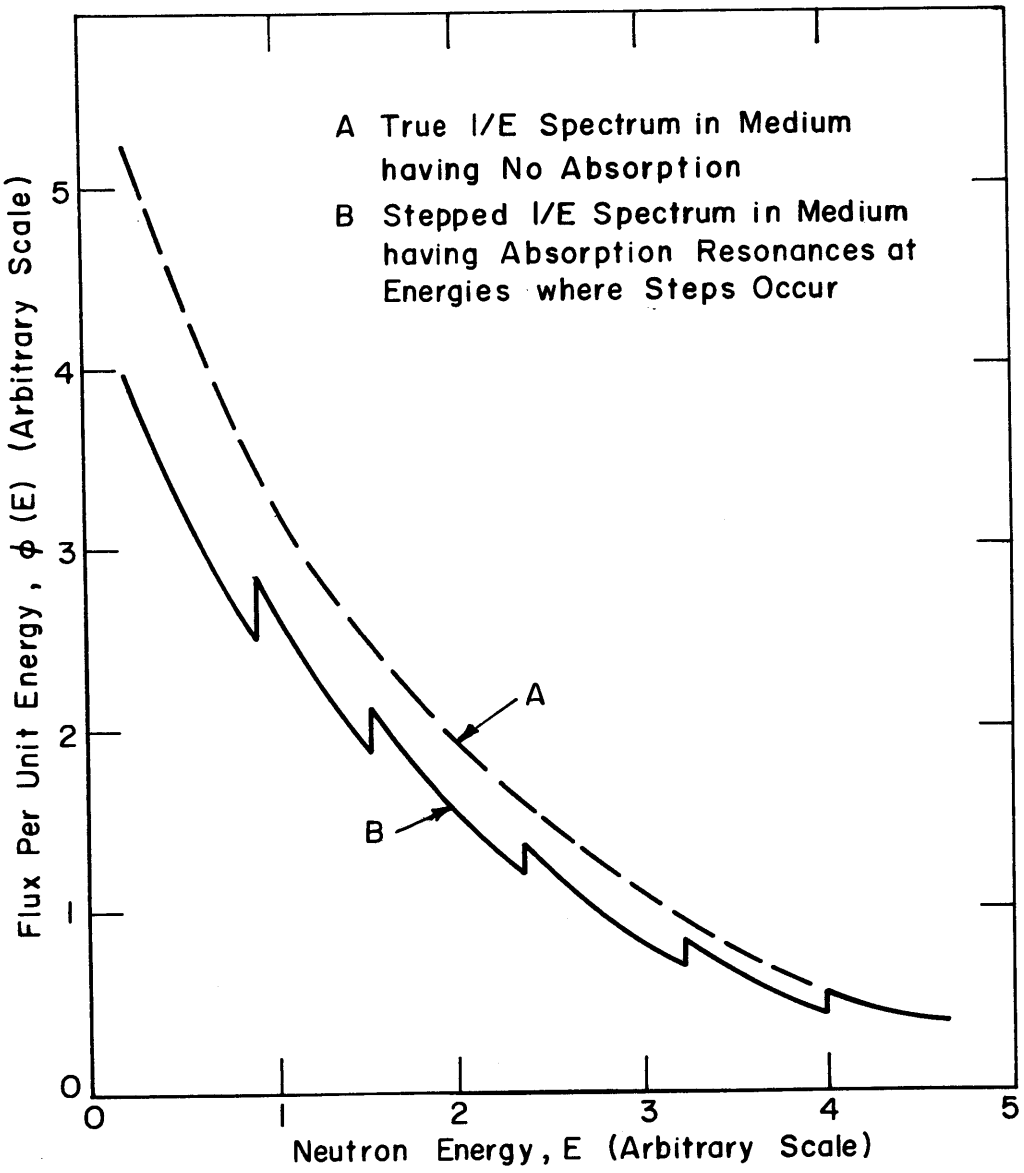

(a) Theoretical Spectrum

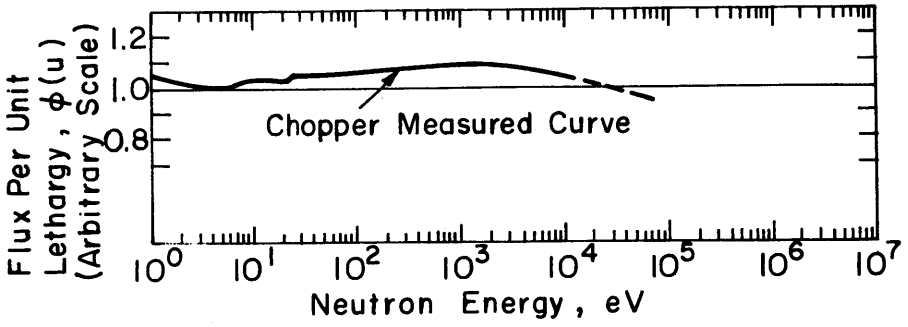

(b) Measured Spectrum

FIG. 5.5 COMPARISON OF FLUX SPECTRA IN MEDIA WITH AND WITHOUT RESONANCE ABSORPTION

density at the effective energy of resonance capture in U^{238} is fairly well described by age theory.

The age theory kernel is completely determined by only one parameter, the effective age τ_{28}, to resonance capture. To determine this age, foils of depleted uranium were irradiated in cadmium-covered foil packets immersed in heavy water around a single, bare fuel rod, which acted as a line source of fission neutrons. The experimental details are described in section 3.3.

Figures 5.6 to 5.8 show the relative values of the resulting Np^{239} activity in the foils, which is proportional to the capture rate in U^{238}. Although each graph has only a few data points, age theory can be used to correlate the data within the region from about 3 or 4 cms to about 20 cms from the source. The effective age has been determined in each case from a least-squares fit of the logarithm of the activity to radius squared over this region. There were not enough data points at large radii to enable the age to be calculated as one-sixth $\overline{r^2}$. However, the age so determined would be somewhat larger than the age as determined here, since at large radii the data points fall above the fit straight line. Although it is evident that age theory correlates the data fairly well in the region considered, the use of a more complicated kernel might result in improved accuracy.

The good agreement between the values of the ages found by using different size foils and source rods indicates that their finite sizes have little effect on the measured age. Sefchovich (S3) has also shown theoretically that to a first approximation the finite extent of the source rod has no effect. The consistency of the various results is further illustrated by plotting on the same graph, Fig. 5.9, all the data obtained between 3 and 20 cm radius. Within the experimental error, they all fall on the same straight line in the region from 3 to 20 cm radius, where 75 percent of the total slowing down occurs.

Table 5.1 lists the values of the age, τ_{28}, obtained from each of the experiments. It is of interest to determine what energy corresponds to the average value of τ_{28}. Since age theory does not apply rigorously to heavy water, it is not true that:

$$\tau(E) = \int_{E_F}^{E} \frac{D}{\xi \Sigma_s} \frac{dE}{E} , \qquad (5.18)$$

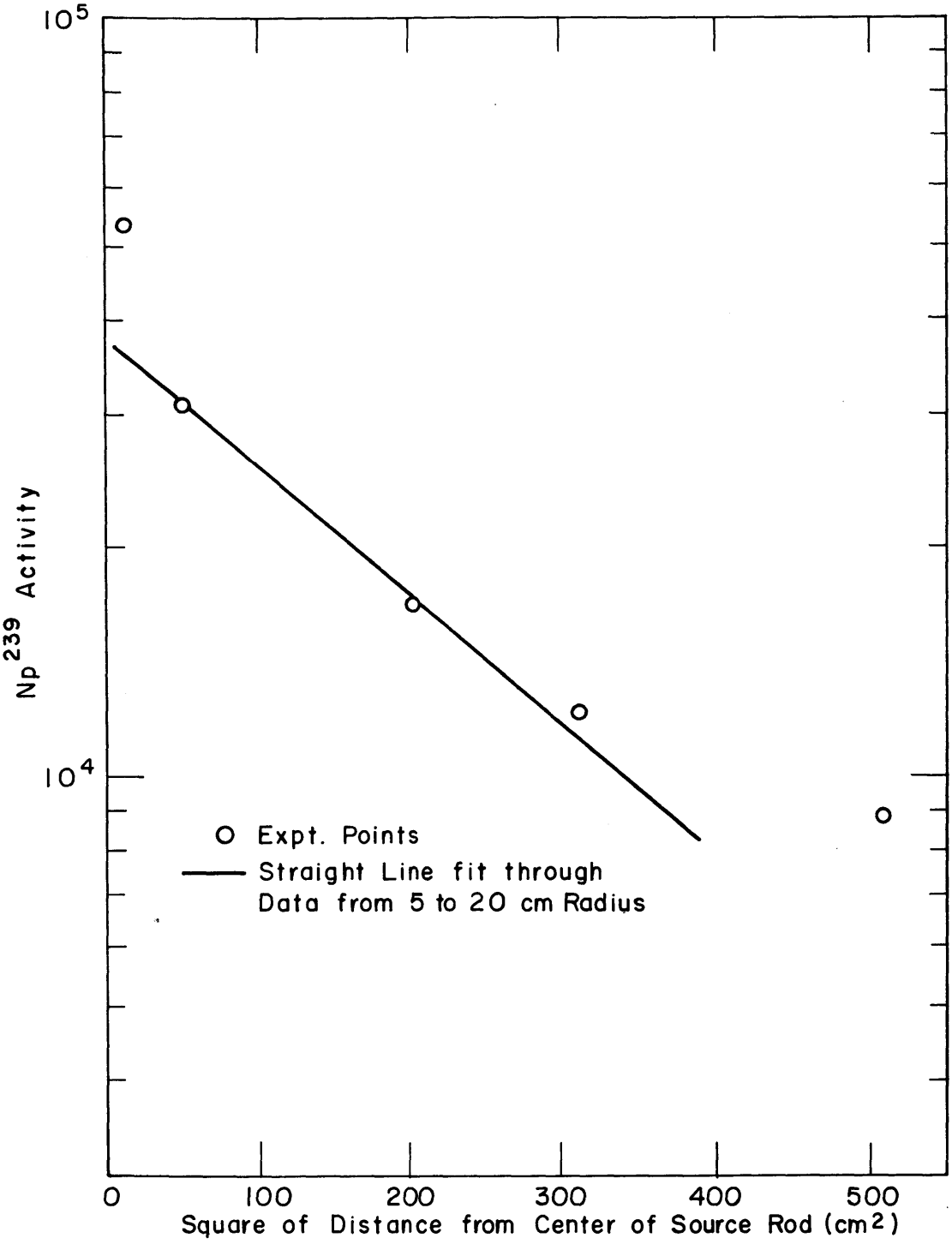

FIG. 5.6 NEPTUNIUM - 239 ACTIVITY IN 1/4 INCH DIAMETER, DEPLETED URANIUM FOILS IN HEAVY WATER AROUND 1 INCH DIAMETER NATURAL URANIUM SOURCE ROD. (SEE SECTION 3.3 FOR DETAILS OF EXPERIMENT)

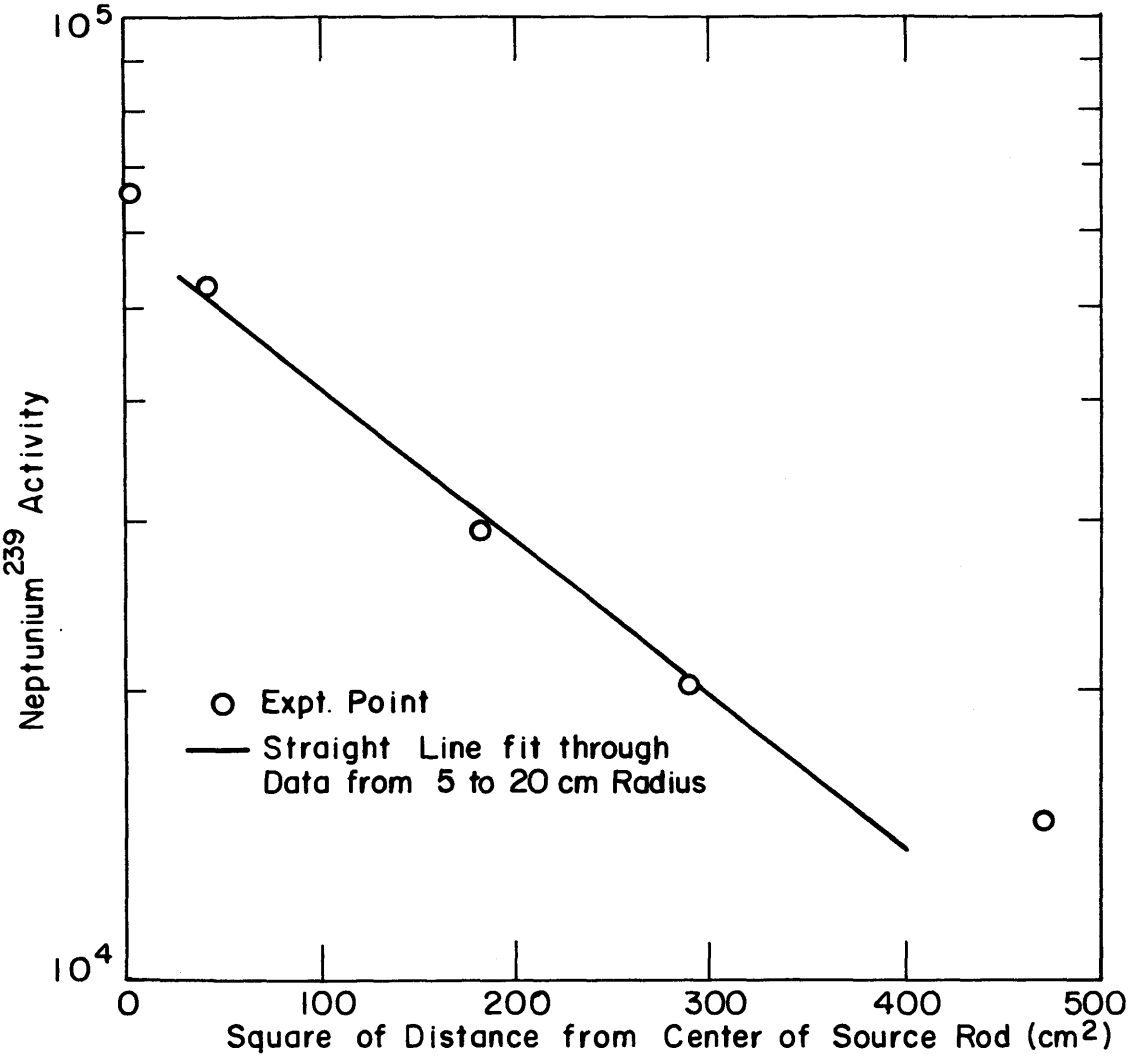

FIG. 5.7 NEPTUNIUM - 239 ACTIVITY IN 1/4 INCH DIAMETER, DEPLETED URANIUM FOILS IN HEAVY WATER AROUND 1/4 INCH DIAMETER, 1.14 % ENRICHED SOURCE ROD. (SEE SECTION 3.3 FOR DETAILS OF EXPERIMENT)

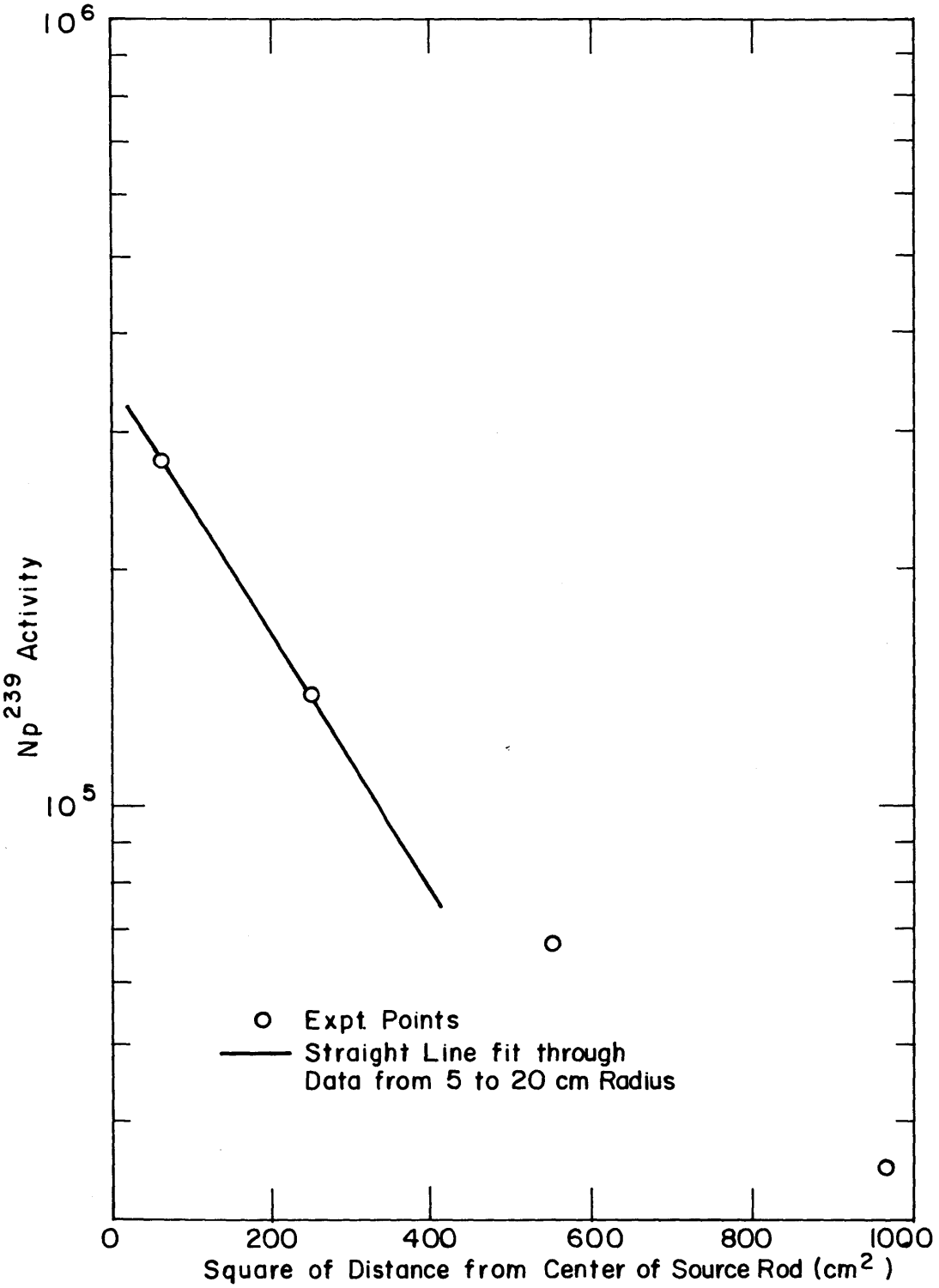

FIG. 5.8 NEPTUNIUM – 239 ACTIVITY IN 3/4 INCH DIAMETER, DEPLETED URANIUM FOILS IN HEAVY WATER AROUND 3/4 INCH DIAMETER, 0.947 % ENRICHED SOURCE ROD. (SEE SECTION 3.3 FOR DETAILS OF EXPERIMENT)

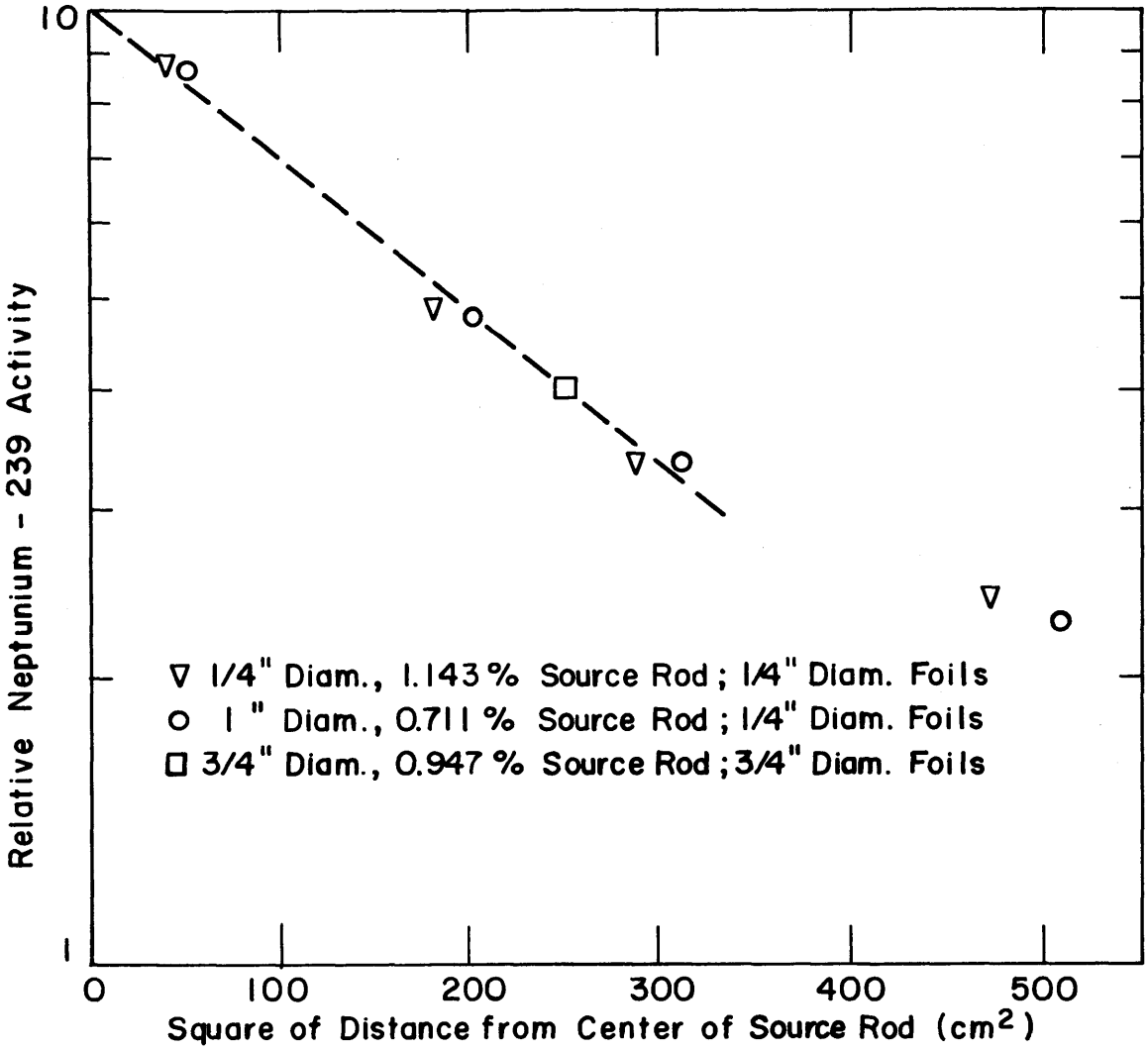

FIG. 5.9 RELATIVE NEPTUNIUM - 239 ACTIVITY IN DEPLETED URANIUM FOILS OF VARIOUS SIZES IN HEAVY WATER

Table 5.1

Values of the Experimentally Determined Age to Resonance Capture in U^{238}

Source Rod Diameter (Inches)	Source Rod Enrichment (Wt. %)	Foil Diameter (Inches)	Effective Age to Resonance Capture (cm^2)
1.00	0.711	0.250	69 ± 5
0.75	0.947	0.750	67
0.25	1.143	0.250	64 ± 3
All points between 6 and 18 cm:			67 ± 3

where E_F is the average energy of fission neutrons. However, it is reasonable to assume that the difference in age corresponding to two nearby energies is given approximately by:

$$\Delta\tau \approx c \ln \frac{E_1}{E_2}, \tag{5.19}$$

where the constant c is determined to fit experimental data. The constant c has been found by using measured values of the age to the indium (W14) and gold (S4) resonances. The data are:

$$\tau(4.91 \text{ ev}) = 95 \pm 3 \text{ cm}^2, \tag{5.20}$$

$$\tau(1.44 \text{ ev}) = 109 \pm 3 \text{ cm}^2, \tag{5.21}$$

These yield a value of:

$$C = 11.4 \pm 3.45 \text{ cm}^2, \tag{5.22}$$

so that:

$$\tau_{AU} - \tau_{28} = 95 - 67 = 11.4 \ln (E_{28}/1.44), \tag{5.23}$$

or:

$$E_{28} = 57 \begin{pmatrix} +73 \\ -32 \end{pmatrix} \text{ ev}. \tag{5.24}$$

Despite its large uncertainty, this experimentally determined value is in agreement with previous theoretical estimates of 25 ev (C1) and 100 ev (T2).

5.4 INFERRED VALUES OF THE VARIOUS RATIOS IN UNIFORM LATTICES

Equations 5.15 and 5.16 of section 5.2, with the experimentally determined value of the age to resonance capture, have been used to infer values of ρ_{28} and C^* in uniform lattices. Table 5.2 lists the material constants and measured values of the ages used in these calculations.

Values of the resonance escape probability for use in these formulas were calculated from Eq. 5.17. The Dancoff corrected effective resonance integral for use in Eq. 5.17 was calculated for each lattice with the aid of Strawbridge's metal-oxide correlation (S5). This correlation is based on the fit of an equivalence formula to measured resonance integrals. For uranium metal rods at room temperature, the correlation is:

$$ERI = 0.561 + 2.638x, \tag{5.25}$$

$$x = \left\{ 10.7\ P_o + \frac{D_{eff}}{\ell_o N_o^{28}} \right\}^{1/2}, \tag{5.26}$$

where:

P_o is the probability that neutrons born in the rod with a uniform source distribution will escape the rod without scattering;

ℓ_o is the mean chord length in the fuel rod;

D_{eff} is the effective shielding factor for the lattice, here approximated by Wigner's rational approximation:

$$D_{eff} = 1 - \frac{1}{1 + \Sigma_{tm}\ell_m}; \tag{5.27}$$

Σ_{tm} is the total cross section of the moderator;

ℓ_m is the mean chord length per unit cell, in the moderator.

Table 5.2

Geometric and Nuclear Constants Used in the Calculation of the Ratios

Concentration of U-235 in Fuel Rod (Wt. %)	Lattice Spacing (Inches)	Volume Ratio V_F/V_c	Slowing-Down Power of Cell $\xi\Sigma_s$ (cm^{-1})	$\left(\frac{\Sigma_a^{25}}{\Sigma_a^{25}+\Sigma_a^{28}}\right)_{SC}$	$\left(\frac{\Sigma_f^{25}}{\Sigma_a^{25}+\Sigma_a^{28}}\right)_{SC}$	$\eta\epsilon$
1.027	1.25	0.03628	0.179	0.2873	0.6101	1.5192*
	1.75	0.01851	0.182	0.2852	0.6115	1.5164
	2.50	0.009069	0.184	0.2832	0.6122	1.5147
1.143	1.25	0.03628	0.179	0.2619	0.6282	1.5707*
	1.75	0.01851	0.182	0.2610	0.6296	1.5643
	2.50	0.009069	0.184	0.2606	0.6304	1.5607
0.711	4.50	0.0448	0.180	0.3646	0.5413	1.3663**
	5.00	0.0363	0.180	0.3649	0.5408	1.3661
	5.75	0.0274	0.180	0.3651	0.5404	1.3481

* Values of ϵ from ref. B3.

** Values of ϵ from ref. W12.

For single rods, this correlation is in excellent agreement with Hellstrand's results for both metal and oxide rods. In addition, it agrees well with measured values in homogeneous mixtures of uranium and moderator.

The calculated values of ERI and resonance escape probability for the lattices studied here are shown in Table 5.3. For lattices of 1.027 percent enriched uranium, these resonance escape probabilities are in excellent agreement with those obtained from measurements of ρ_{28} (D1) with the formula of Kouts and Sher (K4).

Table 5.4 compares the calculated values of ρ_{28} and C^* with results obtained directly from experiments in the large exponential facility at M. I. T., as well as with values obtained by theoretical extrapolation from experiments in the miniature lattice facility at M. I. T. These results are also plotted in Figs. 5.10 to 5.13. In these figures, points which would otherwise lie too close together to resolve have been separated by slight horizontal displacements.

Table 5.5 gives the percent difference in the values obtained by the present method and by extrapolation from miniature lattice results, utilizing the values measured in the large lattice as a basis for comparison. This shows that values obtained from the miniature lattice are generally slightly more accurate than those obtained by the method presented here, but it is not clear that the difference is significant.

There are some anomalies in these results. Thus, considering ρ_{28}, for each method the errors exceed five percent in three cases. In two of these cases, the 1.25-inch spacing and 2.50-inch spacing lattices of 1.143 percent fuel (superscript A in Tables 5.4 and 5.5), both methods differ in the same direction from the values obtained in the large exponential. This suggests that the actual error may lie more in the experiment results than in the calculation. In fact, the inferred values for these lattices are in much better agreement with each other than with the experiments. Reference to Table 5.2 shows that in going from 1.027 percent to 1.143 percent, all the factors in Eq. 5.15 change in such a way as to increase ρ_{28}. This increases the likelihood that the experimentally measured value of ρ_{28} for the 1.143 percent, 1.25-inch lattice is in error, since it lies below the value for the corresponding 1.027 percent lattice.

Table 5.3

Values of the Resonance Integral and Resonance Escape Probability
Used in the Calculation of Lattice Ratios

Concentration of U-235 (Wt. %)	Lattice Spacing (Inches)	Fuel Rod Diameter (Inches)	Effective Resonance Integral* ERI^{28} (Barns)	U-238 Resonance Escape Probability** p
1.027	1.25	0.250	16.95	0.8500
	1.75	0.250	17.32	0.9201
	2.50	0.250	17.58	0.9599
1.143	1.25	0.250	16.95	0.8500
	1.75	0.250	17.32	0.9201
	2.50	0.250	17.58	0.9599
0.711	4.50	1.00	11.40	0.8684
	5.00	1.00	11.40	0.8931
	5.75	1.00	11.40	0.9189

* From Strawbridge's metal-oxide correlation (Eq. 5.25).

** From exponential formula (Eq. 5.17).

Table 5.4

Values of ρ_{28}, the Ratio of Epicadmium to Subcadmium Capture in U-238, and of C^*, the Ratio of Capture in U-238 to Fission in U-235, for 1/4-Inch-Diameter, Uranium Metal Rods in D_2O

Concentration of U-235 in Fuel Rod (Wt. %)	Lattice Spacing (Inches)	Volume Ratio V_F/V_c	ρ_{28}			C^*		
			Direct Experiment (Exponential)	Extrapolation (Miniature Lattice)	Single Element Method	Direct Experiment (Exponential)	Extrapolation (Miniature Lattice)	Single Element Method
1.027[1]	1.25	0.03628	0.8453	0.856	0.7853[B]	0.8028	0.820	0.7991
	1.75	0.01851	0.4373	0.425	0.4207	0.6345	0.646	0.6433
	2.50	0.00907	0.2272	0.242[C]	0.2170	0.5506	0.568	0.5527
1.143[2]	1.25	0.03628	0.8130[A]	0.861	0.8750	0.773	0.733	0.7391
	1.75	0.01851	0.4710	0.476	0.4678	0.617	0.594	0.5888
	2.50	0.00907	0.2220[A]	0.251	0.2412	0.490	0.506	0.5049

(1) "Direct Experiment" values from ref. D1.

(2) "Direct Experiment" values from ref. M5.

A, B, C: See discussion in text.

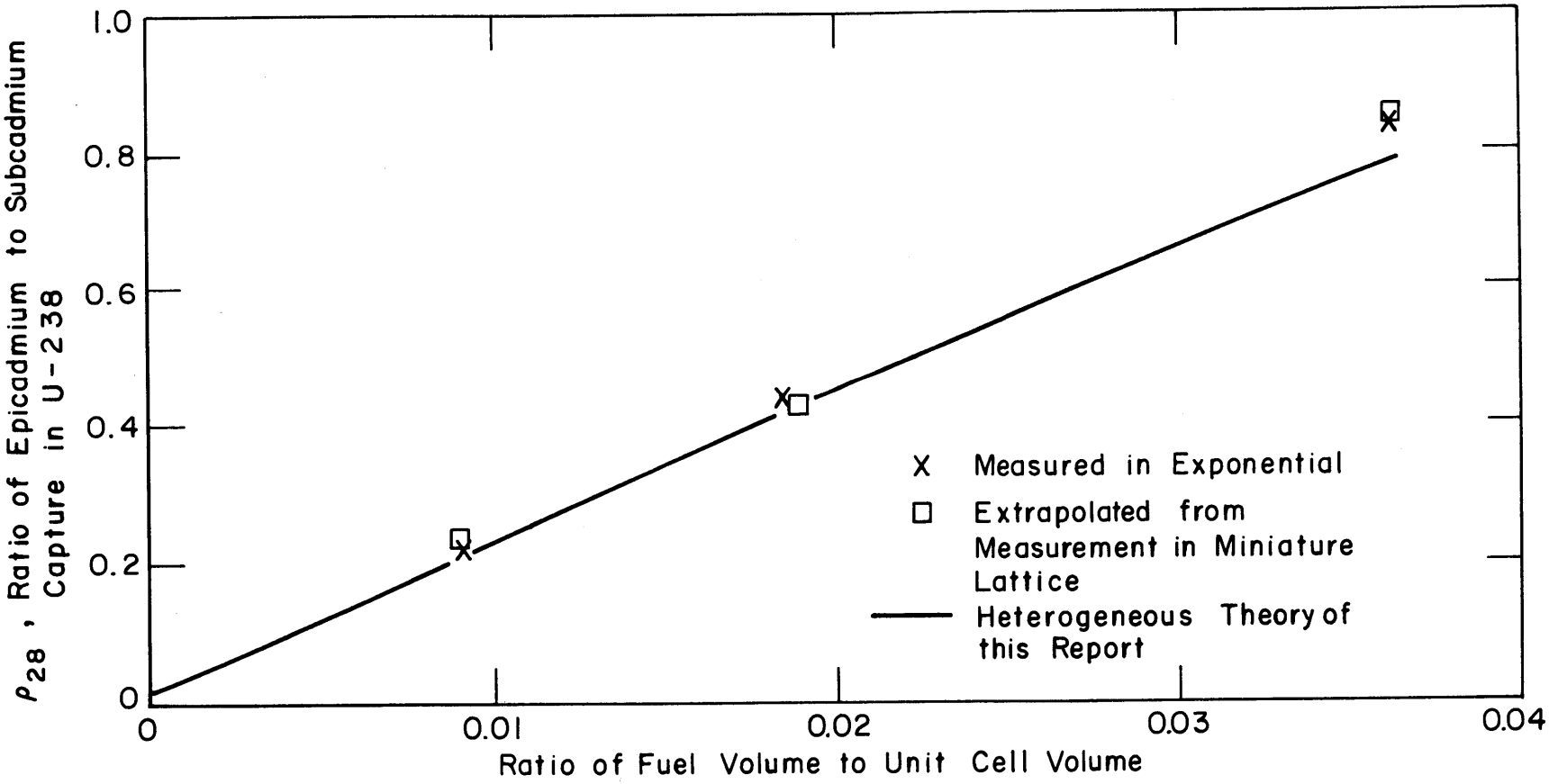

FIG. 5.10 THE RATIO, ρ_{28}, OF EPICADMIUM TO SUBCADMIUM CAPTURE IN U-238 VS. VOLUME FRACTION OF FUEL IN UNIT CELL FOR 1/4" DIAMETER, 1.027 % ENRICHED URANIUM METAL RODS IN D_2O

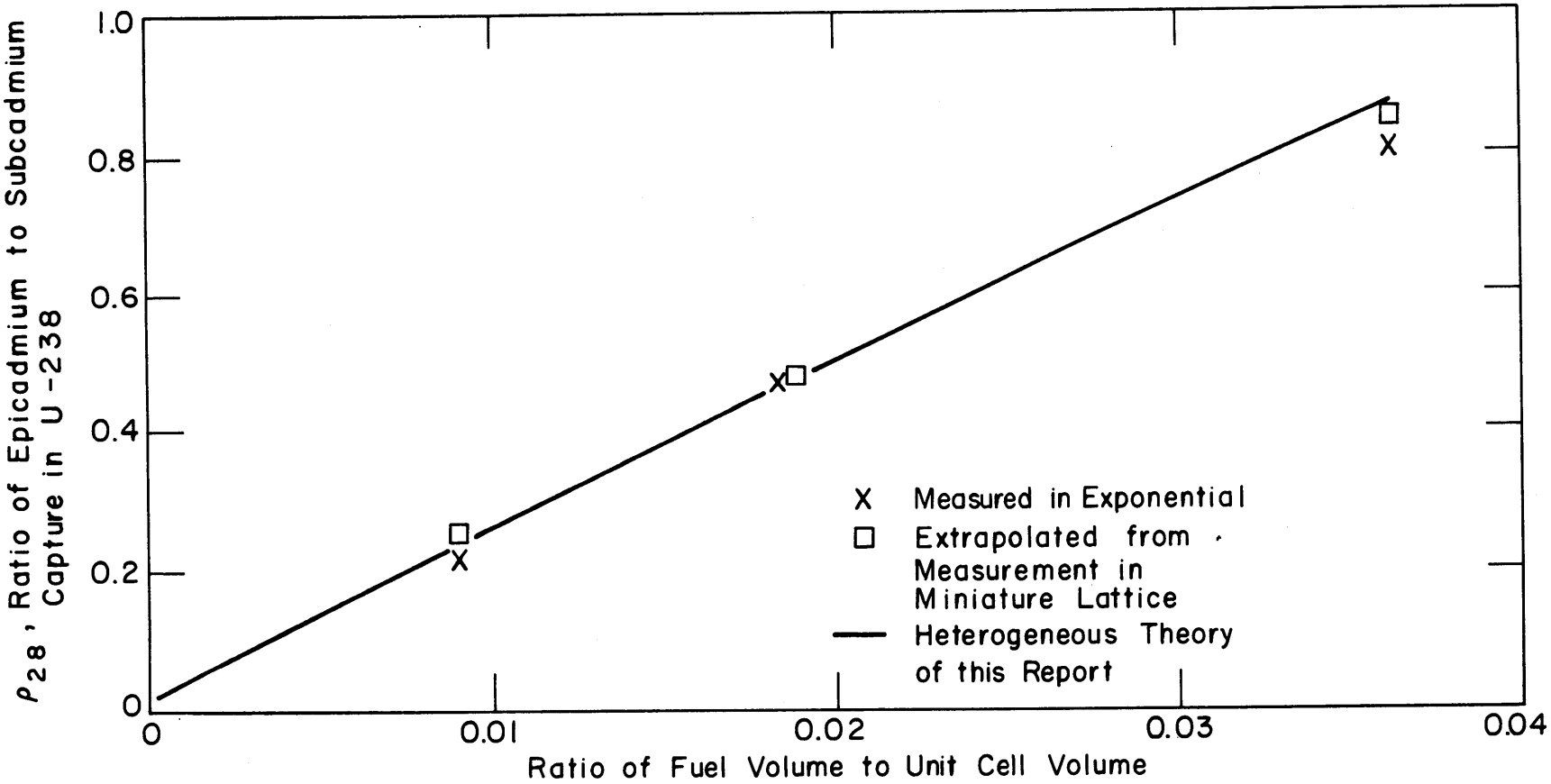

FIG. 5.11 THE RATIO, ρ_{28}, OF EPICADMIUM TO SUBCADMIUM CAPTURE IN U-238 VS. VOLUME FRACTION OF FUEL IN UNIT CELL FOR 1/4" DIAMETER, 1.143 % ENRICHED URANIUM METAL RODS IN D_2O

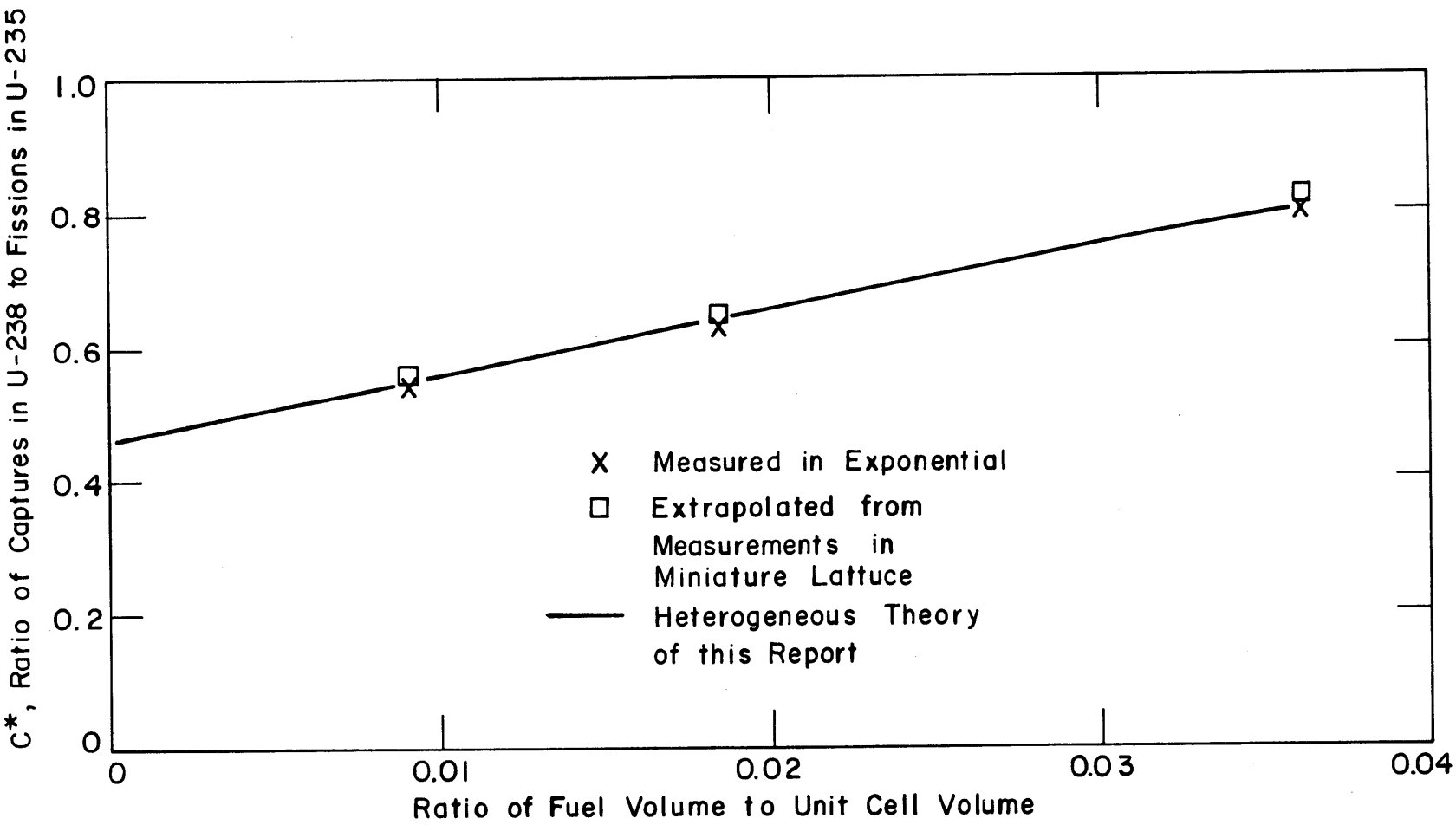

FIG. 5.12 THE RATIO, C* , OF CAPTURES IN U-238 TO FISSIONS IN U-235 VS. VOLUME FRACTION OF FUEL IN UNIT CELL FOR 1/4" DIAMETER, 1.027% ENRICHED URANIUM METAL RODS IN D_2O

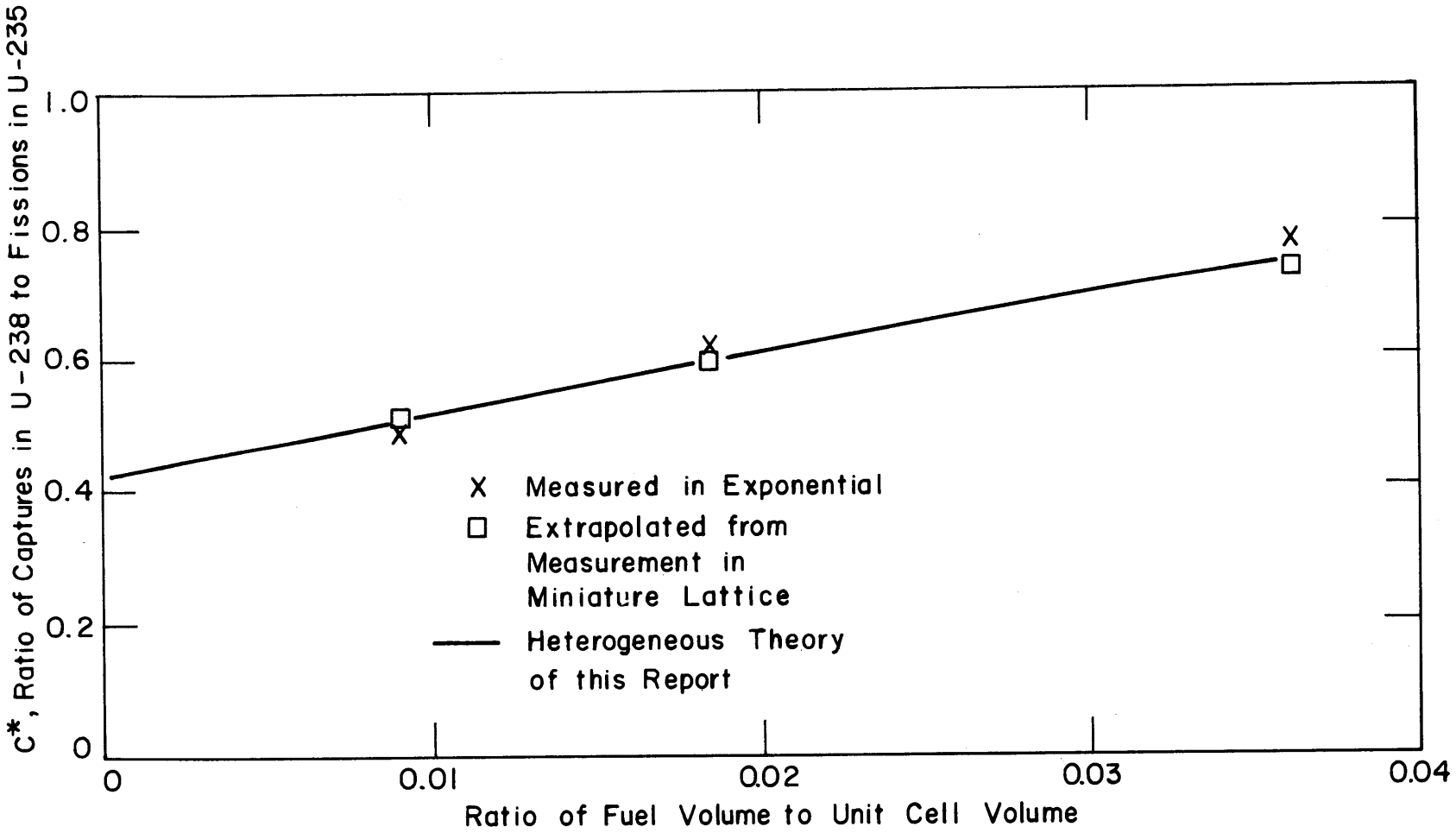

FIG. 5.13 THE RATIO, C*, OF CAPTURES IN U-238 TO FISSIONS IN U-235 VS. VOLUME FRACTION OF FUEL IN UNIT CELL FOR 1/4" DIAMETER, 1.143% ENRICHED URANIUM METAL RODS IN D_2O

Table 5.5

Percentage Differences Between Values of ρ_{28} and C^* Determined by Measurement in Exponential Assembly, and Values Determined by Extrapolation from Measurements in Miniature Lattice or by the Single Element Method

Enrichment (Wt. %)	Pitch (Inches)	V_F/V_c	ρ_{28} Percent Differences		C^* Percent Differences	
			Extrapolation from Miniature Lattice	Single Element Method	Extrapolation from Miniature Lattice	Single Element Method
1.027	1.25	0.03628	+1.3	-7.1[B]	+2.1	-0.5
	1.75	0.01851	-2.8	-3.8	+1.8	+1.4
	2.50	0.00907	+6.5[C]	-4.5	+3.2	+0.4
1.143	1.25	0.03628	+5.9[A]	+7.6[A]	-5.2	-4.4
	1.75	0.01851	+1.1	-0.7	-3.7	-4.6
	2.50	0.00907	+13.1[A]	+8.6[A]	+3.3	+3.0

A, B, C: See discussion in text.

When applied to the 1.25-inch lattice of 1.027 percent enrichment (superscript B in Tables 5.4 and 5.5), the present method gives much too low a value, but the result obtained from the miniature lattice is in good agreement with experiment. Similarly, in the case of the 2.50-inch lattice of 1.027 percent enrichment (superscript C in Tables 5.4 and 5.5), the value from the miniature lattice is much too large, but the method of this paper yields a value in fair agreement with experiment.

Measured and inferred values of C^* generally fall within five percent of one another and are generally in better agreement than are the values of ρ_{28}. This result probably reflects the large single rod contribution to C^*, compared to the negligible single rod contribution to ρ_{28}. Thus, in Figs. 5.10 to 5.13 the values of the intercepts are significant fractions of the lattice values for C^* but not for ρ_{28}. In the method presented here, the single rod contribution to C^* consists mostly of the subcadmium capture (the first term in Eq. 5.16), which is calculated from THERMØS and is thus expected to be accurate. The miniature lattice measurement, of course, includes the single rod contribution, and only the interaction contribution is adjusted by the theoretical extrapolation. Thus, both approximate techniques are expected to give more accurate results for quantities containing a large single rod contribution, and this is in fact observed.

There is no simple, arbitrary correction which could be applied to the results calculated by the present method to improve their agreement with the measured values. In the case of the lattices of 1.027 percent enriched uranium, an increase in the resonance integral would improve the agreement in ρ_{28} but would lessen the agreement in C^*. If the experimental values are accepted as correct, then for lattices such as these the method presented here can evaluate ρ_{28} to within five to eight percent, and C^* to less than five percent.

Values of ρ_{28} and C^* for lattices of one-inch-diameter, natural uranium rods in heavy water are given in Table 5.6 and Figs. 5.14 and 5.15. In this case, values extrapolated from miniature lattice measurements were not available. Agreement between measured and calculated values is better than for the one-quarter-inch diameter rods. The uncertainties in the values of ρ_{28} and C^* are comparable. The theory

Table 5.6

Values of ρ_{28}, the Ratio of Epicadmium to Subcadmium Capture in U-238, and of C^*, the Ratio of Captures in U-238 to Fissions, for One-Inch-Diameter, Natural Uranium Metal Rods in D_2O

Lattice Spacing (Inches)	Volume Ratio V_F/V_c	ρ_{28}			C^*		
		Direct* Experiment (Exponential)	Single Element Method	Percent Difference	Direct* Experiment (Exponential)	Single Element Method	Percent Difference
4.50	0.0448	0.507	0.516	+1.8	1.017	1.001	-1.6
5.00	0.0363	0.401	0.417	+4.0	0.948	0.950	+0.2
5.75	0.0274	0.310	0.315	+1.6	0.859	0.884	+2.9

* "Direct Experiment" values from ref. M6.

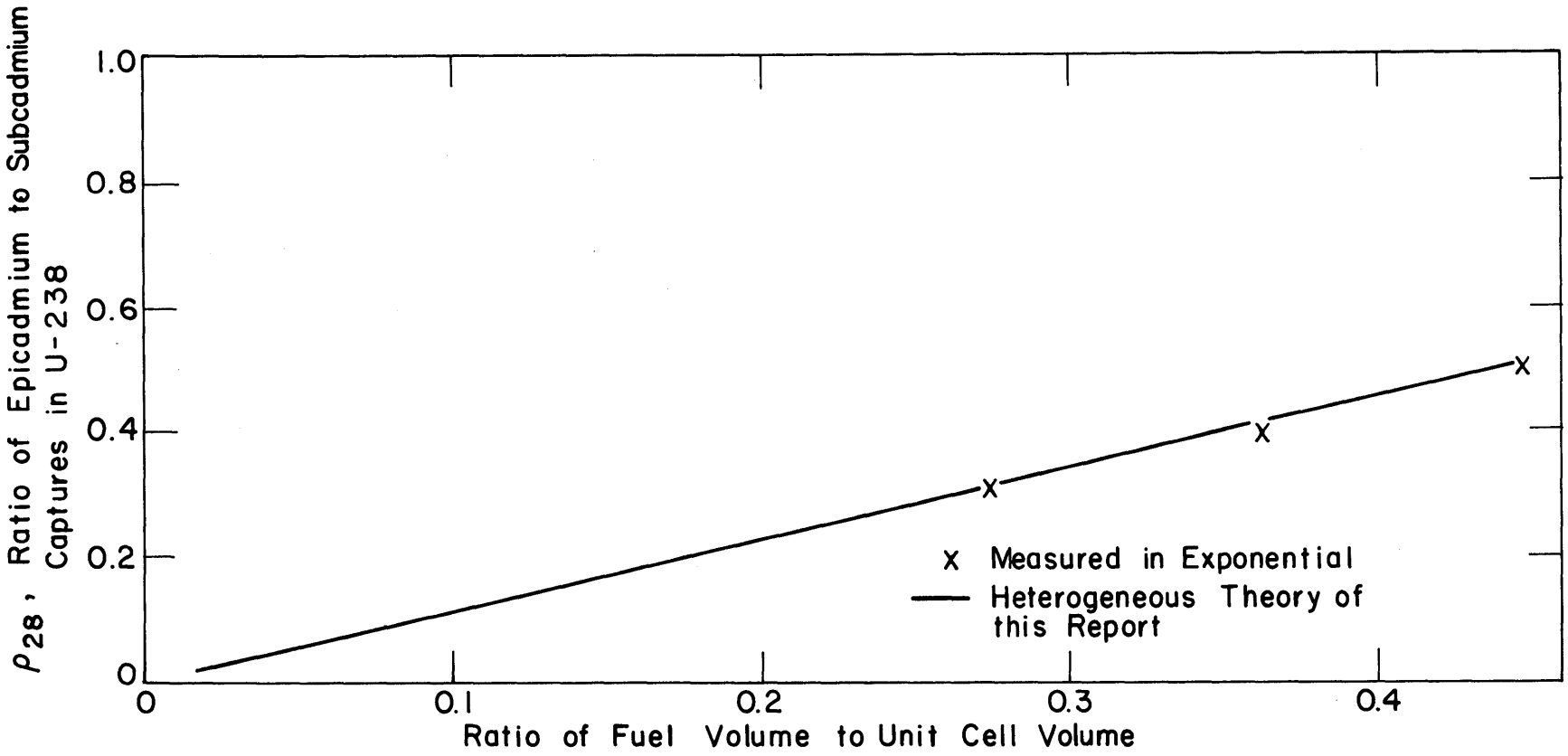

FIG. 5.14 THE RATIO, ρ_{28}, OF EPICADMIUM TO SUBCADMIUM CAPTURE IN U-238 VS. VOLUME FRACTION OF FUEL IN UNIT CELL FOR 1" DIAMETER, NATURAL URANIUM METAL RODS IN D_2O

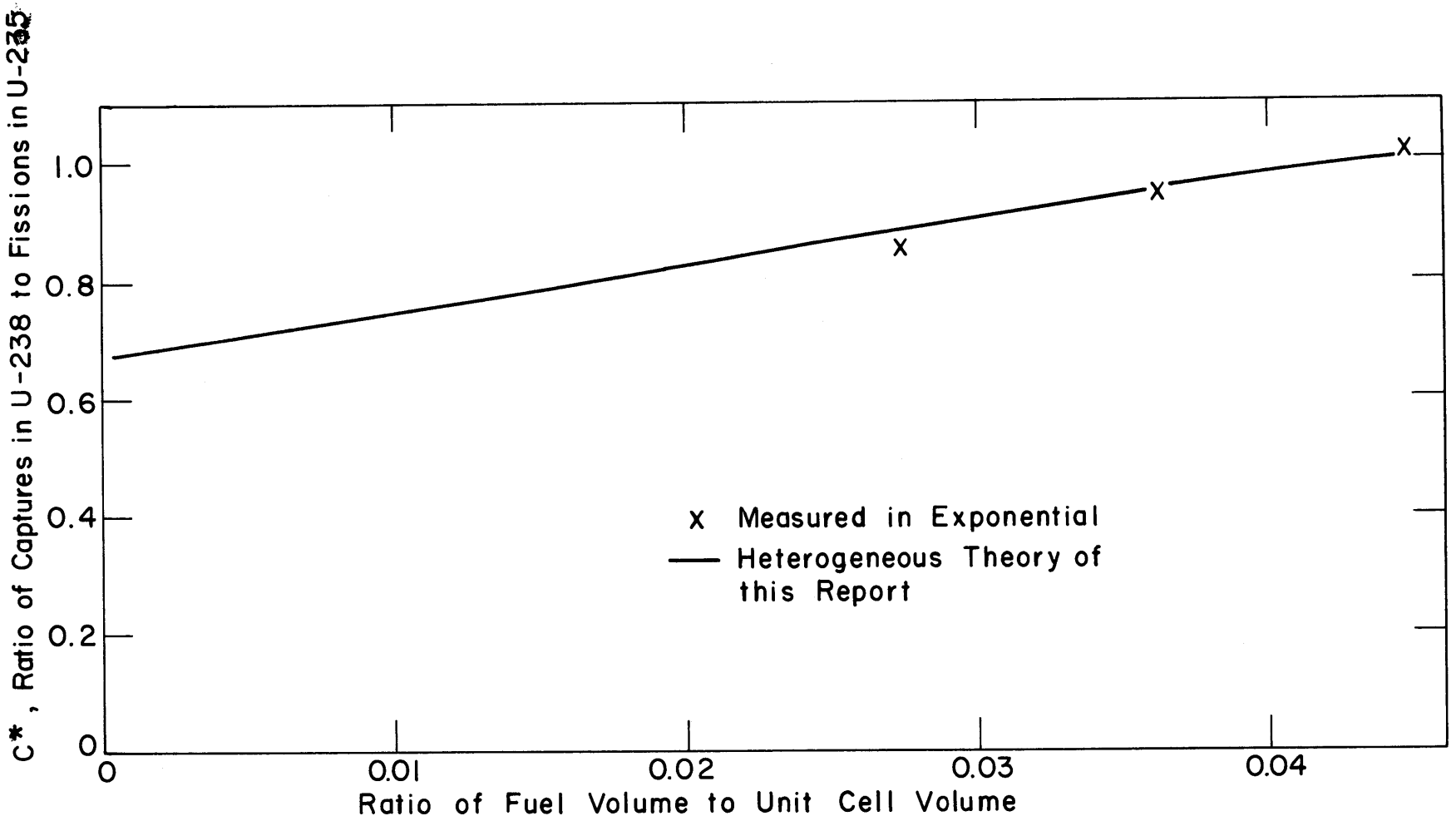

FIG. 5.15 THE RATIO, C*, OF CAPTURES IN U-238 TO FISSIONS IN U-235 VS. VOLUME FRACTION OF FUEL IN UNIT CELL FOR 1" DIAMETER, NATURAL URANIUM METEL RODS IN D_2O

should apply equally well to one-inch-diameter and one-quarter-inch-diameter rods, but experiments with the larger rods are expected to be more accurate. Thus, the good agreement between theory and experiment for the large rods may indicate that some of the difficulty with the smaller rods is experimental more than theoretical.

5.5 INFERRED VALUES OF THE U^{235} FISSION RESONANCE INTEGRAL

Equation 5.13 has been solved for the fission resonance integral, ERI^{25}:

$$ERI^{25} = \frac{\delta_{25}\left(\frac{\Sigma_f^{25}}{\Sigma_a^{25}+\Sigma_a^{28}}\right)_{SC}}{\eta\epsilon \frac{N_{25}V_F}{\xi\Sigma_s V_c} P_{25}^{p}} . \qquad (5.28)$$

This equation has been used to obtain ERI^{25} from measured values of δ_{25}, calculated values of p from Table 5.3, and other nuclear and geometric constants from Table 5.2. The resulting values of the fission resonance integral are given in Table 5.7. These are generally consistent with one another. The average fission resonance integral, 284 barns, is in good agreement with the infinite dilution integral of 274 ± 10 barns given in the latest edition of BNL-325 (H8). This supports the often-heard conjecture that in lattices of slightly enriched uranium the U^{235} behaves as if infinitely dilute, with no noticeable effects resulting from the presence of U^{238}.

Table 5.7

Values of Resonance Integrals for Fission in U-235, as Determined from Measurements of δ_{25}

Concentration of U-235 in Fuel Rod (Wt. %)	Lattice Spacing (Inches)	Volume Ratio V_F/V_c	ERI^{25}_{FISS} (Barns)
1.027[1]	1.25	0.03628	278 ± 50
	1.75	0.01851	300 ± 12
	2.50	0.009069	344 ± 41
1.143[2]	1.25	0.03628	286 ± 52
	1.75	0.01851	300 ± 14
	2.50	0.009069	275 ± 120
0.711[3]	4.50	0.0448	262 ± 10
	5.00	0.0363	256 ± 22
	5.75	0.0274	231 ± 9
Average (with observed standard deviation of the mean):			281 ± 11

(1) Values of δ_{25} from ref. D1.
(2) Values of δ_{25} from ref. M5.
(3) Values of δ_{25} from ref. M6.

Chapter VI

A SINGLE ROD INTERPRETATION OF UNCOLLIDED FLUX MEASUREMENTS

6.1 INTRODUCTION

Several experimenters have measured the macroscopic (W8, B3, W9) and intracellular (W8, K1) distributions of uncollided fission neutrons in exponential and critical assemblies. Woodruff (W8) has summarized the evidence that the various foils used in these experiments are sensitive mainly to uncollided fission neutrons. Of special importance, because it is related to the fast fission ratio, is the quantity δ_{28}, whose dependence on fissions in uranium-238 is generally (W10) assumed to occur only through uncollided fission neutrons. Woodruff (W8) has also shown that the first collision kernel in a cylinder provides an excellent representation of the intracellular distributions when the contributions from all fuel rods in the system are summed to give the total flux at any point.

In this chapter, the results of Chapter II are used to evaluate this sum conveniently, by separating it into two physically meaningful components. To do this, it is necessary to have some information about the kernel representing the uncollided flux around a single fuel rod producing fast neutrons. A semi-analytic representation of this kernel will be developed in terms of an infinite series which converges quickly for most problems. It will then be shown that the change in magnitude of the kernel near the fuel rod is so large that theorem A of Chapter II does not apply. However, the kernel decreases monotonically to zero with increasing distance from the source, and its rate of change is slow outside the unit cell in which the source is situated, so that the results of theorem B of Chapter II are applicable. Thus the uncollided flux within a unit cell in a large array consists of a single-rod component whose magnitude varies within the cell and an interaction component whose magnitude is essentially constant throughout the cell. The

variation, within a unit cell, of the uncollided flux computed with this theory is found to be in good agreement with the relative activities measured in intracellular traverses by Woodruff. In addition, the calculated absolute values of the uncollided flux per source neutron are used to calculate δ_{28}, with results which are in excellent agreement with the measured values.

6.2 THEORY

6.2.1 Semi-Analytic Form of the First Collision Kernel for a Cylindrical Fuel Rod

It will be assumed that there is no axial variation of the source strength.

Nomenclature

$R_o \equiv$ Fuel rod radius,

$\vec{r} \equiv$ radius vector of the field point where the flux is to be evaluated,

$\vec{r}_i \equiv$ radius vector of the i^{th} fuel rod,

$N \equiv$ total number of fuel rods in the system,

$s(R) \equiv$ relative source distribution within each fuel rod (normalized to unity at $R = 0$),

$\Sigma_R \equiv$ removal cross section.

The first-flight kernel giving the uncollided flux at r resulting from a unit annular source at R is derived in Appendix A and has been used in purely numerical form by Woodruff (W8). It is:

$$G_A(R, r) = \frac{\Sigma_R}{2\pi} \int_1^\infty K_o(\Sigma_R r y)\, I_o(\Sigma_R R y)\, dy, \qquad r \geq R, \tag{6.1}$$

$$G_B(R, r) = \frac{\Sigma_R}{2\pi} \int_1^\infty K_o(\Sigma_R R y)\, I_o(\Sigma_R r y)\, dy, \qquad r \leq R. \tag{6.2}$$

It is shown in Appendix B that $G_A(R, r)$ may be evaluated in semi-analytic form by using integral representations of the Bessel functions and doing the y integrations first, with the result:

$$G_A(R,r) = \frac{1}{2\pi r}\left\{ C_2(\Sigma_R r) + \left(\frac{R}{r}\right) I_1(\Sigma_R R)\, C_3(\Sigma_R r) + \left(\frac{R}{r}\right)^2 \left[\frac{I_o(\Sigma_R R) + I_2(\Sigma_R R)}{2}\right] C_4(\Sigma_R r) + \ldots \right\}, \quad r \geq R, \tag{6.3}$$

$$G_B(R,r) = \frac{1}{2\pi R}\left\{ C_2(\Sigma_R R) + \left(\frac{r}{R}\right) I_1(\Sigma_R r)\, C_3(\Sigma_R R) + \left(\frac{r}{R}\right)^2 \left[\frac{I_o(\Sigma_R r) + I_2(\Sigma_R r)}{2}\right] C_4(\Sigma_R R) + \ldots \right\}, \quad r \leq R. \tag{6.4}$$

Here, I_n is the modified Bessel function of the first kind and of order n. The C_n functions are defined by the relations:

$$C_n(z) \equiv \int_1^\infty \frac{e^{-zt}}{t^{n-1}\sqrt{1-t^2}}\, dt, \qquad n = 2, 3, 4, \ldots \tag{6.5}$$

and have been evaluated numerically. Graphs and tables of the first few C_n functions are given in Appendix D.

This representation of the kernels has the advantage that, once tables of the C_n functions have been calculated, the computation of the uncollided flux around a fuel rod of any size with any (cylindrically symmetric) source distribution within it is reduced to a hand calculation. The series converges quickly because of the presence of higher powers of $\left(\frac{r}{R}\right)$ in succeeding terms and because C_n is a decreasing function of n. The C_2 term is usually the dominant one so that survey computations may be done with only this term.

The kernel $\phi_{SR}(r, R_o, \Sigma_R)$, which gives the uncollided flux at r around a single fuel rod of radius R_o, is obtained from Eqs. 6.1 and 6.2 by integration over R with the proper source distribution, s(R), within the fuel rod:

$$\phi_{SR}(r, R_o, \Sigma_R) = \int_0^{R_o} dR\; 2\pi R G(R,r)\, s(R). \tag{6.6}$$

This integration has been done with the parabolic source distribution recommended by Woodruff, who showed that it was a good representation of the thermal flux distributions measured at M.I.T. (W8). The result is:

$$\phi^{A}_{SR}(r, R_o, \Sigma_R) = \frac{1}{r}\left\{C_2(\Sigma_R r)S_2(\Sigma_R, R_o) + \frac{C_3(\Sigma_R r)S_3(\Sigma_R, R_o)}{r} + \frac{C_4(\Sigma_R r)S_4(\Sigma_R, R_o)}{r^2} + \ldots\right\}, \quad r \geq R_o, \tag{6.7}$$

$$\phi^{B}_{SR}(r, R_o, \Sigma_R) = \phi^{A}_{SR}(r, r, \Sigma_R) + I_o(\Sigma_R r)\, f_2(\Sigma_R, R_o, r) + r I_1(\Sigma_R r)\, f_3(\Sigma_R, R_o, r) + \ldots, \quad r \leq R_o. \tag{6.8}$$

The S_n and F_n functions are defined by means of integrations over the source distribution within the rod. The defining integrals and specific formulas for the first few S_n and F_n are given in Appendix E. Except when $r = R_o$, Eq. 6.7 converges rapidly, so that two or three terms, at most, are needed. When $r = R_o$, the higher terms may contribute about 10 percent of the total, but this contribution is well-approximated by the techniques developed in Appendix E. Five or six terms are usually needed in Eq. 6.8.

6.2.2 Calculation of the Total Uncollided Flux Within a Unit Cell

The kernel ϕ_{SR}, giving the uncollided flux around a single fuel rod, has been evaluated for rods of one-quarter-inch and three-quarter-inch diameter, respectively, in heavy water. The kernels given in Eqs. 6.7 and 6.8 are defined on the assumption that the medium is homogeneous. This is nearly true in lattices of uranium and water, whose fast removal cross sections are similar. Hence, in computing ϕ_{SR}, the heterogeneity has been approximately accounted for by defining, for each r, an effective removal cross section which gives approximately the correct optical path length between r and the source. This effective removal cross section is identical with that used by Woodruff (W5):

$$\Sigma_{EFF}(r) \equiv \frac{R_o(\Sigma_R)_{FUEL} + (r - R_o)(\Sigma_R)_{MOD}}{r}, \quad r \geq R_o, \tag{6.9}$$

$$\Sigma_{EFF}(r) \equiv (\Sigma_R)_{FUEL}, \quad r < R_o. \tag{6.10}$$

To calculate the actual removal rate of uncollided neutrons at any point, the uncollided flux at that point should be multiplied by the actual

removal cross section at that point, not by Σ_{EFF}. The only use to which Σ_{EFF} should be put is that for which it was specifically designed — to enable one to use in a heterogeneous system a kernel defined for a homogeneous system.

Figures 6.1 and 6.2 show the single rod kernels computed with this procedure. The dimensions of the smallest unit cell used at M.I.T. with each kind of fuel rod are also marked on the figures. It is evident that ϕ_{SR} undergoes a large change within the unit cell immediately surrounding the source rod but that its variation within the other unit cells is not large. Since ϕ_{SR} decreases monotonically to zero, all the conditions of theorem B of Chapter II are satisfied, except that the kernel used here expresses the uncollided flux rather than the reaction rate. Thus:

$$\phi(r) = \phi_{SR}(r) + \frac{F_1 P}{V_c}, \tag{6.11}$$

with:

$$F_1 = \int_{R_c}^{\infty} 2\pi r \, \phi_{SR}(r) \, dr, \tag{6.12}$$

where R_c is the radius of a unit cell. Since the total number of neutrons produced by the single rod is equal to the number which would be removed throughout the medium, were it infinite, we have:

$$\int_0^{R_o} 2\pi R s(R) \, dR = (\Sigma_R)_{FUEL} \int_0^{R_o} 2\pi r \phi_{SR} \, dr + (\Sigma_R)_{MOD} \int_{R_o}^{\infty} 2\pi r \phi_{SR} \, dr, \tag{6.13}$$

so that:

$$F_1 = \frac{1}{(\Sigma_R)_{MOD}} \left\{ \int_0^{R_o} 2\pi R s(R) \, dR - (\Sigma_R)_{FUEL} \int_0^{R_o} 2\pi r \phi_{SR}(r) \, dr - (\Sigma_R)_{MOD} \int_{R_o}^{R_c} 2\pi r \phi_{SR}(r) \, dr \right\}. \tag{6.14}$$

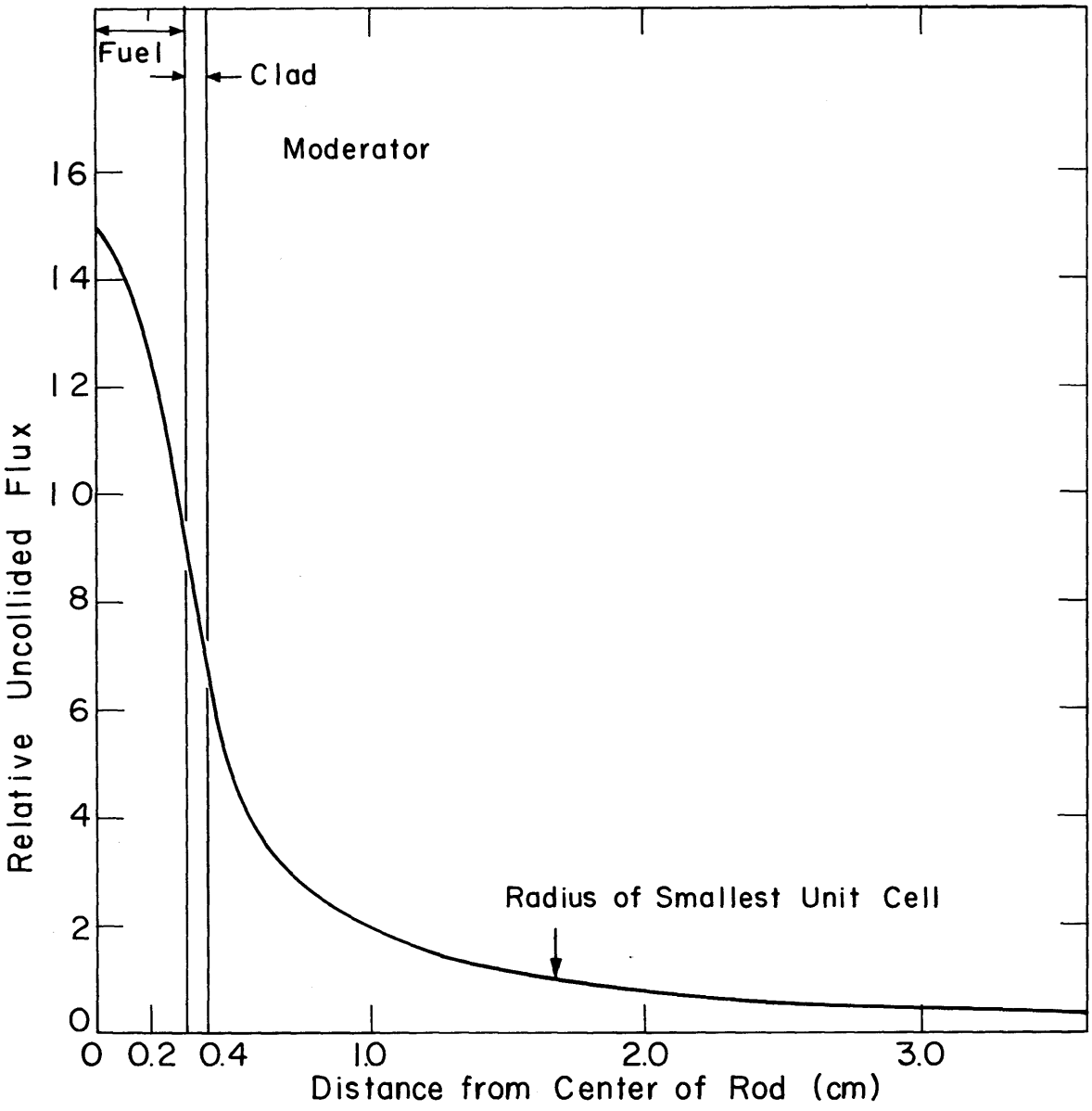

FIG. 6.1 THE SINGLE ROD KERNEL GIVING THE UNCOLLIDED FLUX AROUND A SINGLE, 0.25 INCH DIAMETER, URANIUM ROD IN HEAVY WATER

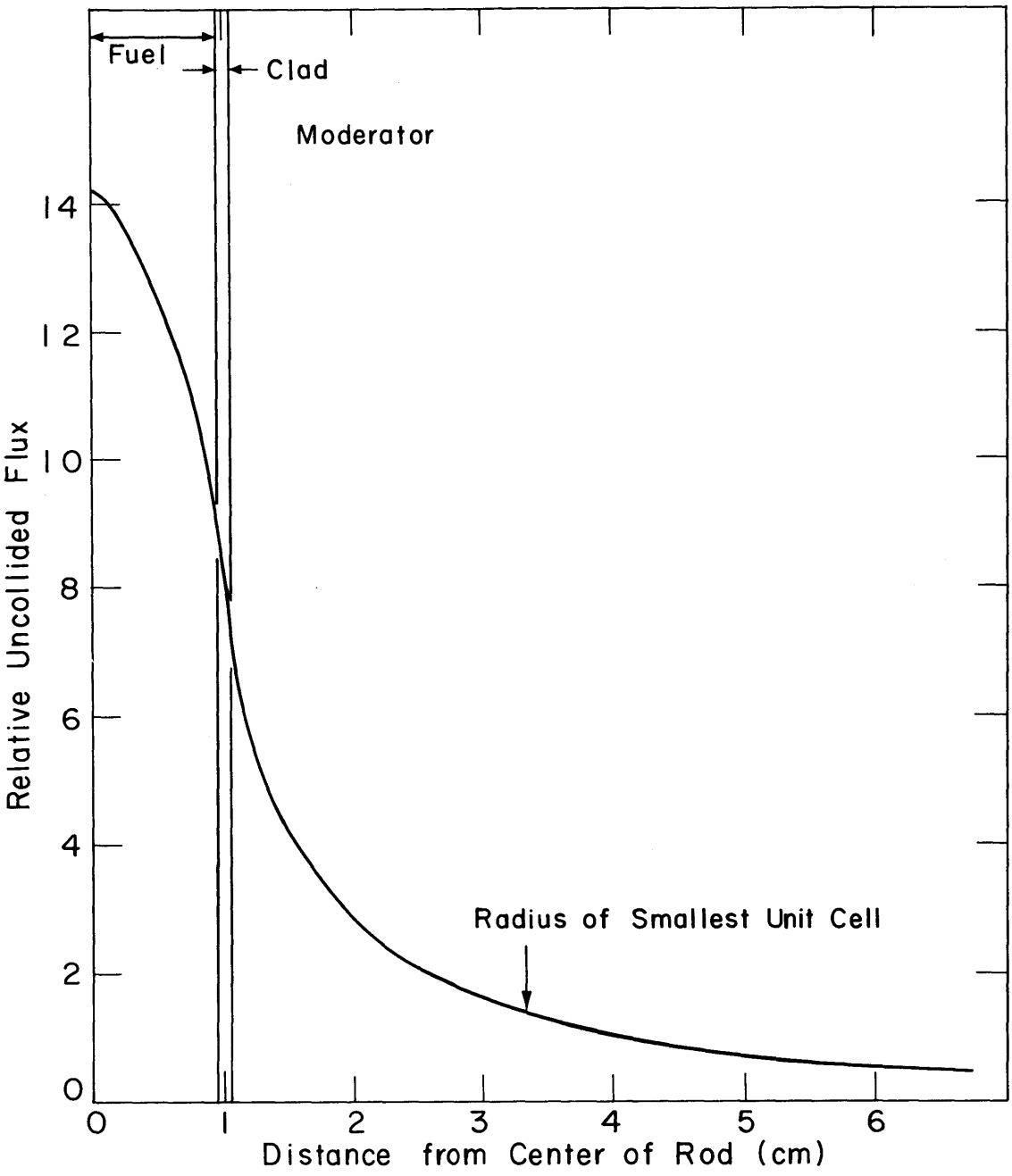

FIG. 6.2 THE SINGLE ROD KERNEL GIVING THE UNCOLLIDED FLUX AROUND A SINGLE, 0.75 INCH DIAMETER, URANIUM ROD IN HEAVY WATER

Thus, F_1 can be evaluated if ϕ_{SR} is known.

The nonleakage probability P, by which the interaction contribution must be multiplied when the system if finite, may be calculated for a macroscopic source distribution which satisfies the wave equation. This is not a restriction since any source distribution can be expanded in eigenfunctions of the wave equation and, in particular, the source distribution in a bare reactor satisfies the wave equation directly. This first-flight nonleakage probability is then (W11):

$$P = \frac{1}{\sqrt{3\tau_F B^2}} \arctan \sqrt{3\tau_F B^2} , \tag{6.15}$$

where B^2 satisfies:

$$\nabla^2 S + B^2 S = 0 . \tag{6.16}$$

The age τ_F is defined as one-sixth the effective mean square distance a neutron travels to first collision. If the medium is homogeneous, this is equivalent to (W11):

$$\tau_F = \frac{2}{\Sigma_R^2} , \tag{6.17}$$

where Σ_R is the average removal cross section of the medium.

6.2.3 Calculation of δ_{28} in Single Fuel Rods and in Lattices

To compute δ_{28} from the preceding results, it is assumed that only uncollided fission neutrons can cause fast fission. Then the number of first generation fast fissions produced per unit length in a fuel rod by one fast neutron from fission in U^{235} is:

$$H = \int_0^{R_o} \phi \Sigma_f \, 2\pi r \, dr, \tag{6.18}$$

or from Eq. 6.11:

$$H = \Sigma_f \int_0^{R_o} dr \, 2\pi r \, \phi_{SR}(r) + \frac{\Sigma_f F_1 P V_F}{V_c} , \tag{6.19}$$

where:

Σ_f = fast fission cross section of uranium fuel,

V_F = volume of fuel rod per unit length.

If we define:

$$\overline{\phi}_{SR} = \frac{1}{V_F} \int_0^{R_o} \phi_{SR}(r)\, 2\pi r\, dr, \tag{6.20}$$

$$\overline{\phi} = \frac{1}{V_F} \int_0^{R_o} \phi(r)\, 2\pi r\, dr, \tag{6.21}$$

Eq. 6.19 becomes:

$$H = \Sigma_f V_F \left(\overline{\phi}_{SR} + \frac{F_1 P}{V_c} \right) = \overline{\phi} V_F \Sigma_f . \tag{6.22}$$

These H fast fissions are not distributed within the fuel rod in the same way as the U^{235} fissions from which they resulted. But δ_{28} is small in a thermal reactor, so that the fractional contribution of later fast neutron generations to δ_{28} is also small. Under these conditions, it suffices to compute the contribution of these later generations by using the same source shape as for the first generation. The total number of fast fissions produced is then:

$$\frac{\text{Total number of fast fissions}}{\text{Fast neutrons from } U^{235} \text{ fission}} = H + \nu_{28} H^2 + \nu_{28}^2 H^3 + \ldots , \tag{6.23}$$

$$= \frac{H}{1 - \nu_{28} H} , \tag{6.24}$$

where ν_{28} is the number of fast neutrons produced per fast fission in U^{238}, averaged over the fission spectrum. The total number of fast fissions per fission in U^{235} is then:

$$\delta_{28} = \frac{\nu_{25} H}{1 - \nu_{28} H} . \tag{6.25}$$

On expanding the denominator and using Eqs. 6.19 and 6.20 to separate $\overline{\phi}$ into single rod and interaction components, we get:

$$\delta_{28} \approx \left\{\nu_{25}\Sigma_f V_F \bar{\phi}_{SR}(1+\nu_{28}\Sigma_f V_F \bar{\phi}_{SR})\right\} + \nu_{25}\Sigma_f F_1 P(1+2\nu_{28}\Sigma_f V_F \bar{\phi}_{SR}) \frac{V_F}{V_c} \cdot \tag{6.26}$$

The term in braces in Eq. 6.26 is the value of δ_{28} in a single, isolated fuel rod. The second term is the interaction contribution to δ_{28}, which depends upon the spacing. In this expression, only terms through the first power in $1/V_c$ have been retained. When $1/V_c$ is changed for a given fuel rod size, the only other terms which vary are F_1 and P, and they vary by only a few percent. Hence, Eq. 6.26 predicts that δ_{28} should be approximately linear with $1/V_c$, a relation which has been observed experimentally.

6.3 RESULTS AND COMPARISON WITH EXPERIMENT

6.3.1 Lattices Studied at M.I.T.

The theory just developed has been applied to some of the lattices which have been studied at M.I.T. Figures 6.3, 6.4 and 6.5 show the relative uncollided flux in lattices consisting of one-quarter-inch diameter, 1.027% enriched uranium rods in heavy water, as calculated from the present theory and as measured by Woodruff. Table 6.1 explains the symbols on the graphs. Table 6.2 gives the cross sections used in the calculation. These are similar to those recommended by Woodruff and, like his, have been chosen to yield the best agreement between the theoretical and experimental microscopic traverses. The value of

Table 6.1

Symbols Used on the Graphs of Relative Activity in Figs. 6.3-6.6

×	$In^{115}(n, n')\ In^{115m}$ Activity
○	$U^{238}(n, f)$ Activity
▽	$Ni^{58}(n, p)\ Co^{58}$ Activity
□	$Zn^{64}(n, p)\ Cu^{64}$ Activity
—	Relative uncollided flux from semi-analytic calculation $[(\Sigma_R)_{FUEL} = 0.1\ cm^{-1},\ (\Sigma_R)_{MOD} = 0.085\ cm^{-1}]$
	All experimental data are from reference W8.

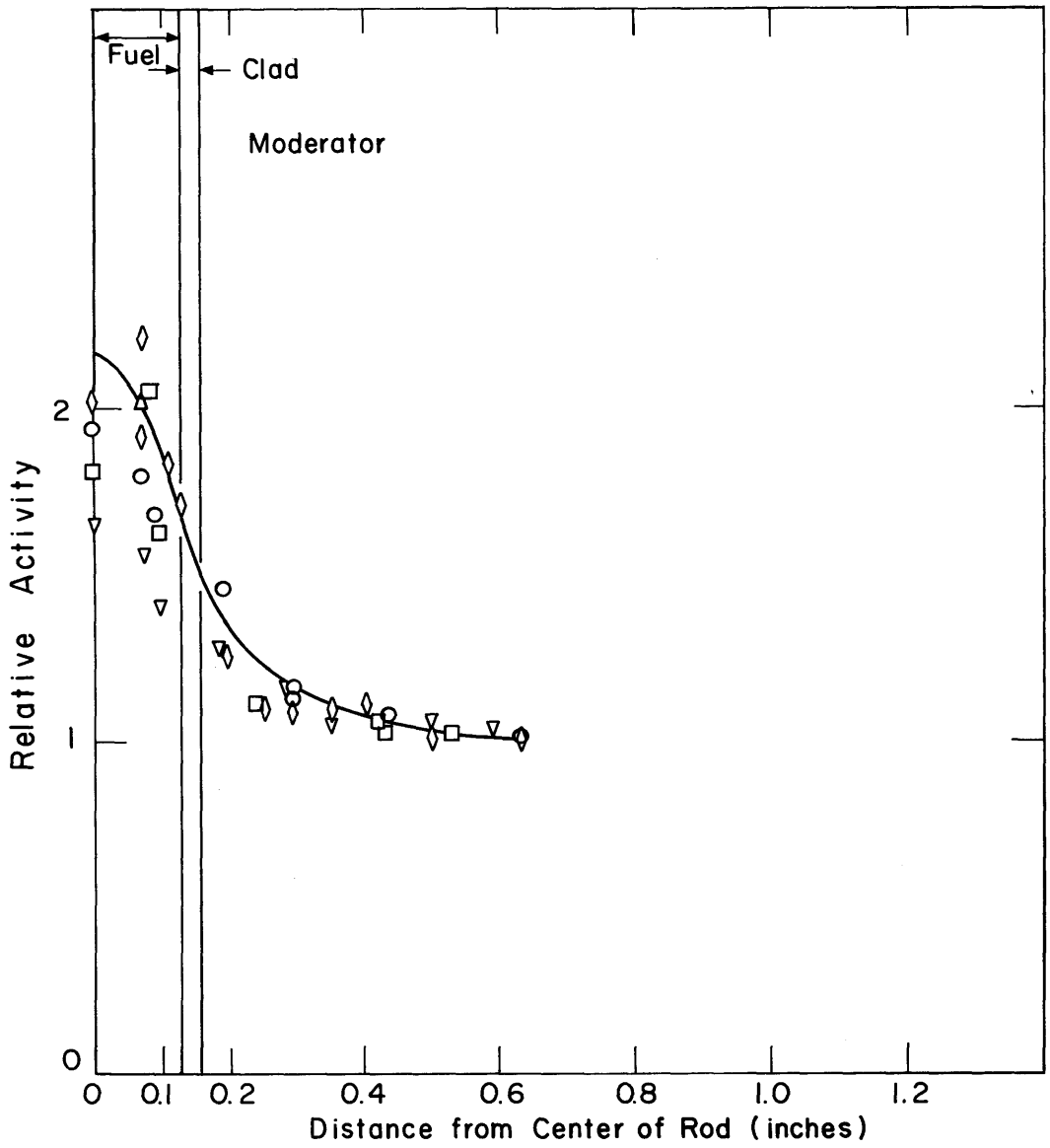

FIG. 6.3 RELATIVE ACTIVITY IN TRIANGULAR LATTICE OF 0.25 INCH DIAMETER, 1.027% ENRICHED URANIUM METAL FUEL RODS ON A 1.25 INCH SPACING IN D_2O

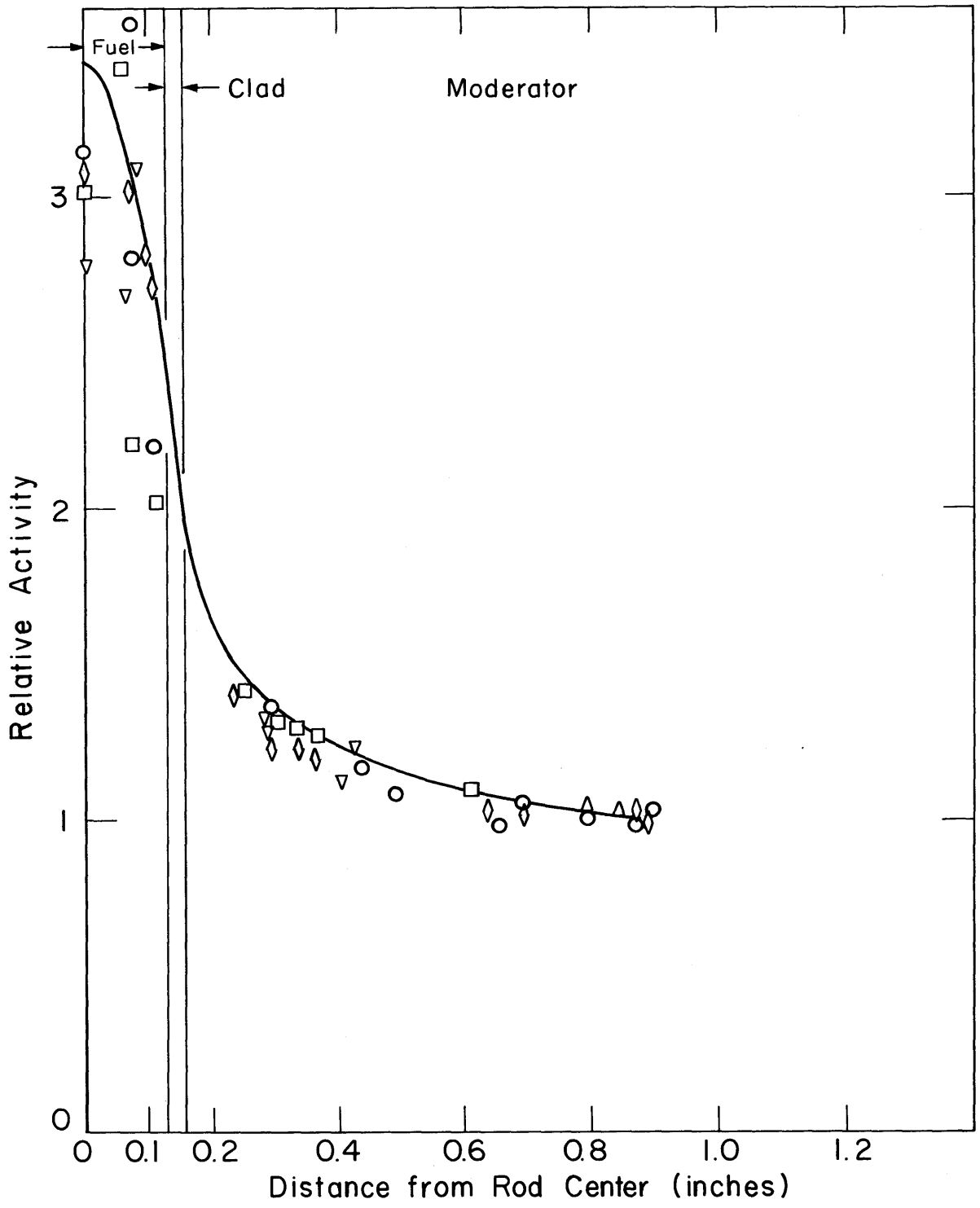

FIG. 6.4 RELATIVE ACTIVITY IN TRIANGULAR LATTICE OF 0.25 INCH DIAMETER, 1.027% ENRICHED URANIUM METAL FUEL RODS ON A 1.75 INCH SPACING IN D_2O

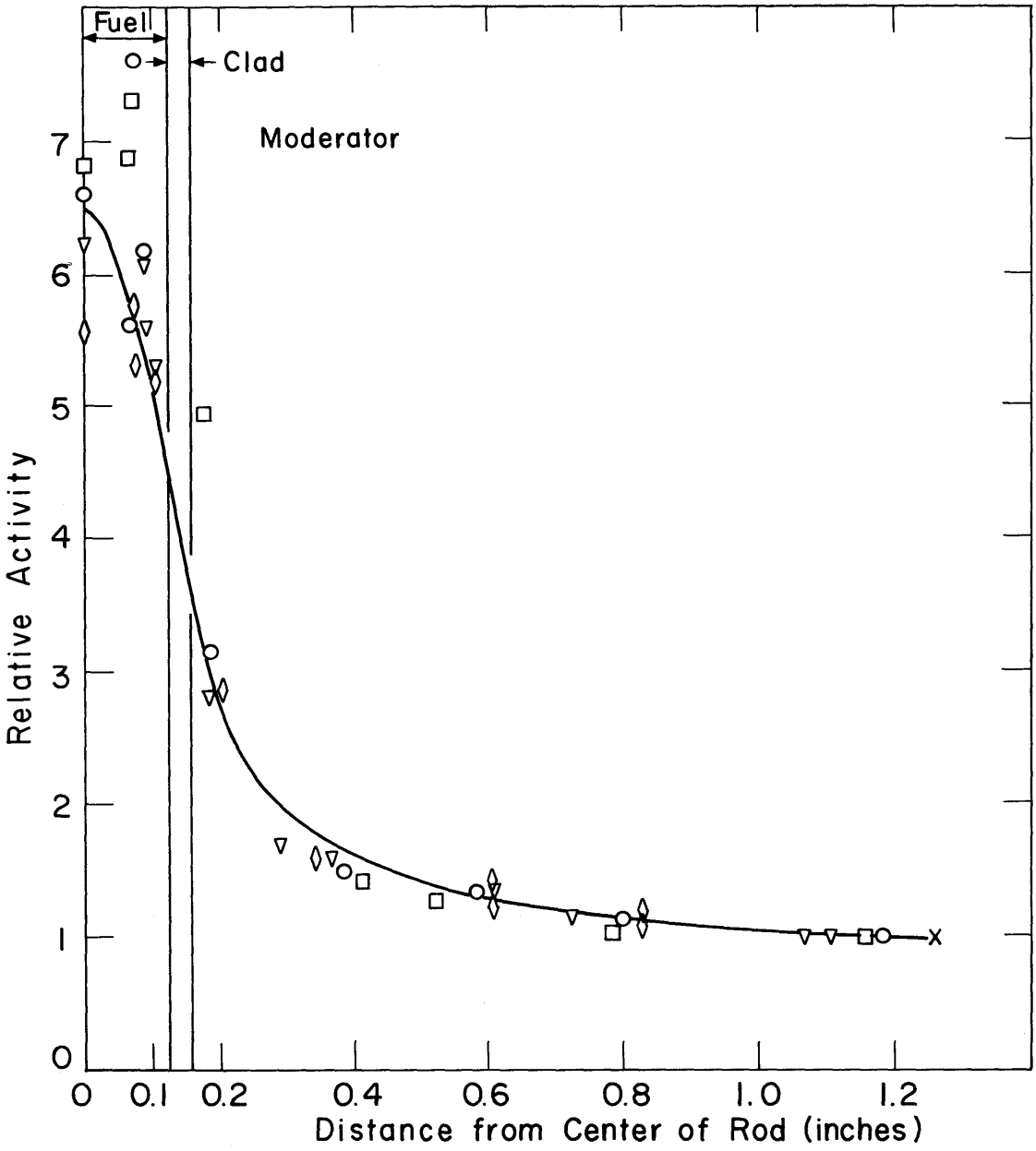

FIG. 6.5 RELATIVE ACTIVITY IN TRIANGULAR LATTICE OF 0.25 INCH DIAMETER, 1.027% ENRICHED URANIUM METAL FUEL RODS ON A 2.50 INCH SPACING IN D_2O

Table 6.2
Nuclear Data Used in Uncollided Flux Calculations

$(\Sigma_R)_{FUEL} = 0.100\ cm^{-1}$
$(\Sigma_R)_{D_2O} = 0.085\ cm^{-1}$
$(\Sigma_R)_{H_2O} = 0.105\ cm^{-1}$
$(\Sigma_R)_{CLAD} = 0$
$\nu_{25} = 2.45$
$\nu_{28} = 2.84$
$\Sigma_f = 0.0146\ cm^{-1}$

$0.085\ cm^{-1}$ for the moderator removal cross section is somewhat lower than the value of 0.0899 recommended by Woodruff. The difference is not considered significant because both values are only estimates of the best value of the cross section. The difficulty in assessing the relative accuracy of the measurements made with each of the four different reactions used to measure the fast flux precluded the use of a least squares method to obtain the "best" value of the cross section. Figure 6.6 shows the relative uncollided flux in a lattice of three-quarter-inch diameter, 0.947% enriched uranium rods in heavy water. The same values of the cross sections also lead to good agreement here.

Values of δ_{28} for these lattices have been computed by means of Eq. 6.25. These, along with the experimentally determined values, are listed in Table 6.3 and are shown in Figs. 6.7 and 6.8. It is evident that the values of δ_{28} calculated with the present theory are in excellent agreement with the measured values, both for single rods and lattices. This suggests that δ_{28} can be calculated for any lattice by means of the theory presented here if the effective removal cross sections in fuel and moderator are known. As the present examples show, these cross sections can be obtained by fitting microscopic traverses made with foils (preferably of U^{238}) sensitive only to uncollided neutrons. The traverses may be made either in a lattice or around a single rod immersed in moderator. Those made in a lattice are preferable because

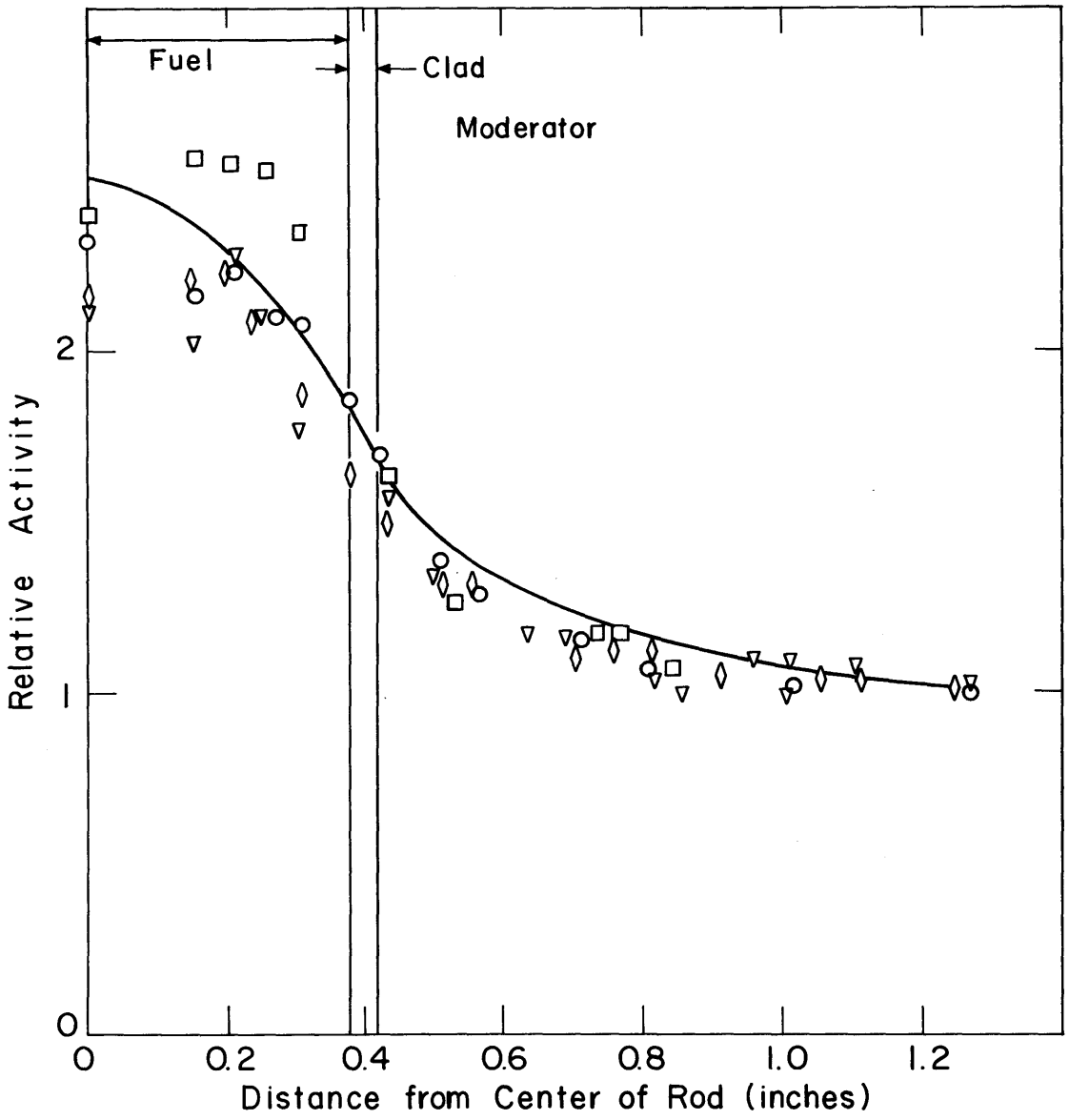

FIG. 6.6 RELATIVE ACTIVITY IN TRIANGULAR LATTICE OF 0.75 INCH DIAMETER, 0.947 % ENRICHED, URANIUM METAL FUEL RODS ON 2.50 INCH SPACING IN D_2O

Table 6.3

Values of δ_{28} for Slightly Enriched Uranium Rods in Heavy Water

Fuel Rod Diameter (Inches)	Fuel Rod Enrichment (%)	Fuel Rod Spacing (Inches)	(V_F/V_c)	δ_{28} (a) (Expt.)	δ_{28} (b) (Calc.)	δ_{28}^{∞} (c) (Calc.)
0.25	1.03	∞	0	0.0133 ±0.0004	0.0140	0.0140
	1.14			0.0151 ±0.0004		
	1.03	2.50	0.009069	0.0183 ±0.0007	0.0166	0.0167
	1.14			0.0164 ±0.0010		
	1.03	1.75	0.01851	0.0217 ±0.0007	0.0200	0.0203
	1.14			0.0204 ±0.0030		
	1.03	1.25	0.03628	0.0274 ±0.0012	0.0265	0.0270
	1.14			0.0265 ±0.0070		
0.75	0.947	∞	0	0.0409 ±0.0012	0.0383	0.0383
		5.0	0.0204	0.0489 ±0.0017	0.0425	0.0428
		3.5	0.0416	0.0516 ±0.0032	0.0490	0.0494
		2.5	0.0816	0.0615 ±0.0021	0.0631	0.0640

(a) From refs. M7 and B3.

(b) From calculations made with the semi-analytic method. Leakage in lattices of finite spacing assumed the same as in critical system.

(c) From calculations made with the semi-analytic method, with no leakage correction.

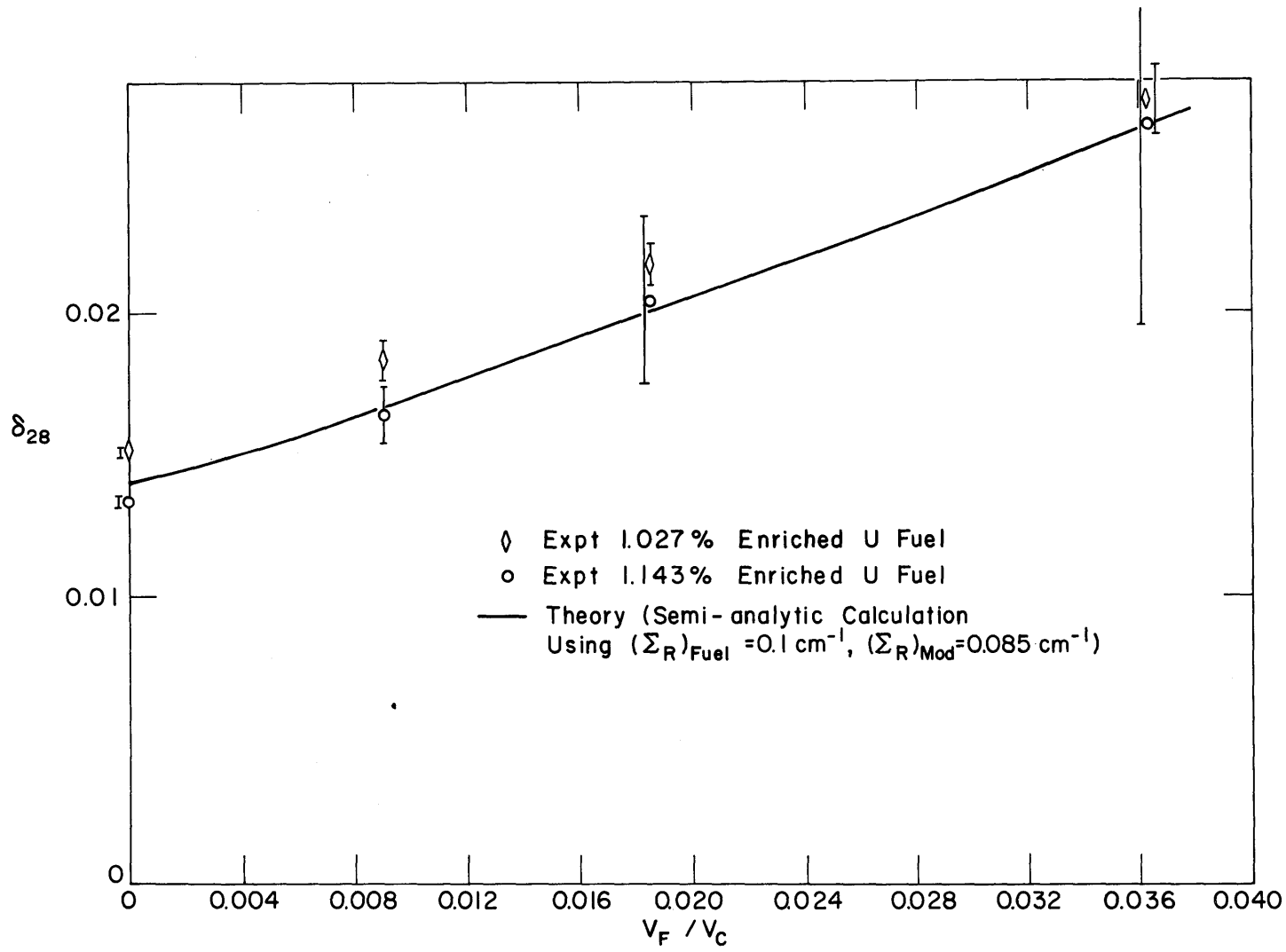

FIG. 6.7 FAST FISSION RATIO VS RATIO OF FUEL VOLUME TO UNIT CELL VOLUME FOR 1/4" DIAM FUEL RODS IN D_2O

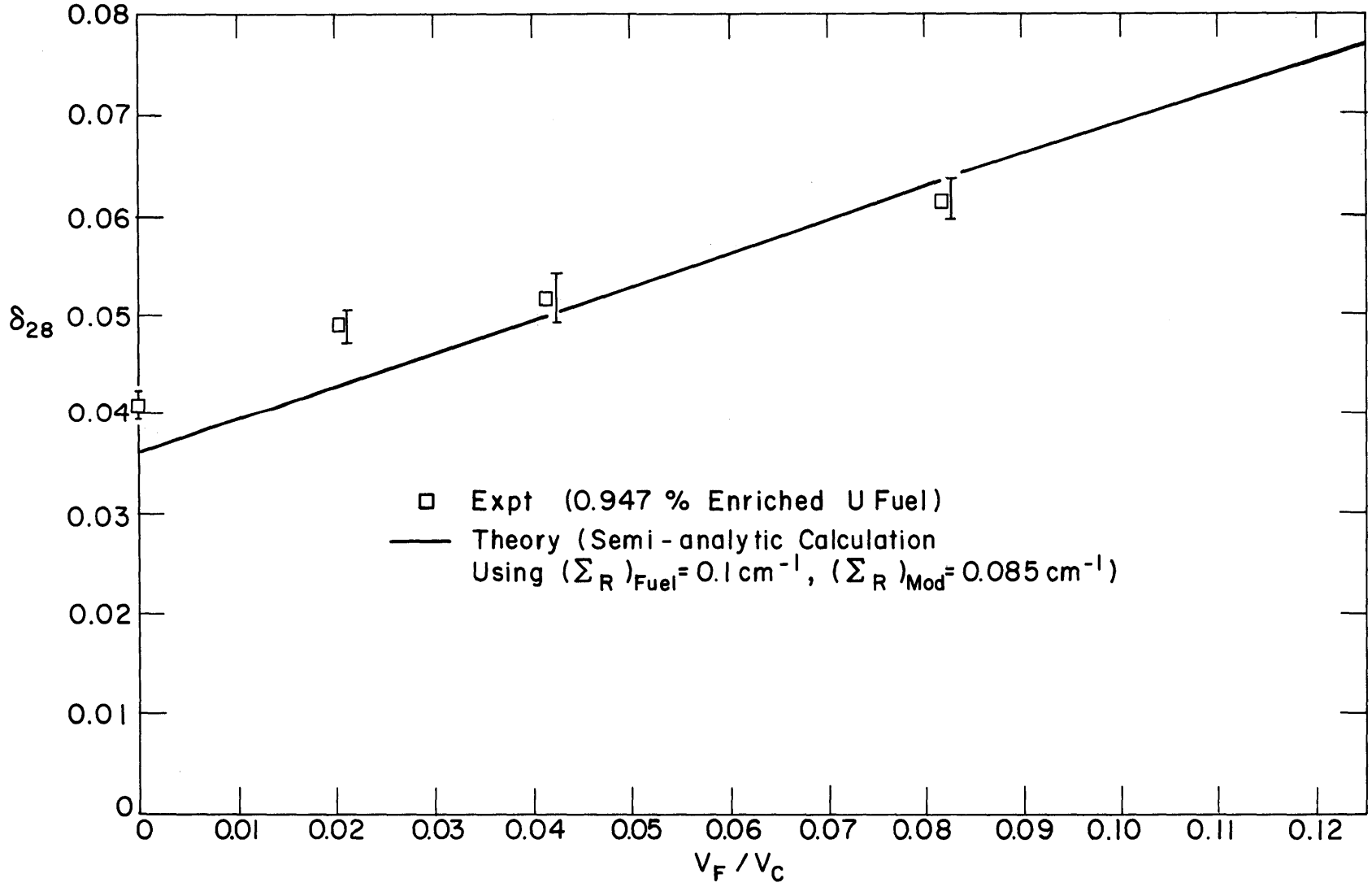

FIG. 6.8 FAST FISSION RATIO VS RATIO OF FUEL VOLUME TO UNIT CELL VOLUME FOR 3/4" DIAM FUEL RODS IN D_2O

the ratio of the activity at the center of the rod to the activity at the edge of the cell is especially sensitive to the moderator removal cross section. Furthermore, cross sections for reactions with uncollided neutrons are small, so that low activity and poor counting statistics may present a problem in the single rod experiment. If the fuel rod is large enough, however, an accurate traverse can be made around it and the cross sections may be obtained from it.

6.3.2 Applications to Light Water Systems

The theory of section 6.2 has also been applied to lattices of slightly enriched uranium rods in light water which have been investigated experimentally at Brookhaven National Laboratory. Table 6.2 gives the cross sections used in the calculations. The removal cross section of uranium has not been changed from the value used in the calculations for heavy water lattices. For the light water, a removal cross section of 0.105 cm^{-1} has been used. This is the value recommended by Woodruff as giving the best agreement between a calculation based on the UNCOL code and the measured microscopic distribution in a lattice of three-eighths-inch rods in light water.

For fuel rods of one-quarter-inch diameter, there are no measurements of uncollided flux with which the theory can be compared, but many measurements of δ_{28} have been made at Brookhaven. Figure 6.9 and Table 6.4 provide a comparison of these measured values of δ_{28} with the values obtained from the theory of section 6.2. Agreement is generally good, although the theoretical curve may have a slightly smaller slope than the experimental points indicate. This difference might be alleviated by the use of slightly different cross sections in the theoretical calculations. The experimental values of δ_{28} are nearly linear with the volume fraction of fuel in the unit cell, as predicted by Eq. 6.26.

Figure 6.10 is a comparison of the values of δ_{28} for these lattices, as predicted by various theories. The present theory, which involves only hand calculations, gives good agreement with the results of the more complicated, and time-consuming, calculations made with the Monte Carlo and multigroup collision probability methods.

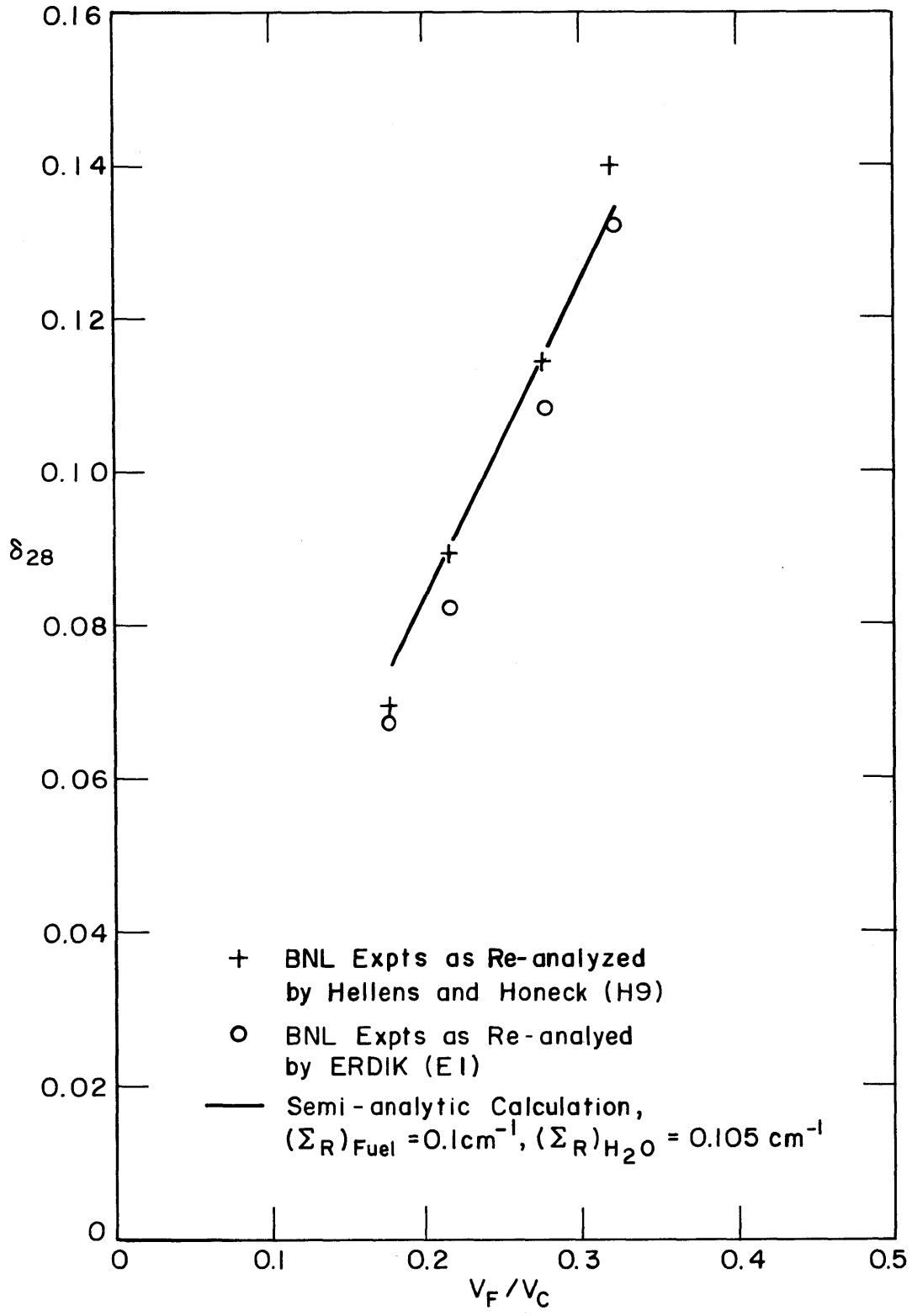

FIG. 6.9 FAST FISSION RATIO, δ_{28}, VS. VOLUME FRACTION OF FUEL IN CELL FOR SLIGHTLY ENRICHED URANIUM RODS, OF 1/4 INCH DIAMETER IN LIGHT WATER

Table 6.4

Values of δ_{28} in Light Water Lattices
0.25-Inch-Diameter Rods, 1.03% Enriched

Water to Uranium Volume Ratio $\frac{V_w}{V_u}$	Fuel to Cell Volume Ratio $\frac{V_F}{V_c}$	δ_{28} Experimental Values		δ_{28}^{∞} Calculated by the Semi-Analytic Method
		(Hellens-Honeck)*	(Erdik)**	
1.5	0.3211	0.140	0.132	0.134
2.0	0.2767	0.114	0.108	0.115
3.0	0.2167	0.089	0.082	0.0898
4.0	0.1781	0.069	0.067	0.0746

* From reference H9.

** From reference E1.

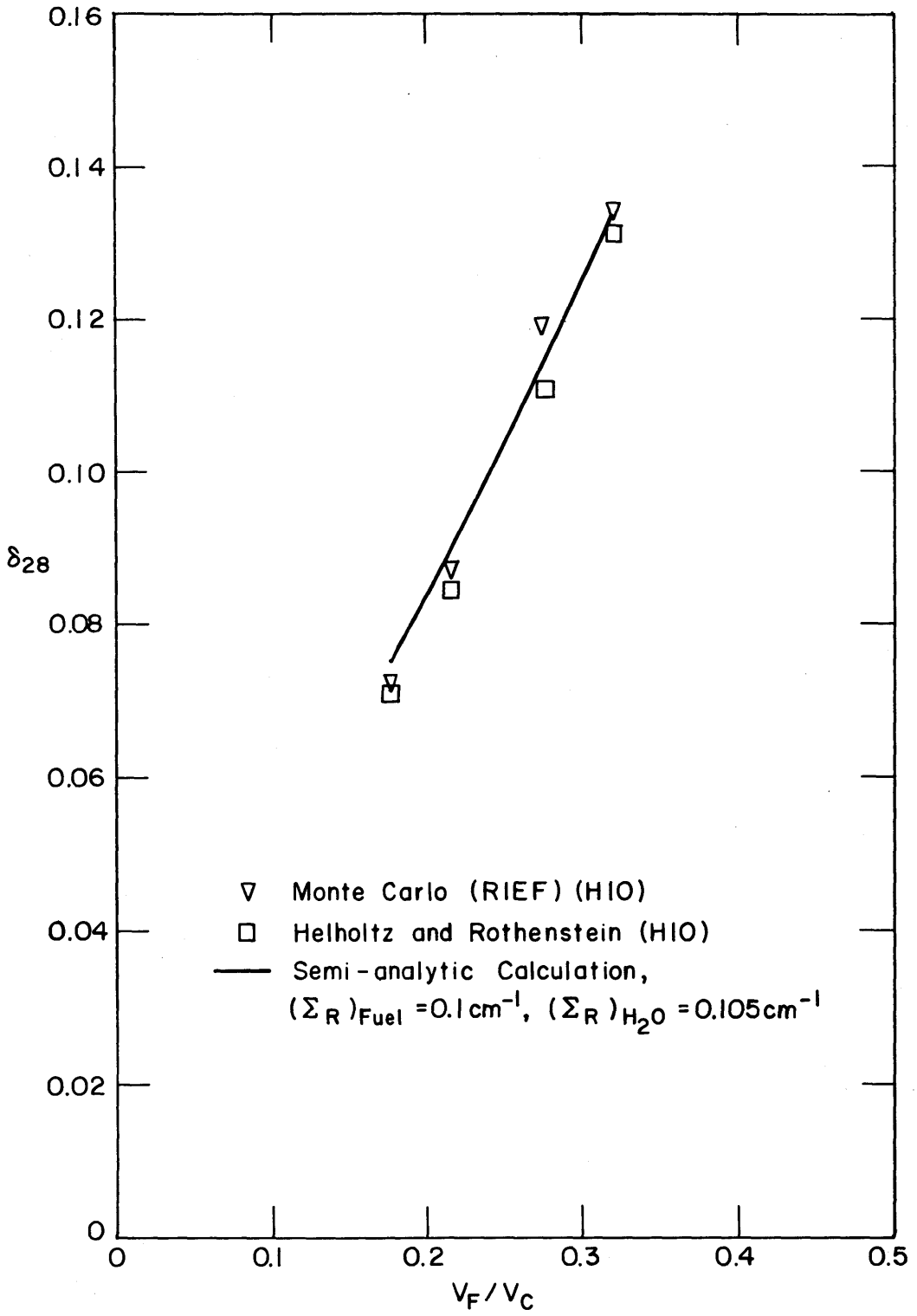

FIG. 6.10 COMPARISON OF CALCULATED VALUES OF δ_{28} FOR 1/4 INCH DIAMETER, SLIGHTLY ENRICHED URANIUM RODS IN LIGHT WATER VS. VOLUME FRACTION OF FUEL IN CELL

Chapter VII

SUMMARY AND RECOMMENDATIONS FOR FURTHER WORK

7.1 INTRODUCTION

In the previous chapters, it has been shown that the Single Element Method of analyzing reactor physics problems produces both useful numerical results and considerable insight into the reactor physics processes occurring in thermal nuclear reactors. This final chapter contains a summary of the results which have been established, together with suggestions for applications to related problems. The chapter will conclude with some comments on the possibility of using these methods to treat other problems in reactor physics.

7.2 THEORETICAL METHODS

The theoretical foundation of the Single Element Method was presented in Chapter II. It was pointed out there that the reaction rate at any point in a unit cell can be viewed as the sum of the reaction rates of neutrons originating in each separate fuel element of the system. These individual reaction rates are simply values of the same kernel function, evaluated at a different argument for each source element and weighted with the relative production rate in that element. The kernel represents the reaction rate per source neutron as a function of distance from the single fuel element providing the source of neutrons. It was then shown that in a large uniform lattice, the sum can be evaluated analytically if the kernel satisfies the important condition that it be a monotonically decreasing function of distance from the single fuel element providing the neutron source. When this condition is satisfied, only the first few terms need be summed explicitly. These terms represent the contribution of neutrons originating from the fuel element in the unit cell where the reaction rate is to be evaluated and from fuel elements in nearby unit cells. The Poisson summation was used to

demonstrate that the sum of all the remaining terms gives a result which is effectively constant throughout the unit cell considered. The number of terms which must be summed explicitly equals the number of unit cells, surrounding and including the one of interest, in each of which the magnitude of the kernel suffers a large fractional change. Two special cases of this result are particularly simple and important. They are useful for a large number of problems in reactor physics.

In the first special case, there are no unit cells within which the kernel experiences a large change in magnitude; thus, the total reaction rate in the unit cell of interest is effectively constant. This state of affairs is found for neutrons in the epithermal energy region of many thermal reactors. The slowing-down density in these reactors is often assumed to be constant within a unit cell, both in treating resonance absorption and in calculating the slowing-down source into the region of thermal energies.

The second special case is that in which the kernel changes magnitude significantly only within the unit cell of interest itself. When this is so, the reaction rate in that cell may be expressed as the sum of a space-dependent term and a space-independent term. The space-dependent term is the kernel which represents the reaction rate of neutrons originating from the fuel element contained in the cell of interest; the space-independent term is a constant which represents the contribution of neutrons originating outside the cell of interest. These are usually denoted as the "single rod" and "lattice" contributions (H9), although there have heretofore been no systematic attempts to calculate their magnitudes from first principles. It was shown in Chapter VI that the distribution of fast neutrons in reactors moderated by light or heavy water is well described by these two terms.

The results of Chapter II thus provide a generalization of the usual assumption that the slowing-down density is constant throughout a unit cell. They show what conditions are required for any reaction rate to be effectively constant across a unit cell, and also what space dependence must be included when these conditions are not met.

Chapters IV, V, and VI comprised the application of this method to the thermal, resonance, and fast neutron energy regions.

7.3 APPLICATIONS IN THE THERMAL REGION

In Chapter IV, an expression was deduced for the value of the thermal utilization in a uniform lattice in terms of a parameter Γ, pertaining to an individual fuel element. This parameter, which is analogous to an impedance, is the ratio of a flux to current. The flux is that subcadmium flux which would exist at the center of the element if all fast neutron sources in the system remained unchanged but if, in the calculation of the subcadmium neutron transport, all fuel elements were replaced by moderator. The current is the actual current of subcadmium neutrons into the element. The parameter depends upon the particular moderator in which the fuel is placed but is essentially independent of neighboring fuel elements and of the boundaries of the system.

It was shown in section 4.2.1 that, in heavy water, values of this parameter can be obtained from experiments around a single fuel rod immersed in moderator. Values of the thermal utilization obtained by this method for lattices of cylindrical, uranium metal rods are given in Table 4.3. On the average, they agree with those obtained from THERMØS to within about 0.3 percent. For these lattices, the method presented here may not be quite as accurate as the ABH method or methods such as THERMØS which solve a discrete form of the transport equation. In lattices composed of more complex fuel elements, the method presented here becomes increasingly attractive because the transport equation becomes increasingly difficult to solve efficiently (in terms of computer time and core storage) as the geometric complexity increases; the single element method characterizes the whole fuel element by the experimentally measured parameter Γ and is thus practically indifferent to the internal structure of the element. In the single element treatment, any lack of cylindrical symmetry inside the fuel element is accounted for in the experimentally measured parameter Γ and need not be considered explicitly in calculating values of the thermal utilization.

It is recommended that the applicability of the single element method to clustered fuel elements in heavy water be verified experimentally. The elements used for the single element experiment should have been fully investigated in lattices, so that measured values of the

thermal utilization are available for comparison. A comparison should also be made with various theoretical methods of calculating values of the thermal utilization of the clusters.

It was pointed out that the SEM is expected to be useful, too, in determining values of the thermal utilization in graphite-moderated lattices but that its usefulness for lattices containing light water is uncertain. These applications should be investigated experimentally and theoretically.

7.4 APPLICATIONS IN THE RESONANCE REGION

In Chapter V, the SEM expression for the slowing-down density in a unit cell was related to the flux by the assumption that $\phi = q/\xi\Sigma_s E$. By this means, expressions were derived for the values of the ratios ρ_{28}, δ_{25}, and C^* in a large, uniformly spaced lattice. The ratios are defined in section 5.1.1. Three results of interest were obtained.

First, these expressions show that in a large, uniform, heavy water lattice, all three ratios are nearly proportional to $1/V_c$, the reciprocal of the volume of a unit cell. It was pointed out that this is of great usefulness in evaluating experimental results because values of a particular ratio, for the same fuel elements at different lattice spacings, should lie on a nearly straight line when plotted against $1/V_c$. This dependence makes it easier both to discern bad or doubtful data and to interpolate experimental values to other lattice spacings. A very useful approximation consists in assuming that the line is exactly straight so that, to establish its position, experiments need be done at only two different lattice spacings. Once determined, the line can be used to estimate values of the ratio of interest for the same fuel elements at any other lattice spacing. It was pointed out that a further saving can result if one of the "lattices" used to establish the position of the line is that lattice for which the abscissa, $1/V_c$, is zero. The physical realization of such a "lattice" is a single fuel element immersed in a large amount of moderator. Thus, measurements on a single fuel element can contribute to the experimental estimation of ρ_{28}, δ_{25}, and C^* in lattices. That such a procedure is indeed feasible is evident from an examination of Figs. 5.10 through 5.15.

The second result of interest is that the formulas derived in Chapter V for ρ_{28} and C^* may be used to evaluate these ratios directly from calculation. The required data for this purpose are: a) the value of the effective age τ_{28} to resonance capture in U^{238}; b) the values of the ratio of cross sections averaged over the subcadmium energy spectrum in the fuel; c) the value of $\eta\epsilon$, the effective number of fast neutrons produced per thermal absorption in the fuel. The age τ_{28} was obtained from an experiment around a single fuel element and was found to be reasonably independent of the size of fuel rod used; values of η were obtained from THERMØS; values of ϵ were obtained from Chapter VI. The values of ρ_{28} and C^* computed in this way were found to agree to about 5 percent with values measured in the large exponential at M.I.T.

The third result of interest is that values of δ_{25} measured in lattices in the large exponential at M.I.T. can be used with the single element formula to obtain values of the fission resonance integral of U^{235} in lattices. Values of the fission resonance integral found in this way exhibited no systematic trend with lattice spacing. The average value was in excellent agreement with the infinite dilution value given in the Second Supplement to the Second Edition of BNL-325.

Several plots of data obtained at other laboratories for different moderators were included in Chapter V. The expected linear dependence was observed in all cases.

The single element expressions for the ratios involve the ERI's for resonance capture in U^{238}. These vary with the lattice spacing, but no extensive set of measurements has ever been made in heavy water lattices. It is therefore recommended that a program be instituted to measure resonance integrals in lattices. The effect of the lattice spacing is small but should be resolvable in a careful experiment designed for that purpose. In one-quarter-inch-diameter rods, for example, theory (S5) predicts that the resonance integral changes from 17.77 barns for an isolated rod to 16.95 barns in a lattice with a triangular spacing of 1.25 inches. The values obtained for the resonance

integrals should be compared with values from Kier's theoretical calculation (K3).

7.5 APPLICATIONS IN THE HIGH ENERGY REGION

In Chapter VI, a semi-analytic expression for the first-flight kernel was developed. Using the methods of Chapter II, it was shown that the uncollided flux within a unit cell in a large, uniform array may be expressed as the sum of a single element component, arising in the fuel element contained in the cell of interest, and a lattice component, arising from all other fuel elements in the system. Throughout the unit cell of interest, the lattice component is constant and inversely proportional to cell volume. The constant of proportionality varies slightly with lattice spacing and may be determined, as shown in section 2.2.5, from an integration over the single element component.

Formulas expressing the spatial dependence of the single element component were developed in Appendix B by an expansion of the first-flight kernel for infinitely long annular sources. The expansion is useful in obtaining numerical results and also shows clearly how the kernel for an annular or cylindrical source reduces to that for a line source at large enough distances from the source. This expansion was used in section 6.3 to evaluate the single element and lattice contributions to the uncollided flux in the heavy water lattices studied at M.I.T. The predicted spatial dependence of the uncollided flux agrees well with that obtained experimentally by G. Woodruff (W8). This flux was used with a theoretically developed fission cross section to compute values of δ_{28} in these lattices. The results are in good agreement with the measured values, as shown in Table 6.3. Because of its dependence on the uncollided flux, δ_{28} was shown theoretically to exhibit a linear dependence on the inverse of unit cell volume, and this was verified in Figs. 6.7 and 6.8 by comparison with the results of experiments made in the exponential assembly.

It was pointed out that the only parameter appearing in the single collision kernel is the removal cross section of the moderator. This can be determined from an experimental measurement of the uncollided

flux distribution near a single element immersed in moderator and can then be used in the calculation of δ_{28}.

The same method was used in analyzing experiments on uranium metal rods in light water. Again, the resulting values of δ_{28}, shown in Fig. 6.9, were in good agreement with the experimental results.

The method presented here is extremely useful, since it yields results having an accuracy comparable to more complicated methods but requiring only a modest amount of time and computation. Even if more complicated models, such as Woodruff's UNCOL code (W8), are employed, the use of the expansion presented (in Appendices B and E) for the first-flight kernel should save considerable computer time.

7.6 SUMMARY AND SUGGESTIONS FOR FURTHER APPLICATIONS

It has been shown that use of the single element method is advantageous in several ways. First, it permits the data to be presented in a particularly lucid and meaningful way. Second, it suggests methods by which values of various parameters in lattices may be obtained by experiments on single fuel elements. Such experiments have the advantage of automatically including any complicating effects which may arise because of the complex structure of an individual fuel element. Third, the single element method suggests new and useful computational procedures for evaluating reactor parameters theoretically.

Of the advantages suggested in Chapter I for the Single Element Method, only its applicability to clustered fuel elements and to nonuniform arrays has not been demonstrated here. Because the method works so well for lattices of individual fuel rods in heavy water, its use should be investigated for lattices of clustered fuel elements in heavy water. The possibility of analyzing nonuniform arrays by the Single Element Method may be particularly valuable in considering multiregion reactors. The theoretical analysis in Chapter II suggests that a region which is far enough from the unit cell of interest contributes only a space-independent background to the neutron density within that cell.

The applicability of the Single Element Method to the regions of thermal and resonance energies in light water reactors ought to be

investigated. The results of Klahr et al. (K2) on the use of self-consistent kernels obtained from experiments on full lattices and the straight lines which appear in Figs. 5.1 to 5.3 of the present report suggest that the SEM will prove useful. It is not yet clear just how accurately kernels for light water lattices can be obtained from experiments on single fuel rods, and this problem should be studied by experiment.

Finally, the SEM may be useful in studying the reactor physics of fuel which has undergone considerable burnup. This would be especially valuable because the high radiation levels of such fuel preclude the use of full exponential or critical assemblies for detailed studies in reactor physics.

Appendix A

DERIVATION OF THE FIRST COLLISION KERNEL FOR AN INFINITELY LONG ANNULAR SOURCE IN A HOMOGENEOUS MEDIUM

The first collision kernel expressing the uncollided flux from an annular source of infinitesimal thickness will be derived, starting with the first collision kernel for a point source. The kernel for a line source will be derived first, and from it the kernel for an annular source will be derived. The system is assumed to be infinitely long in the axial direction; the source is uniform along its length and is normalized to one source neutron per unit length of source. The medium is homogeneous, with a removal cross section of Σ.

Consider the geometry shown in Fig. A.1. The line source lies along the z axis. The kernel $G_\ell(r)$, representing the uncollided flux at radius r, may be expressed as an integral over the kernel for a point source:

$$G_\ell(r) \equiv \int_{-\infty}^{\infty} \frac{dz\ e^{-\Sigma\rho}}{4\pi\rho^2}. \tag{A.1}$$

By means of the relation:

$$z^2 = \rho^2 - r^2, \tag{A.2}$$

Eq. A.1 may be put into the form of an integral over z:

$$G_\ell(r) = 2\int_{r}^{\infty} \frac{d\rho\ \rho e^{-\Sigma\rho}}{4\pi\rho^2\sqrt{\rho^2 - r^2}}, \tag{A.3}$$

and with the further substitution:

$$u = \frac{\rho}{r}, \tag{A.4}$$

the expression for the kernel becomes:

$$G_\ell(r) = \frac{1}{2\pi}\int_{1}^{\infty} \frac{du\ e^{-\Sigma ru}}{ru\sqrt{u^2 - 1}}. \tag{A.5}$$

But:

$$\frac{e^{-\Sigma ru}}{ru} = \Sigma \int_1^\infty dy\, e^{-\Sigma ruy}, \tag{A.6}$$

which may be introduced into Eq. A.5, with the result:

$$G_\ell(r) = \frac{1}{2\pi} \int_1^\infty \frac{du\, \Sigma}{\sqrt{u^2 - 1}} \int_1^\infty dy\, e^{-\Sigma ruy}. \tag{A.7}$$

When the order of integration is interchanged in Eq. A.7, one gets:

$$G_\ell(r) = \frac{\Sigma}{2\pi} \int_1^\infty dy \int_1^\infty \frac{du\, e^{-\Sigma ryu}}{\sqrt{u^2 - 1}}. \tag{A.8}$$

But the zeroeth order modified Bessel function of argument z is defined as (W5):

$$K_o(z) = \int_1^\infty \frac{du\, e^{-zu}}{\sqrt{u^2 - 1}}, \tag{A.9}$$

so that:

$$G_\ell(r) = \frac{\Sigma}{2\pi} \int_1^\infty dy\, K_o(\Sigma ry), \tag{A.10}$$

which is the desired expression for the line kernel and agrees with that given by Weinberg and Wigner (W4).

The first collision kernel for an annular source may be expressed as an integral over line source kernels. Consider the geometry shown in Fig. A.2. The kernel G(R, r), giving the uncollided flux at r from an annular source of unit strength and of radius R, is:

$$G(R, r) = \frac{\int_0^{2\pi} G_\ell(w)\, R d\theta}{\int_0^{2\pi} R d\theta}, \tag{A.11}$$

where the denominator effects the normalization to unit source strength. By means of the cosine law:

$$w^2 = R^2 + r^2 - 2Rr \cos\theta, \tag{A.12}$$

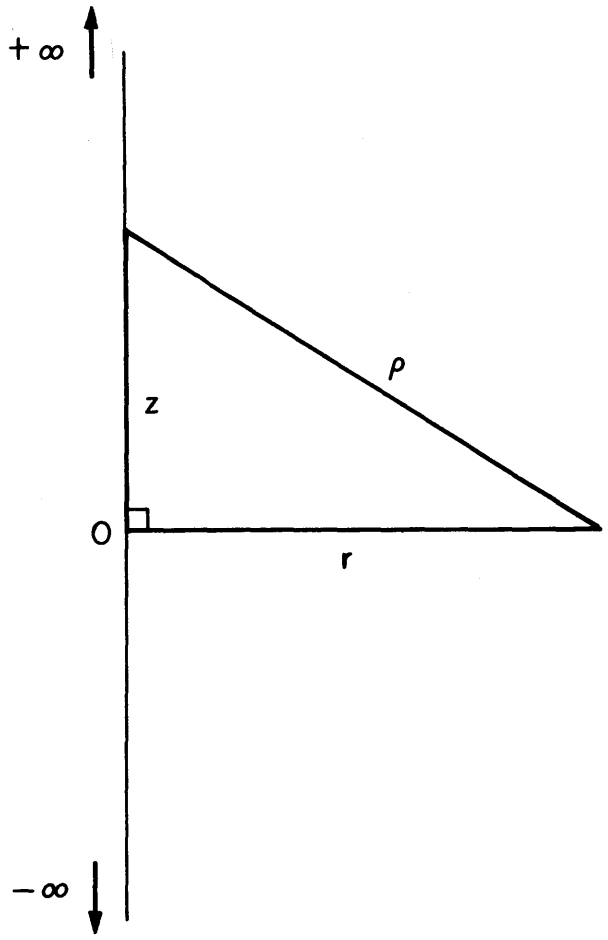

FIG. A.1 GEOMETRIC CONFIGURATION USED IN DERIVING THE FIRST FLIGHT KERNEL FOR A LINE SOURCE

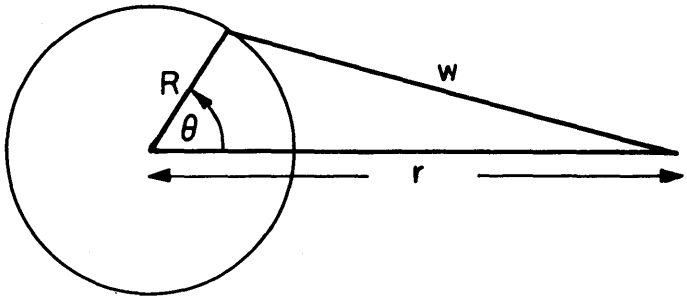

FIG. A2 GEOMETRIC CONFIGURATION USED IN DERIVING THE FIRST FLIGHT KERNEL FOR AN ANNULAR SOURCE

and Eq. A.10, the kernel for the annular source may be expressed as:

$$G(R, r) = \frac{\Sigma}{(2\pi)^2} \int_0^{2\pi} d\theta \int_1^{\infty} K_o(\Sigma w y)\, dy, \tag{A.13}$$

$$G(R, r) = \frac{\Sigma}{(2\pi)^2} \int_0^{2\pi} d\theta \int_1^{\infty} K_o\left(\Sigma y \sqrt{R^2 + r^2 - 2Rr\cos\theta}\,\right) dy. \tag{A.14}$$

When the order of integration is changed, this becomes:

$$G(R, r) = \frac{\Sigma}{(2\pi)^2} \int_1^{\infty} dy \int_0^{2\pi} d\theta\, K_o\left(\Sigma y \sqrt{R^2 + r^2 - 2Rr\cos\theta}\,\right). \tag{A.15}$$

But by the addition theorem for Bessel functions (W16):

$$K_o\left(\Sigma y \sqrt{R^2 + r^2 - 2Rr\cos\theta}\,\right) = \sum_{m=-\infty}^{\infty} K_m(\Sigma y r)\, I_m(\Sigma y R)\cos m\theta. \tag{A.16}$$

When this result is substituted into Eq. A.15 and the integration over θ is done, only the m=0 term will yield a nonzero result because:

$$\int_0^{2\pi} d\theta \cos m\theta = \begin{cases} 0, & m = \pm 1, \pm 2, \ldots \\ 2\pi, & m = 0 \end{cases} \tag{A.17}$$

The result is:

$$G_A(R, r) = \frac{\Sigma}{2\pi} \int_1^{\infty} K_o(\Sigma r y)\, I_o(\Sigma R y)\, dy, \qquad r \geq R, \tag{A.18}$$

which is the desired result and agrees with the form given by Weinberg and Wigner (W4). This kernel is labelled with the subscript "A" to denote that it is valid only when $r \geq R$.

When $r \leq R$, the roles of R and r must be interchanged in the addition theorem, Eq. A.12. The net result is to interchange r and R in the final form of the kernel:

$$G_B(R, r) = \frac{\Sigma}{2\pi} \int_1^{\infty} dy\, K_o(\Sigma R y)\, I_o(\Sigma r y)\, dy, \qquad r \leq R. \tag{A.19}$$

Appendix B

SEMI-ANALYTIC FORM OF THE FIRST COLLISION KERNEL FOR AN ANNULAR SOURCE IN A HOMOGENEOUS MEDIUM

The first collision kernel describes the spatial dependence of the uncollided flux from a unit source in a homogeneous medium. In Appendix A, an exact but numerically intractable expression was derived for the first collision kernel in the case of an annular source of infinitesimal thickness and infinite length. The source distribution along the length of the annulus was assumed to be uniform. In this appendix, the exact expression for the kernel will be reduced to a numerically useful and physically meaningful approximation. There are three cases:

Case A. Field Point Outside the Annular Source

The kernel, as derived in Appendix A, is:

$$G_A(R, r) = \frac{\Sigma}{2\pi} \int_1^\infty dy\, K_o(\Sigma r y)\, I_o(\Sigma R y), \qquad r \geq R . \tag{B.1}$$

For the Bessel functions, we substitute the integral representations (W5):

$$K_o(\Sigma r y) = \int_1^\infty \frac{dt\, e^{-(\Sigma r y)t}}{\sqrt{t^2 - 1}}, \tag{B.2}$$

$$I_o(\Sigma R y) = \frac{1}{\pi} \int_{-1}^{+1} \frac{dx\, e^{-(\Sigma R y)x}}{\sqrt{1 - x^2}} . \tag{B.3}$$

Doing the integration over y in Eq. B.1 now gives:

$$G_A(R, r) = \frac{\Sigma}{2\pi} \frac{1}{\pi} \int_{-1}^{+1} \frac{dx\, e^{-\Sigma R x}}{\sqrt{1 - x^2}} \int_1^\infty \frac{dt\, e^{-\Sigma r t}}{\sqrt{t^2 - 1}} \frac{1}{\Sigma R x + \Sigma r t} . \tag{B.4}$$

We now use the expansion:

$$\frac{1}{\Sigma Rx + \Sigma rt} = \frac{1}{\Sigma rt\left(1 + \frac{Rx}{rt}\right)}, \tag{B.5}$$

$$\frac{1}{\Sigma Rx + \Sigma rt} = \frac{1}{\Sigma rt}\left\{1 - \left(\frac{Rx}{rt}\right) + \left(\frac{Rx}{rt}\right)^2 - \left(\frac{Rx}{rt}\right)^3 + \ldots\right\}, \tag{B.6}$$

which is valid since:

$$\left|\frac{Rx}{rt}\right| \leq 1 \tag{B.7}$$

because:

$$\left.\begin{aligned} &R \leq r, \\ &|x| \leq 1, \\ &t > 1, \end{aligned}\right\} \tag{B.8}$$

and the expansion:

$$\frac{1}{\sqrt{t^2 - 1}} = \frac{1}{t\sqrt{1 - \left(\frac{1}{t}\right)^2}}, \tag{B.9}$$

$$\frac{1}{\sqrt{t^2 - 1}} = \frac{1}{t}\left\{1 + \frac{1}{2}\left(\frac{1}{t}\right)^2 + \frac{3}{8}\left(\frac{1}{t}\right)^4 + \ldots + \frac{(2n-1)(2n-3)\ldots(1)}{2^n n!}\left(\frac{1}{t^2}\right)^n + \ldots\right\}. \tag{B.10}$$

When the resulting expressions are grouped according to powers of x, the result is:

$$\begin{aligned} G_A(R, r) = \frac{1}{2\pi r}\frac{1}{\pi}\int_{-1}^{+1}\frac{e^{-\Sigma Rx}}{\sqrt{1 - x^2}}\Bigg[&\int_1^\infty \frac{dt\ e^{-\Sigma rt}}{t^2}\left\{1 + \frac{1}{2}\left(\frac{1}{t}\right)^2 + \frac{3}{8}\left(\frac{1}{t}\right)^4 + \ldots\right\} \\ &- \left(\frac{Rx}{r}\right)\int_1^\infty \frac{e^{-\Sigma rt}}{t^3}\left\{1 + \frac{1}{2}\left(\frac{1}{t}\right)^2 + \frac{3}{8}\left(\frac{1}{t}\right)^4 + \ldots\right\} \\ &+ \left(\frac{Rx}{r}\right)^2\int_1^\infty \frac{e^{-\Sigma rt}}{t^4}\left\{1 + \frac{1}{2}\left(\frac{1}{t}\right)^2 + \frac{3}{8}\left(\frac{1}{t}\right)^4 + \ldots\right\} - \ldots\Bigg]. \end{aligned} \tag{B.11}$$

With the definition:

$$C_n(z) = \int_1^\infty \frac{dt\, e^{-zt}}{t^n} \left\{ 1 + \frac{1}{2}\left(\frac{1}{t}\right)^2 + \frac{3}{8}\left(\frac{1}{t}\right)^4 + \ldots \right\} ; \tag{B.12}$$

the kernel becomes:

$$G_A(R, r) = \frac{1}{2\pi r} \frac{1}{\pi} \int_{-1}^{+1} \frac{dx\, e^{-\Sigma R x}}{\sqrt{1 - x^2}} \left[C_2(\Sigma r) - \left(\frac{Rx}{r}\right) C_3(\Sigma r) \right.$$

$$\left. + \left(\frac{Rx}{r}\right)^2 C_4(\Sigma r) + \ldots + (-1)^n \left(\frac{Rx}{r}\right)^n C_{n+2}(\Sigma r) + \ldots \right] . \tag{B.13}$$

But from Eq. B.3 defining the integral representation of I_o, there follows:

$$\frac{1}{\pi} \int_{-1}^{+1} dx \frac{x^k\, e^{-zx}}{\sqrt{1 - x^2}} = (-1)^k \frac{d^k}{dz^k} [I_o(z)] . \tag{B.14}$$

Thus:

$$G_A(R, r) = \frac{1}{2\pi r} \left\{ I_o(\Sigma R)\, C_2(\Sigma r) + \left(\frac{R}{r}\right) I_o'(\Sigma R)\, C_3(\Sigma r) \right.$$

$$+ \left(\frac{R}{r}\right)^2 I_o''(\Sigma R)\, C_4(\Sigma r) + \ldots$$

$$\left. + \left(\frac{R}{r}\right)^n I_o^{(n)}(\Sigma R)\, C_{n+2}(\Sigma r) + \ldots \right\} . \tag{B.15}$$

Each function here is the weighted sum of an infinite series of exponential integrals. The convergence of this sum is examined in Appendix F.

The derivatives of the Bessel functions can be expressed in terms of the Bessel functions, themselves, by using (A1):

$$I_o^{(k)}(z) = \frac{1}{2^k} \left\{ I_{-k} + \binom{k}{1} I_{-k+2} + \binom{k}{2} I_{-k+4} + \ldots + \binom{k}{k} I_k \right\} , \tag{B.16}$$

and:

$$I_{-k}(z) = I_k(z), \tag{B.17}$$

so that the first few derivatives become:

$$I_o'(z) = I_1(z), \tag{B.18}$$

$$I_o''(z) = \frac{I_o(z) + I_2(z)}{2}, \tag{B.19}$$

$$I_o'''(z) \equiv \frac{3I_1(z) + I_3(z)}{4}, \tag{B.20}$$

$$I_o^{(IV)}(z) = \frac{3I_o(z) + 4I_2(z) + I_4(z)}{8}. \tag{B.21}$$

Case B. Field Point Enclosed by the Annular Source

The kernel, as derived in Appendix A, is:

$$G_B(R, r) = \frac{\Sigma}{2\pi} \int_1^\infty dy\, K_o(\Sigma R y)\, I_o(\Sigma r y), \qquad r \leq R. \tag{B.22}$$

This is just the form given in Eq. B.1, except that R and r have been interchanged. However, r is now smaller than R, so that all the previous manipulations are still valid and G_B may be obtained by interchanging R and r in Eq. B.15:

$$G_B(R, r) = \frac{1}{2\pi R}\left\{ C_2(\Sigma R) I_o(\Sigma r) + \left(\frac{r}{R}\right) C_3(\Sigma R) I_o'(\Sigma r) + \left(\frac{r}{R}\right)^2 C_4(\Sigma R) I_o''(\Sigma r) + \ldots + \left(\frac{r}{R}\right)^n I_o^{(n)}(\Sigma r)\, C_{n+2}(\Sigma R) + \ldots \right\}. \tag{B.23}$$

Case C. Semi-Analytic Form of the Line Source First-Flight Kernel

The annular source kernel reduces to a line source kernel when the radius of the annulus is zero. Alternatively, from the definition of the line source kernel given in Appendix A:

$$G_\ell(r) = \frac{\Sigma}{2\pi} \int_1^\infty dy\, K_o(\Sigma r y), \tag{B.24}$$

it is clear that:

$$G_{\ell}(r) = G_A(0, r) \ . \tag{B.25}$$

From Eq. B.15, this is:

$$G_{\ell}(r) = \frac{C_2(\Sigma r)}{2\pi r} \ . \tag{B.26}$$

This form of the kernel displays clearly the line singularity at $r = 0$. $C_2(\Sigma r)$ accounts for attenuation by removal, since the total geometric attenuation appears in the denominator.

Appendix C

PROPERTIES OF THE FIRST COLLISION KERNELS AND OF THE C_n FUNCTIONS USED IN THE SEMI-ANALYTIC FORMS OF THE KERNELS

Several useful properties of the first collision kernels derived in Appendix A and of the C_n functions defined by Eq. B.12 will be demonstrated. These properties follow from mathematical manipulations of the defining expressions.

Property (i):

$C_n(z)$ is a positive, smooth, monotonically decreasing function of z. This is clear from the definition:

$$C_n(z) = \int_1^\infty \frac{dt\, e^{-zt}}{t^{n-1}\sqrt{t^2-1}} . \tag{C.1}$$

Property (ii):

$$C_{n+1}(z) < C_n(z). \tag{C.2}$$

The defining integrals show that the integrands are everywhere positive and the integrand used for $C_n(z)$ is always larger than or equal to that used for $C_{n+1}(z)$.

Property (iii):

$$\int_Z^\infty C_n(z)\, dz = C_{n+1}(Z). \tag{C.3}$$

The integral definition of $C_n(z)$ may be rewritten as:

$$\int_Z^\infty C_n(z)\, dz = \int_Z^\infty dz \int_1^\infty \frac{dt\, e^{-zt}}{t^{n-1}\sqrt{t^2-1}} . \tag{C.4}$$

Interchanging the order of integration proves the result.

Property (iv):

$$\left|\frac{dC_{n+1}(z)}{dz}\right| < \left|\frac{dC_n(z)}{dz}\right| . \tag{C.5}$$

This is proved by differentiating Eq. C.3 with respect to z to get:

$$C_{n+1}(z) = -\frac{dC_n(z)}{dz}, \tag{C.6}$$

replacing n by n+1 to get:

$$C_{n+2}(z) = -\frac{dC_{n+1}(z)}{dz}, \tag{C.7}$$

and noting that theorem (ii) proves that:

$$C_{n+2}(z) < C_{n+1}(z) . \tag{C.8}$$

The theorem now follows from the fact that the C_n functions are always positive so that:

$$|C_k(z)| = C_k(z) . \tag{C.9}$$

Property (v):

$$C_2(0) = \pi/2, \tag{C.10}$$

$$C_3(0) = 1, \tag{C.11}$$

$$C_4(0) = \pi/4 . \tag{C.12}$$

These can be evaluated directly from integration formulas (H2) after setting z = 0 in the defining integrals.

Property (vi):

At large enough distances, the uncollided flux around a finite, cylindrical source has the same shape as that around a line source. That this must be so is clear from physical principles, but not obvious from the integral form of the kernels as given in Weinberg and Wigner (W4).

The flux around the finite source is:

$$\phi_F = \int_0^{R_o} 2\pi R G_A(R, r)\, s(R)\, dR\,; \tag{C.13}$$

that around the line source is:

$$\phi_\ell = G_\ell(r)\,. \tag{C.14}$$

A comparison of the semi-analytic forms of G_A and G_ℓ given in Eqs. B.15 and B.26 shows that the first term of G_A has the same spatial (r) dependence as G_ℓ and that when $r \gg R$, the remaining terms of G_A are negligible. This shows that the flux shape will be the same as for the line source, although its magnitude will differ by a factor of $\int_0^{R_o} I_o(\Sigma R)\, 2\pi R s(R)\, dR$. However, $I_o(\Sigma R)$ differs negligibly from unity, except for very large sources. Thus, if the finite and line sources are normalized to the same source strengths, not only their asymptotic flux shapes but also their asymptotic flux magnitudes will be equal.

The semi-analytic form of G_A may be used to determine quantitatively the difference for any source shape and rod size.

Property (vii):

$$\int_0^\infty C_2(z)\, dz = 1\,. \tag{C.15}$$

This follows from the principle of conservation of neutrons; the total neutron removal rate around a unit (per unit length) line source must be one. Thus:

$$\int_0^\infty 2\pi r \Sigma G_\ell(r)\, dr = 1, \tag{C.16}$$

$$\int_0^\infty 2\pi r \Sigma \frac{C_2(\Sigma r)}{2\pi r}\, dr = 1\,. \tag{C.17}$$

Let:

$$w = \Sigma r, \tag{C.18}$$

so that:

$$dw = \Sigma\, dr\,. \tag{C.19}$$

Then:

$$\int_0^\infty C_2(w)\, dw = 1\,, \tag{C.20}$$

as stated. This agrees with the value obtained using:

$$\int_0^\infty C_2(w)\, dw = C_3(0), \tag{C.21}$$

from property (iii), together with the value of $C_3(0)$ obtained by direct integration.

Property (viii):

For large values of z, the asymptotic formula for $C_n(z)$ is:

$$C_n(z) \sim \sqrt{\frac{\pi}{2}}\,\frac{e^{-z}}{\sqrt{z}}\,. \tag{C.22}$$

It is evident from the defining integral:

$$C_n(z) = \int_1^\infty \frac{dt\, e^{-zt}}{t^{n-1}\sqrt{t^2-1}}\,, \tag{C.23}$$

that, as z increases, the major contribution to the integral becomes increasingly concentrated near t = 1. Thus, if the integral is written:

$$C_n(z) = \int_1^\infty \frac{dt}{t^{n-1}\sqrt{t+1}}\left(\frac{e^{-zt}}{\sqrt{t-1}}\right), \tag{C.24}$$

then the expression in parentheses is quickly varying near t=1 while the rest is slowing varying, so that t may be replaced by one in the slowing varying part. Making the substitution:

$$t - 1 = w, \tag{C.25}$$

then yields:

$$C_n(z) \sim \frac{e^{-z}}{\sqrt{2}} \int_0^\infty \frac{dw\, e^{-wz}}{w}\,, \tag{C.26}$$

$$C_n(z) \sim \sqrt{\frac{\pi}{2}}\,\frac{e^{-z}}{\sqrt{z}}\,. \tag{C.27}$$

Appendix D

CALCULATION OF THE C_n FUNCTIONS USED IN THE SEMI-ANALYTIC EXPRESSIONS FOR THE FIRST COLLISION KERNELS

The C_n functions are defined by Eq. B.12 as:

$$C_n(z) \equiv \int_1^\infty \frac{dt\, e^{-zt}}{t^n} \left\{ 1 + \frac{1}{2}\left(\frac{1}{t}\right)^2 + \frac{3}{8}\left(\frac{1}{t}\right)^4 + \ldots \right\}, \tag{D.1}$$

which is the expanded form of:

$$C_n(z) = \int_1^\infty \frac{dt\, e^{-zt}}{t^n \sqrt{1 - \left(\frac{1}{t}\right)^2}}. \tag{D.2}$$

This is, in turn, equivalent to:

$$C_n(z) = \int_1^\infty \frac{dt\, e^{-zt}}{t^{n-1}\sqrt{t^2 - 1}}. \tag{D.3}$$

The C_n functions have been evaluated for n = 2, 3, and 4 by starting with Eq. D.1 in its most general form:

$$C_n(z) = \int_1^\infty \frac{dt\, e^{-zt}}{t^n} \left\{ 1 + \frac{1}{2}\left(\frac{1}{t}\right)^2 + \frac{3}{8}\left(\frac{1}{t}\right)^4 + \ldots + \frac{(2k-1)(2k-3)\ldots(1)}{2^k k!}\left(\frac{1}{t}\right)^{2k} + \ldots \right\}, \tag{D.4}$$

$$C_n(z) = \sum_{k=0}^{\infty} a_k E_{n+2k}(z), \tag{D.5}$$

where $E_j(z)$ is the exponential integral (A2). The series in Eq. D.5 is barely convergent; in fact, neither the coefficient series alone nor the exponential integral series alone is convergent. That the series in Eq. D.5 does indeed converge can be proved by use of the following theorem (W6):

"A series $u_1 + u_2 + u_3 + \ldots$, in which $\lim_{n\to\infty} \left|\frac{u_{n+1}}{u_n}\right| = 1$, will be absolutely convergent if a positive number c exists such that

$$\overline{\lim_{n\to\infty}}\, n\left\{\left|\frac{u_{n+1}}{u_n}\right| - 1\right\} = -1 - c ." \tag{D.6}$$

Using the asymptotic formula (A3), $E_{n+2k}(z) \sim \frac{e^{-z}}{z + n + 2k}$, valid for large values of $n+2k$, one gets:

$$\overline{\lim_{k\to\infty}}\, k\left\{\left|\frac{a_{k+1}E_{n+2(k+1)}}{a_k E_{n+2k}}\right| - 1\right\} = \overline{\lim_{k\to\infty}}\, k\left\{\frac{e^{-z}}{(z+n+2k+2)} \cdot \frac{(z+n+2k)}{e^{-z}} \cdot \frac{(2k+1)(2k-1)\ldots(1)}{2^{k+1}(k+1)!} \cdot \frac{2^k k!}{(2k-1)(2k-3)\ldots(1)} - 1\right\}, \tag{D.7}$$

$$= \overline{\lim_{k\to\infty}}\, k\left\{\frac{z+n+2k}{z+n+2k+2} \cdot \frac{(2k+1)}{2(k+1)} - 1\right\}, \tag{D.8}$$

$$= -1 - \frac{1}{2} . \tag{D.9}$$

Thus, $c = -\frac{1}{2}$ and the series converges.

Equation D.5 has been used in a FORTRAN program to evaluate $C_n(z)$ for representative values of z and for $n = 2, 3, 4$. Because of the slow convergence, 5000 terms in the series were used. This is a sufficient number to yield the values of $C_2(0)$, $C_3(0)$, $C_4(0)$ to better than one percent (by comparison with the exact values in Appendix C). Further, the asymptotic formula for E_{n+2k} shows that for $k \geq 5000$ and for reasonable values of z:

$$E_{n+2k}(z) \sim \frac{e^{-z}}{z + n + 2k} \sim \frac{e^{-z}}{n + 2k} . \tag{D.10}$$

Since a_k is independent of z, the error $\epsilon_n(z)$ incurred by omitting terms beyond the five-thousandth is:

$$\epsilon_n(z) \approx e^{-z} \sum_{k=5001}^{\infty} \frac{a_k}{n + 2k} . \tag{D.11}$$

But the sum is just $\epsilon_n(0)$, which for $n = 2, 3, 4$ is known because the

exact values have been calculated by direct integration. Thus:

$$\epsilon_n(z) \approx e^{-z}\epsilon_n(0) . \qquad (D.12)$$

Figure D.1 shows the behavior of $C_2(z)$, $C_3(z)$, and $C_4(z)$ for small values of z. It may be seen that these are smooth functions, amenable to simple interpolation. A short table of the same functions is given by Table D.1.

Table D.1

Values* of the C_n Functions**
Used in the Semi-Analytic Forms of the First-Flight Kernels

z	$C_2(z)$	$C_3(z)$	$C_4(z)$
0	1.571	1.000	0.786
.03	1.424	0.947	0.748
.05	1.358	0.920	0.730
.10	1.221	0.855	0.685
.15	1.111	0.797	0.644
.20	1.017	0.744	0.606
.25	0.935	0.695	0.570
.30	0.863	0.650	0.536
.35	0.798	0.609	0.505
.40	0.740	0.570	0.475
.45	0.687	0.535	0.448
.50	0.639	0.502	0.422

* Correct to at least 1%.

** $C_n(z) \equiv \int_1^\infty \frac{dt\, e^{-zt}}{t^{n-1}\sqrt{t^2-1}}$.

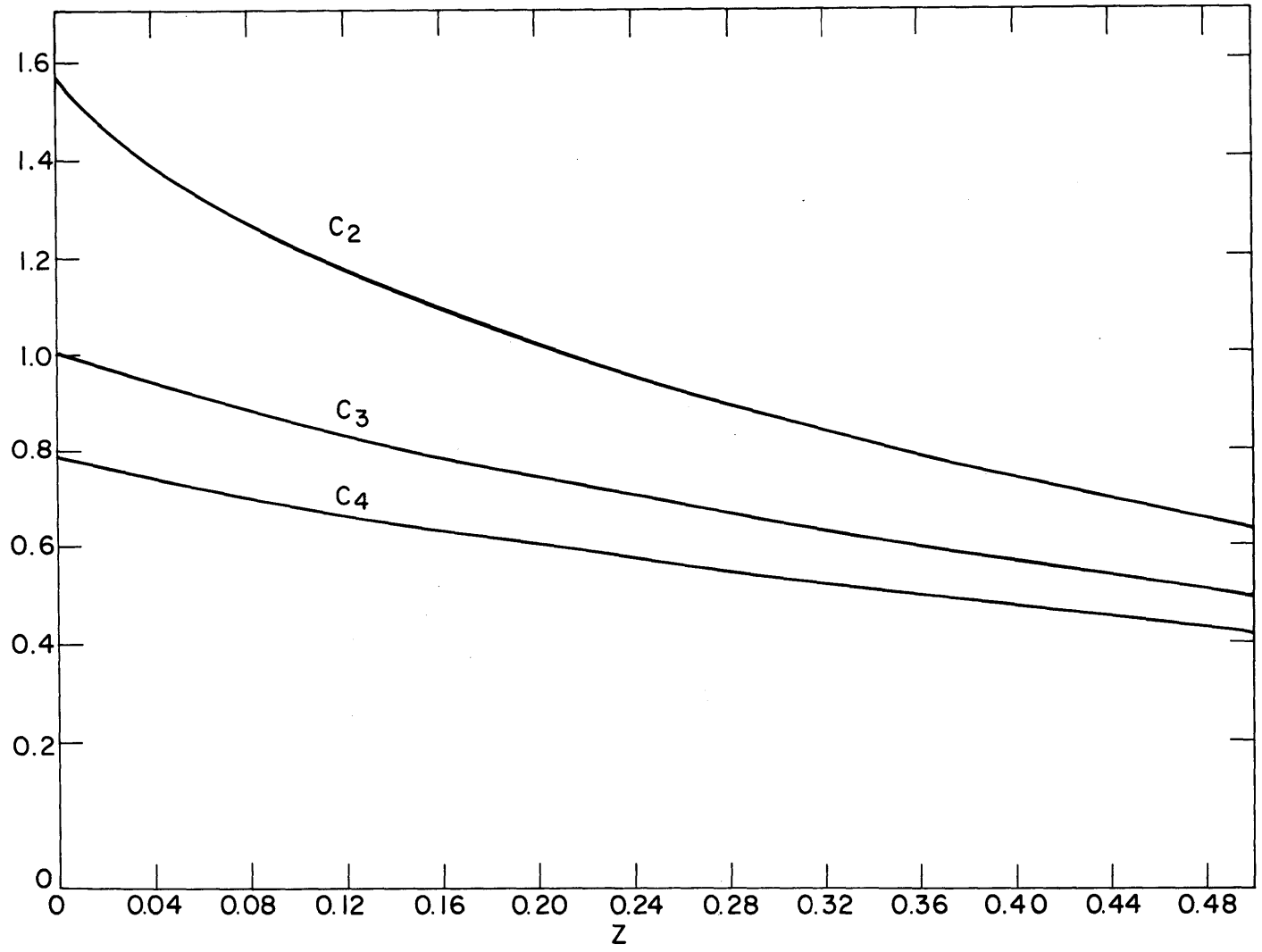

FIG. DI FUNCTIONS $c_n(z)$ APPEARING IN INTEGRATED FORM OF LINE, ANNULAR, AND ROD FIRST FLIGHT KERNELS

Appendix E

COEFFICIENTS IN THE SEMI-ANALYTIC FORM OF THE SINGLE ROD FLUX

The uncollided flux at radius r around a single homogeneous fuel rod of radius R_o is obtained by integrating the kernels G_A or G_B (defined in Appendix A) over the source distribution s(R) within the rod. For field points outside the rod, denoted by subscript or superscript "A":

$$\phi^A_{SR}(r, R_o, \Sigma) = \int_0^{R_o} G_A(R, r)\, 2\pi R s(R)\, dR, \qquad r \geq R_o, \tag{E.1}$$

and for field points inside, denoted by subscript or superscript "B":

$$\phi^B_{SR}(r, R_o, \Sigma) = \int_0^{r} G_A(R, r)\, 2\pi R s(R)\, dR + \int_r^{R_o} 2\pi R G_B(R, r) s(R)\, dR, \tag{E.2}$$

$$\phi^B_{SR}(r, R_o, \Sigma) = \phi^A_{SR}(r, r, \Sigma) + \phi^C_{SR}(r, R_o, \Sigma), \tag{E.3}$$

where:

$$\phi^C_{SR}(r, R_o, \Sigma) = \int_r^{R_o} 2\pi R G_B(R, r)\, s(R)\, dR\,. \tag{E.4}$$

The origin of coordinates is at the center of the fuel rod. When the semi-analytic form of the kernels defined in Appendix B is used, the result of the integrations is:

$$\phi^A_{SR}(r, R_o, \Sigma) = \frac{1}{r}\left\{ C_2(\Sigma r) S_2(\Sigma, R_o) + \frac{C_3(\Sigma r) S_3(\Sigma, R_o)}{r} + \frac{C_4(\Sigma r) S_4(\Sigma, R_o)}{r^2} + \frac{C_5(\Sigma r) S_5(\Sigma, R_o)}{r^3} + \cdots \right\}, \qquad r \geq R_o, \tag{E.5}$$

$$\phi^{C}_{SR}(r, R_o, \Sigma) = I_o(\Sigma r) f_2(r, R_o) + r I_1(\Sigma r) f_3(r, R_o) + \frac{r^2}{2}\left[I_o(\Sigma r)+I_2(\Sigma r)\right] f_4(r, R_o) + \ldots, \qquad r \leq R_o . \tag{E.6}$$

The coefficients in these expansions are:

$$S_2(u) = \int_0^u R I_o(\Sigma R) s(R)\, dR, \tag{E.7}$$

$$S_3(u) = \int_0^u R^2 I_1(\Sigma R) s(R)\, dR, \tag{E.8}$$

$$S_4(u) = \int_0^u \frac{R^3}{2}\left\{I_o(\Sigma R)+I_2(\Sigma R)\right\} s(R)\, dR, \tag{E.9}$$

$$S_5(u) = \int_0^u \frac{R^4}{4}\left\{3I_1(\Sigma R)+I_3(\Sigma R)\right\} s(R)\, dR, \tag{E.10}$$

$$S_6(u) = \int_0^u \frac{R^5}{8}\left\{3I_o(\Sigma R)+4I_2(\Sigma R)+I_4(\Sigma R)\right\} s(R)\, dR, \tag{E.11}$$

$$S_7(u) = \int_0^u \frac{R^6}{16}\left\{10I_1(\Sigma R)+5I_3(\Sigma R)+I_5(\Sigma R)\right\} s(R)\, dR, \tag{E.12}$$

$$S_j(u) = \int_0^u R^{j-1} I_o^{(j-2)}(\Sigma R)\, s(R)\, dR, \tag{E.13}$$

$$S_j(u) = \int_0^u R^{j-1}\left\{I_{-(j-2)}(\Sigma R) + \binom{j-2}{1} I_{-(j-2)+2}(\Sigma R) + \binom{j-2}{2} I_{-(j-2)+4}(\Sigma R) + \ldots + \binom{j-2}{j-2} I_{+(j-2)}(\Sigma R)\right\} s(R)\, dR, \tag{E.14}$$

and:

$$f_2(r, R_o) = \int_r^{R_o} C_2(\Sigma R)\, s(R)\, dR, \tag{E.15}$$

$$f_3(r, R_o) = \int_r^{R_o} C_3(\Sigma R)\, s(R)\, \frac{dR}{R}, \tag{E.16}$$

$$f_4(r, R_o) = \int_r^{R_o} C_4(\Sigma R)\, s(R)\, \frac{dR}{R^2} , \tag{E.17}$$

$$\vdots$$

$$f_k(r, R_o) = \int_r^{R_o} C_k(\Sigma R)\, s(R)\, \frac{dR}{R^{k-2}} . \tag{E.18}$$

Appendix F

COMPUTER PROGRAM ØNE-ROD

This code is used to compute values of J_{rod}/D and $\eta\epsilon P J_{rod}/D$ from values of relative subcadmium activity at various distances from a single fuel element at the center of a cylindrical exponential facility. The details of such an experiment are described in Chapter III and the notation is defined in Chapter IV.

Input is of the "programmed" kind, in which each fixed point variable is associated with a given location in one array, and each floating point variable is associated with a given location in a second array. Input is provided to the program by punching on cards the value of each variable and the location of the variable in the array. This is convenient because only the values which are different from those used in the previous case need be provided. For each case, all fixed point input must precede all floating point input. Each case must contain at least one card of fixed point input and one card of floating point input. Each card may contain values for up to five variables, which will be stored consecutively in the input array. Thus, separate cards must be used for values which are not to be stored consecutively. The input format is as follows:

Col. 2	Number of input values given on this card in Cols. 13-72.
Cols. 9-12	I3 format; array location of the variable corresponding to the input value in Cols. 13-24 of this card.
Cols. 13-72	5I12 or 5E12.8 format; values for up to 5 variables, which will be stored consecutively in the input array.

The array locations for the input variables are:

Fixed Point Array Locations	Variable
1	Run number.
2	Case number.
3	Number of data points.
8	0 Unity weighting factor used.
	1 Use weighting factors from input cards (see floating point location 60).

Floating Point Array Locations	Variable
1	Radius of the foil closest to the fuel rod; radii of the other foils are entered consecutively after this.
61	Relative weight assigned to the activity of the foil closest to the fuel rod; weights for the other foils are entered consecutively after this.
101	Activity of the foil closest to the fuel rod; activities of the other foils are entered consecutively after this.
51	Value of $(\gamma^2-\kappa^2)$; see Chapter IV for definitions of these quantities.
52	Value of the age from fission to thermal in the moderator.
53	Initial value of the activity to be used in the integration.
54	Always set to 1.0 .

Restriction: The number of data points may not exceed 40.

```
*       LIST
*       LABEL
C       REVISION TO ONE ROD TO FIT ONLY PART OF POINTS
C       INCLUDES VARIABLE PHI AT ZERO
        EQUIVALENCE (IARRAY(9),IFIRST),(IARRAY(10),ILAST),(ARRAY(61),W)
        DIMENSIONW(40),DIF(40)
        COMMON IFIRST,ILAST,IP
     1  CALL INPUTE
        DO122K=1,21
        ARRAY(150)=ARRAY(56)+FLOATF(K-1)*(ARRAY(57)-ARRAY(56))/20.0
    22  CALL INTONE(A,AA)
        ARRAY(150)=0.0
        CALL INTTWO
        CALL INTONE(AB,AC)
        CALL INTSOR
        IP=ILAST-IFIRST+1
        CALL MATR
        CALL VECTR
        CALL PHIT(S,D,W,U,IP,2,IC,DIF)
        SQUERR=0.0
        DO113I=1,IP
   113  SQUERR=SQUERR+DIF(I)**2
   122  SQUERR=SQUERR
        GOTO1
        END
*       LIST
*       LABEL
CMATR
        SUBROUTINE MATR
        DIMENSIONW(40),DIF(40)
        EQUIVALENCE (IARRAY(9),IFIRST),(IARRAY(10),ILAST),(ARRAY(61),W)
        COMMON IFIRST,ILAST,IP
        DO22I=1,IP
        III=IFIRST+I-1
        S(I,1)=-R(III)
    22  S(I,2)=R(III)-SOURCE(III)
   999  RETURN
        END
*       LIST
*       LABEL
CVECTR
        SUBROUTINE VECTR
        DIMENSIONW(40),DIF(40)
        EQUIVALENCE (IARRAY(9),IFIRST),(IARRAY(10),ILAST),(ARRAY(61),W)
        COMMON IFIRST,ILAST,IP
        PI=3.1415927
        DO22I=1,IP
        III=IFIRST+I-1
    22  D(I)=2.*PI*(AA(III)-ASQ*AC(III)-R(III)*A(III))
   999  RETURN
        END
*       LIST
*       LABEL
CSQFW
*       SYMBOL TABLE
        SUBROUTINE SQFIT
        DIMENSION R(50),A(50),      S(50,2),ST(2,50),STS(2,2),STSI(2,2),
       1D(50),AA(50),AC(50),AB(50),SOURCE(50),U(50),DIF(50),DATCAL(50),
       2ARRAY(150) ,IARRAY(10)
        EQUIVALENCE(ARRAY(1),R(1)),(ARRAY(101),A(1)),(ARRAY(51),ASQ),
       1(ARRAY(52),TAU),(ARRAY(53),REFF),(IARRAY(1),NRUN),(IARRAY(2),NUM),
       2(IARRAY(3),IMAX),(IARRAY(4),IDATA),(IARRAY(5),ISOUR),(IARRAY(6),IA
       3),(IARRAY(7),IB),(IARRAY(8),IC),(IARRAY(9),ID),(IARRAY(10),IE)
```

```
      COMMON R,A,S,D,AA,AC,AB,ST,STS,STSI,U,DATCAL,DIF,SQUERR,M,IMAX,
     1ASQ,SOURCE,TAU,IDATA,ISOUR,IA,IB,IC,ID,IE,REFF,NRUN,NUM
      DIMENSION SEMI(50)
      DIMENSION WS(50,2),WD(50),W(40)
      COMMON WS,WD
      EQUIVALENCE (ARRAY(61),W(1))
      M=2
C     GET S TRANSPOSE
      DO22I=1,M
      DO22J=1,IB
   22 ST(I,J)=S(J,I)
C
C     GET WS
C
      IF(IC) 25,23,25
   23 DO24I=1,IMAX
      DO24J=1,M
   24 WS(I,J)=S(I,J)
      GOTO29
   25 DO27I=1,IMAX
      DO27J=1,M
   27 WS(I,J)=W(I)*S(I,J)
C
C     MULTIPLY BY S
C
   29 DO33I=1,M
      DO33 J=1,M
      STS(I,J)=0.0
      DO33K=1,IB
   33 STS(I,J)=STS(I,J)+ST(I,K)*WS(K,J)
C
C     GET STS INVERSE
C     THIS FORMULA FOR 2X2 MATRIX ONLY
C
      DET=STS(1,1)*STS(2,2)-STS(1,2)*STS(2,1)
      STSI(1,1)=STS(2,2)/DET
      STSI(2,2)=STS(1,1)/DET
      STSI(1,2)=-STS(1,2)/DET
      STSI(2,1)=-STS(2,1)/DET
C
C     GET WD
C
      IF(IC)37,35,37
   35 DO36I=1,IMAX
   36 WD(I)=D(I)
      GOTO41
   37 DO39I=1,IMAX
   39 WD(I)=W(I)*D(I)
C
C     MULTIPLY BY DATA VECTOR
C
   41 DO44 I=1,M
      SEMI(I)=0.0
      DO44K=1,IB
   44 SEMI(I)=ST(I,K)*WD(K)+SEMI(I)
C
C     MULTIPLY STS INVERSE BY SEMI TO GET UVECTOR
C     U IS VECTOR TO BE FOUND
C
      DO 55 I=1,M
      U(I)=0.0
      DO 55 K=1,M
   55 U(I)=U(I)+STSI(I,K)*SEMI(K)
```

```
C
  999 RETURN
      END
*     LIST
*     LABEL
*     SYMBOL TABLE
      SUBROUTINE INTSOR
      DIMENSION R(50),A(50),      S(50,2),ST(2,50),STS(2,2),STSI(2,2),
     1D(50),AA(50),AC(50),AB(50),SOURCE(50),U(50),DIF(50),DATCAL(50),
     2ARRAY(150) ,IARRAY(10)
      EQUIVALENCE(ARRAY(1),R(1)),(ARRAY(101),A(1)),(ARRAY(51),ASQ),
     1(ARRAY(52),TAU),(ARRAY(53),REFF),(IARRAY(1),NRUN),(IARRAY(2),NUM),
     2(IARRAY(3),IMAX),(IARRAY(4),IDATA),(IARRAY(5),ISOUR),(IARRAY(6),IA
     3),(IARRAY(7),IB),(IARRAY(8),IC),(IARRAY(9),ID),(IARRAY(10),IE)
      COMMON R,A,S,D,AA,AC,AB,ST,STS,STSI,U,DATCAL,DIF,SQUERR,M,IMAX,
     1ASQ,SOURCE,TAU,IDATA,ISOUR,IA,IB,IC,ID,IE,REFF,NRUN,NUM
      DIMENSION T(50),X(50)
C     DOUBLE INTEGRAL OF SLOWING DOWN (AGE) SOURCE)
C
      PI=3.1415927
      COEF=SQRTF(PI*TAU)
      A1=.3480242
      A2=-.0958798
      A3=.7478556
      P=.47047
      DO22I=1,IMAX
      X(I)=.5*R(I)/SQRTF(TAU)
      T(I)=1.0/(1.0+P*X(I))
      POLY=T(I)*(A1+T(I)*(A2+A3*T(I)))
   22 SOURCE (I)=COEF*(1.0-POLY*EXPF(-X(I)*X(I)))
  999 RETURN
      END
*     LIST
*     LABEL
*     SYMBOL TABLE
      SUBROUTINE INTTWO
      DIMENSION R(50),A(50),      S(50,2),ST(2,50),STS(2,2),STSI(2,2),
     1D(50),AA(50),AC(50),AB(50),SOURCE(50),U(50),DIF(50),DATCAL(50),
     2ARRAY(150) ,IARRAY(10)
      EQUIVALENCE(ARRAY(1),R(1)),(ARRAY(101),A(1)),(ARRAY(51),ASQ),
     1(ARRAY(52),TAU),(ARRAY(53),REFF),(IARRAY(1),NRUN),(IARRAY(2),NUM),
     2(IARRAY(3),IMAX),(IARRAY(4),IDATA),(IARRAY(5),ISOUR),(IARRAY(6),IA
     3),(IARRAY(7),IB),(IARRAY(8),IC),(IARRAY(9),ID),(IARRAY(10),IE)
      COMMON R,A,S,D,AA,AC,AB,ST,STS,STSI,U,DATCAL,DIF,SQUERR,M,IMAX,
     1ASQ,SOURCE,TAU,IDATA,ISOUR,IA,IB,IC,ID,IE,REFF,NRUN,NUM
      DIMENSION E(50)
C     COMPUTES INTEGRAL(U*A(U))DU  FROM ZERO TO W WHERE
C     W IS THE SET R(I)
C     USES INTONE
      DO 22 I=1,IMAX
   22 E(I)=R(I)*A(I)
      CALL INTONE(E,AB)
  999 RETURN
      END
*     LIST
*     LABEL
*     SYMBOL TABLE
      SUBROUTINE INTONE(G,SUM)
      DIMENSION R(50),A(50),      S(50,2),ST(2,50),STS(2,2),STSI(2,2),
     1D(50),AA(50),AC(50),AB(50),SOURCE(50),U(50),DIF(50),DATCAL(50),
     2ARRAY(150) ,IARRAY(10)
      EQUIVALENCE(ARRAY(1),R(1)),(ARRAY(101),A(1)),(ARRAY(51),ASQ),
     1(ARRAY(52),TAU),(ARRAY(53),REFF),(IARRAY(1),NRUN),(IARRAY(2),NUM),
```

```
     2(IARRAY(3),IMAX),(IARRAY(4),IDATA),(IARRAY(5),ISOUR),(IARRAY(6),IA
     3),(IARRAY(7),IB),(IARRAY(8),IC),(IARRAY(9),ID),(IARRAY(10),IE)
      COMMON R,A,S,D,AA,AC,AB,ST,STS,STSI,U,DATCAL,DIF,SQUERR,M,IMAX,
     1ASQ,SOURCE,TAU,IDATA,ISOUR,IA,IB,IC,ID,IE,REFF,NRUN,NUM
      DIMENSION G(50),SUM(50)
C     COMPUTES INTEGRAL (G(U)DU) FROM ZERO TO W WHERE W IS THE SET
C     R(I)            USES TRAPEZOIDAL RULE
      SUM(1)=(G(1)+ARRAY(150))*R(1)/2.
      DO22I=2,IMAX
   22 SUM(I)=SUM(I-1)+(G(I)+G(I-1))*(R(I)-R(I-1))/2.
  999 RETURN
      END
```

Appendix G

REFERENCES

A1 Abramowitz, M., and I. A. Stegun, editors, Handbook of Mathematical Functions, pp. 375, 376, National Bureau of Standards, USGPO, Washington, D. C. (1964).

A2 Abramowitz, M., and I. A. Stegun, loc. cit., ref. A1, p. 228.

A3 Abramowitz, M., and I. A. Stegun, loc. cit., ref. A1, p. 231.

A4 Avery, R., editor, "Argonne National Laboratory Reactor Physics Division Annual Report, July 1, 1964 to June 30, 1965," ANL-7110, p. 31 (1966).

A5 "Reactor Physics Constants," ANL-5800, p. 281 (1963).

A6 Ibid., p. 275.

A7 Amouyal, A., and P. Benoist, "New Method for the Determination of the Thermal Utilization Factor of a Cell," CEA-571 (1956).

B1 Brown, P. S., T. J. Thompson, I. Kaplan, and A. E. Profio, "Measurements of the Spatial and Energy Distribution of Thermal Neutrons in Uranium, Heavy Water Lattices," NYO-10205, MITNE-17 (1962).

B2 Bliss, H. E., I. Kaplan, and T. J. Thompson, "Use of a Pulsed Neutron Source to Determine Nuclear Parameters of Lattices of Partially Enriched Uranium Rods in Heavy Water," MIT-2344-7, MITNE-73 (1966).

B3 Bliss, H. E., "Measurement of the Fast Fission Effect in Heavy Water, Partially Enriched Uranium Lattices," S. M. Thesis, Nuclear Engineering Department, M. I. T (June 1964).

B4 Butler, M., editor, "Proceedings of the Conference on the Application of Computing Methods to Reactor Problems," pp. 110, 111, ANL-7050 (1965).

B5 Barry, R. F., "The Revised Leopard Code – A Spectrum Dependent, Non-Spatial Depletion Program," WCAP-2759 (1965).

C1 Critoph, E., "Comparison of Theory and Experiment for (a) Lattice Properties of D_2O-U Reactors; (b) Control Rod Experiments; (c) Foreign Rod Experiments," CRRP-655, AECL-350 (1956).

D1 D'Ardenne, W. H., T. J. Thompson, D. D. Lanning, and I. Kaplan, "Studies of Epithermal Neutrons in Uranium, Heavy Water Lattices," MIT-2344-2, MITNE-53 (1964).

D2 Driscoll, M., Private communication (1966).

E1 Erdik, E. J., Reactor Sci. Tech., 15, 98 (1961).

G1 Green, R. E., et al., "Highlights of Chalk River Work on the Physics of Heavy Water Lattices Since the 1959 IAEA Panel," in Heavy Water Lattices, Second Panel Report, IAEA, Vienna (1965).

G2 Galanin, A. D., International Conf. on Peaceful Uses of Atomic Energy, Vol. 5, p. 477, United Nations Publications, New York, N. Y. (1956).

G3 Glasstone, S., and M. C. Edlund, The Elements of Nuclear Reactor Theory, D. Van Nostrand Co., Inc., Princeton, N. J. (1952).

H1 Harrington, J., D. D. Lanning, I. Kaplan, and T. J. Thompson, "Use of Neutron Absorbers for the Experimental Determination of Lattice Parameters in Subcritical Assemblies," MIT-2344-6, MITNE-69 (1966).

H2 Hodgman, C. D., R. C. Weast, and S. M. Selby, editors, Handbook of Chemistry and Physics, Thirty-eighth Edition, pp. 256, 257, Chemical Rubber Publishing Co., Cleveland, Ohio (1956).

H3 Hellman, S. P., "Measurements of δ_{28} and ρ_{28} in a Two-and-One-Half Inch Triangular Lattice of Three-Quarter Inch Metallic Uranium Rods in Heavy Water Moderator," M. S. Thesis, Nuclear Engineering Department, M. I. T. (1965).

H4 Honeck, H., "THERMOS, A Thermalization Transport Theory Code for Reactor Lattice Calculations," BNL-5826 (1961).

H5 Hemmig, P. B., editor, "Conference on Neutron Cross Section Technology," pp. 148, 149, CONF-660303 (1966).

H6 Hellstrand, Eric, "Measurement of Resonance Integrals," in Reactor Physics in the Resonance and Thermal Regions, Vol. 2, p. 160, Goodjohn and Pomraning, editors, M. I. T. Press (1966).

H7 Loc. cit., ref. H6, p. 151.

H8 Hughes, D. J., and R. B. Schwartz, "Neutron Cross Sections," BNL-325, 2nd Edition, 2nd Supplement (1965).

H9 Hellens, R. L., and H. C. Honeck, "Summary and Preliminary Analysis of the BNL Slightly Enriched Uranium, Water Moderated Lattice Measurements," in Light Water Lattices, IAEA (1962).

H10 Helholtz, J. and W. Rothenstein, "Multigroup Calculations of the Fast Spectrum and Fast Fission Effect," Nucl. Sci. Eng., 24, 349 (1966).

K1 Klein, D., A. Z. Kranz, et al., "Measurement of Thermal Utilization, Resonance Escape Probability, and Fast Effects in Water Moderated, Slightly Enriched Uranium and Uranium Oxide Lattices," Nucl. Sci. and Eng., 3, 403-427 (1958).

K2 Klahr, C. N., et al., "Heterogeneous Reactor Calculation Methods," NYO-2680 (1961).

K3 Kier, P. H., "RIFF-RAFF, A Program for Computation of Resonance Integrals in a Two-Region Cell," ANL-7033 (1965).

K4 Kouts, H., and R. Sher, "Experimental Studies of Slightly Enriched Uranium, Water Moderated Lattices, Part I: 0.600-Inch-Diameter Rods," BNL-486 (1957).

K5 Kouts, H., et al., "Physics of Slightly Enriched Normal Water Lattices," Proc. 1958 Geneva Conf., 12, P/1841.

M1 Malaviya, B. K., I. Kaplan, D. D. Lanning, A. E. Profio, and T. J. Thompson, "Studies of Reactivity and Related Parameters in Slightly Enriched Uranium, Heavy Water Lattices," MIT-2344-1, MITNE-49 (1964).

M2 Morse, P. M., and H. Feshbach, Methods of Theoretical Physics, pp. 453, 467, McGraw-Hill Book Co. (1953).

M3 Madell, J. T., T. J. Thompson, A. E. Profio, and I. Kaplan, "Spatial Distribution of the Neutron Flux on the Surface of a Graphite-Lined Cavity," NYO-9657, MITNE-18 (1962).

M4 Meghreblian, R. V., and D. K. Holmes, Reactor Analysis, p. 646, McGraw-Hill Book Co. (1960).

M5 Thompson, T. J., I. Kaplan, F. M. Clikeman, and M. J. Driscoll, "Heavy Water Lattice Project Annual Report," MIT-2344-4, MITNE-65 (1965).

M6 Kaplan, I., D. D. Lanning, A. E. Profio, and T. J. Thompson, "Summary Report on Heavy Water, Natural Uranium Lattice Research," NYO-10209, MITNE-35 (1963).

M7 Thompson, T. J., et al., loc. cit., ref. M5, pp. 51, 52.

P1 Palmedo, P. F., I. Kaplan, and T. J. Thompson, "Measurements of the Material Bucklings of Lattices of Natural Uranium Rods in D_2O," NYO-9660, MITNE-13 (1962).

P2 Peak, J. C., I. Kaplan, and T. J. Thompson, "Theory and Use of Small Subcritical Assemblies for the Measurement of Reactor Parameters," NYO-10204, MITNE-16 (1962).

P3 Papay, L., et al., "Heavy Water Lattice Project Annual Report," p. 53, MIT-2344-4, MITNE-65 (1965).

P4 Petersen, G., and F. G. Warzek, "AEC Superheat Criticals – A Comparison of Theory and Experiment on Uniform Lattices," GEAP-3882 (1962).

S1 Simms, R. I., I. Kaplan, T. J. Thompson, and D. D. Lanning, "Analytical and Experimental Investigations of the Behavior of Thermal Neutrons in Lattices of Uranium Metal Rods in Heavy Water," NYO-10211, MITNE-33 (1963).

S2 Sefchovich, E., I. Kaplan, and T. J. Thompson, "The Measurement of Reactor Parameters in Slightly Enriched Uranium, Heavy Water Moderated Miniature Lattices," MIT-2344-8, MITNE-76 (1966).

S3 Ibid., p. 191.

S4 Ibid., p. 192.

S5 Strawbridge, L. E., "Calculation of Lattice Parameters and Criticality for Uniform, Water Moderated Lattices," WCAP-3742 (1963).

T1 Thompson, T. J., "Research Program at the M.I.T. Nuclear Reactor," in Programming and Utilization of Research Reactors, Academic Press, New York (1962).

T2 Thie, J. A., Heavy Water Exponential Experiments Using ThO_2 and UO_2, p. 89, Pergamon Press, New York (1961).

U1 Uotinen, V. O., "Physics Research Quarterly Report – Jan. - Mar. 1966," p. 17, BNWL-284.

W1 Weitzberg, A., I. Kaplan, and T. J. Thompson, "Measurements of Neutron Capture in U-238 in Lattices of Uranium Rods in Heavy Water," NYO-9659, MITNE-11 (1962).

W2 Wolberg, J. R., T. J. Thompson, and I. Kaplan, "A Study of the Fast Fission Effect in Lattices of Uranium Rods in Heavy Water," NYO-9661, MITNE-15 (1962).

W3 Woodruff, G. L., I. Kaplan, and T. J. Thompson, "A Study of the Spatial Distribution of Fast Neutrons in Lattices of Slightly Enriched Uranium Rods Moderated by Heavy Water," MIT-2344-5, MITNE-67 (1965).

W4 Weinberg, A. M., and E. P. Wigner, The Physical Theory of Neutron Chain Reactors, p. 217, Univ. of Chicago Press (1958).

W5 Watson, G. N., A Treatise on the Theory of Bessel Functions, p. 172, Cambridge Univ. Press (1944).

W6 Whittaker, E. T., and G. N. Watson, A Course of Modern Analysis, p. 23, Cambridge Univ. Press (1927).

W7 Weinberg, A. M., and E. P. Wigner, loc. cit., ref. W4, p. 326.

W8 Woodruff, G. W., et al., "A Study of the Spatial Distribution of Fast Neutrons in Lattices of Slightly Enriched Uranium Rods Moderated by Heavy Water," MIT-2344-5, MITNE-67 (1965).

W9 Wolberg, J. R., T. J. Thompson, and I. Kaplan, "A Study of the Fast Fission Effect in Lattices of Uranium Rods in Heavy Water," NYO-9661, MITNE-15 (February 1962).

W10 Weinberg, A. M., and E. P. Wigner, loc. cit., ref. W1, pp. 700, 702.

W11 Ibid., p. 402.

W12 Weitzberg, A., I. Kaplan, and T. J. Thompson, "Measurements of Neutron Capture in U-238 in Lattices of Uranium Rods in Heavy Water," NYO-9659, MITNE-11 (1962).

W13 Weinberg, A. M., and E. P. Wigner, The Physical Theory of Neutron Chain Reactors, p. 670, Univ. of Chicago Press (1958).

W14 Wehmeyer, D., Private communication to J. C. Peak (1961).

W15 Wade, J. W., "Neutron Age in Mixtures of D_2O and H_2O," Nuclear Sci. Eng., 4, 12 (1958).

W16 Watson, G. N., loc. cit., ref. W5, p. 361.

W17 Seitz, F., and E. P. Wigner, Phys. Rev., 43, 804 (1933).

Appendix H

LIST OF SYMBOLS

A	Activity of a foil.
A_{epi}	Epicadmium absorption rate in U^{238} per unit length in the fuel element of interest.
A_{sub}	Subcadmium absorption rate in U^{238} per unit length in the fuel element of interest.
a	Lattice spacing.
B^2	Material buckling.
b	Lattice spacing.
$C(X)$	The error incurred in the calculated value of the reaction rate at point X in a uniform, infinite, slab lattice when only the first term in the Poisson summation is used.
C^*	Ratio of the total U^{238} capture rate in the fuel to the U^{235} fission rate in the fuel.
c	A constant.
c_o	A constant.
c_1	A constant.
D	Diffusion coefficient.
D_{eff}	Effective shielding factor for a lattice in Strawbridge's formulation of the resonance integral.
d	A constant.
E	Energy of a neutron.
E_c	Cadmium cutoff energy.
E_F	Average energy of fission neutrons.
E_{28}	Average energy of neutrons captured in the resonances of U^{238}.

ERI^{25} Effective resonance integral for epicadmium fission in U^{235}, including the contribution of the smooth fission cross section.

ERI^{28} Effective resonance integral for epicadmium absorption in U^{238}, excluding the 1/v component.

$(ERI)^{28}_{1/E}$ Value of ERI^{28} in a 1/E flux spectrum.

F The integral of the kernel K over all space, the integration being over the variable representing the field point.

F_1 The integral of the kernel K_1 over all space, the integral being over the variable representing the field point.

f Thermal utilization.

$f_k(r,R_o)$ Coefficient defined in Appendix E.

G(r) The kernel giving the slowing-down density to subcadmium energies per unit of area (in the radial plane) at radius r from the center of a fuel element.

$G_A(R,r)$ Kernel giving the uncollided flux at radius r around an infinitesimally thick annular source at radius R ($r \geq R$).

$G_B(R,r)$ Kernel giving the uncollided flux at radius r around an infinitesimally thick annular source at radius R ($r \leq R$).

$G_\ell(r)$ Kernel giving the uncollided flux at radius r around a line source at the origin.

H Integral of the total uncollided flux over the volume of a fuel element.

J_{rod} Net current of subcadmium neutrons into a fuel element, per unit length of element.

K(r) Kernel representing, in cylindrical geometry, the flux or reaction rate at radius r around a line or finite source in an infinite medium.

$K_1(r)$ Kernel which is identical to K except within those unit cells in which K experiences a large fractional change in magnitude. Within these unit cells, K_1 is zero.

L Lattice spacing in a uniform, infinite, one-dimensional system.

ℓ_o Mean chord length in a fuel rod.

ℓ_m Mean chord length in the moderator, per unit cell.

M A real number.

m An integer.

N A real number.

N_{28} Density of U^{238} atoms in a fuel element.

n An integer.

P Nonleakage probability.

$P_{1/v}$ Probability that a fission neutron does not leak out of the system before reaching the effective energy at which 1/v capture in U^{238} occurs.

P_{Res} Probability that a fission neutron does not leak out of the system before reaching the effective energy at which resonance capture in U^{238} occurs.

P_o Probability that neutrons born in a fuel rod with a uniform source distribution will escape the rod without scattering.

p Resonance escape probability.

$Q(\vec{r}, \vec{r}_i, E)$ Kernel giving the reaction rate at $\vec{r}$ of neutrons having energy E and born at $\vec{r}_i$.

$Q(|\vec{r} - \vec{r}_i|, E)$ Kernel giving the reaction rate at $\vec{r}$ of neutrons having energy E and born at $\vec{r}_i$ in an infinite medium.

$q(E)$ Slowing-down density past energy E.

R Radius of an annular source.

$R(\vec{r})$ Reaction rate at position $\vec{r}$.

R_o Radius of a cylindrical fuel rod.

$\vec{r}$ Radius vector to field position.

$\vec{r}_i$	Radius vector to position of i^{th} source.
r	Radius.
S	Macroscopic source distribution.
$S_j(\Sigma,R_o)$	Coefficient defined in Appendix E.
s	Source distribution within a cylindrical fuel rod.
$T(\vec{r}_i)$	Absorption rate of subcadmium neutrons in the i^{th} fuel element, normalized to unity at the fuel element of interest.
V_F	Volume of a fuel element, per unit length.
V_c	Volume of a unit cell, per unit length.
V_{H_2O}	Volume of water per unit length of a unit cell, in a light water lattice.
X	Coordinate of field point.
x	Resonance parameter defined by Eq. 5.26.
x_m	x coordinate of m^{th} fuel element.
Y	Coordinate of a field point.
y_n	y coordinate of n^{th} fuel element.
Γ	Ratio of the subcadmium flux at the surface of a fuel element to the net current, J_{rod}, of subcadmium neutrons into the element.
Γ'	Ratio of ϕ_o to J_{rod}.
γ	Inverse of the axial relaxation length in an exponential assembly.
∇_R^2	Radial Laplacian.
δ_{25}	Ratio of epicadmium to subcadmium fission rates in a fuel element.
δ_{28}	Ratio of the fission rate in U^{238} of a fuel element to the fission rate in U^{235} in the same element.
ϵ	Fast fission factor.
η	Number of fast neutrons produced directly by one subcadmium absorption in a fuel element.

θ	An angle.
κ	Inverse of the thermal diffusion length in the moderator.
μ	An integer.
ν	An integer.
ν_{25}	Average number of neutrons produced by one U^{235} fission.
ν_{28}	Average number of neutrons produced by one U^{238} fission.
ξ	Average logarithmic energy decrement.
ρ_{28}	Ratio of the epicadmium to subcadmium capture rates in U^{238}.
Σ	Macroscopic removal cross section.
Σ_s	Macroscopic scattering cross section.
Σ_{am}	Macroscopic absorption cross section of the moderator.
Σ_{EFF}	Effective removal cross section of heterogeneous medium (defined in Eqs. 6.9 and 6.10).
Σ_f	Macroscopic fission cross section of a fuel element.
Σ_R	Macroscopic removal cross section.
Σ_{tm}	Macroscopic total cross section of moderator.
$\sigma^{28}_{1/v}(E)$	Microscopic cross section for 1/v capture in U^{238}.
σ^{28}_{o}	2200 m/s value of $\sigma^{28}_{1/v}(E)$.
$\sigma^{28}_{Res}(E)$	Microscopic cross section for capture in the resonances of U^{238}.
$\sigma_{A(r)}$	Standard deviation of the activity A(r).
σ_N	Standard deviation of the observed number of counts, N.
σ_r	Standard deviation of the uncertainty in radial positions of foils.
σ_z	Standard deviation of the uncertainty in axial positions of foils.

τ	Neutron age.
τ_{28}	Age from fission to the effective energy at which neutrons are captured in the resonances of U^{238}.
τ_{Au}	Age from fission to the energy of the lowest resonance of Au^{197}.
τ_F	Effective age from fission to first collision.
$\phi(E)$	Neutron flux as a function of energy.
$\phi(r)$	Radial dependence of the subcadmium flux around a fuel element immersed in moderator.
ϕ_o	Value of the subcadmium flux which would exist at the center of a fuel element if all fast neutron sources in the system remained unchanged, but if in calculating the subcadmium neutron transport the properties of all fuel elements were replaced by those of the moderator.
$\phi_{SR}(r)$	The uncollided fast flux at radius r around an infinitely long, cylindrical fuel element which is the source of neutrons.

APPENDIX I

BIBLIOGRAPHY

In this bibliography we list a selection of references which deal with various aspects of single fuel element neutronics, but which were not cited as specific references in the body of the report. A brief comment is included on each.

1. Corno, S. E., "Interpretazione Teorica Delle Esperienze di Moltiplicazione Neutronica su un Solo Elemento di Combustible," Energia Nucleare, 10, 11, (1963). A highly theoretical application of small source theory to the problem of a single rod in an exponential pile. (Series of three articles.)

2. Feinberg, S. M., "Heterogeneous Methods for Calculating Reactors," Proc. 1955 Geneva Conf., P/669. One of the original and basic theoretical papers on heterogeneous methods.

3. Galanin, A. D., "The Thermal Coefficient in a Heterogeneous Reactor," Proc. 1955 Geneva Conf., P/666. One of the original and basic theoretical papers on heterogeneous methods.

4. Horning, W. A., "Small Source Model of a Thermal Pile," HW-24282 (1957). An early attempt at an analysis that could be used to relate theory and experiment.

5. Corno, S. E., "Theory of Pulsed Neutron Experiments in Highly Heterogeneous Multiplying Media," in Pulsed Neutron Research, Vol. II, IAEA, Vienna, 1965. A theory of pulsed neutron experiments applicable to a single fuel element.

6. Lanning, D. D., "Heterogeneous Reactor Critical Conditions Using Small Source Theory," TID-7532, Part I (1957). The application of heterogeneous analysis using age theory, to reactors containing control rods.

7. Meetz, K., "Exact Treatment of Heterogeneous Core Structures," Proc. 1958 Geneva Conf., P/968. A theoretical paper which develops a mathematical formalism for such problems.

8. Zink, J. and G. Rodeback, "The Determination of Lattice Parameters by Means of Measurements on a Single Fuel Element," NAA-SR-5392 (1960). Actual experiments on a single fuel rod are used to infer parameters of graphite uranium lattices, with best results in the thermal energy region. Also reported in Nucl. Sci. Eng., 9, p. 16-25 (1961).

9. Durrani, S., E. Etherington, and J. Ford, "Determinations of Reactor Lattice Parameters from Measurements on a Single Fuel Element Channel," APC/TN 1054. Another application of the method in (8)above.

10. G. W. Rodeback, C. H. Skeen and J. W. Zink, "Single Element Measurements," Trans. Amer. Nuc. Soc., 2, 1, June 1959. A preliminary report on (8).

11. O. W. Heinzman and S. W. Kash, NAA-SR-1546, August 1956, "Intracell Flux Distributions for an Extensive Series of Heavy Water, Uranium Rod Lattices." Reports radial flux traverses about 1-inch diameter single rods.

12. F. B. Estabrook, NAA-SR-925, p. 13, "Single Rod Exponential Experiments." Reports other data on same experiments as in (11).

13. B. Pershagen, G. Andersson and I. Carlvik, "Calculation of Lattice Parameters for Uranium Rod Clusters in Heavy Water and Correlation with Experiments," ICPUAE, Geneva 1958, Vol. 12. An example of the application of the Poisson summation in heterogeneous lattices.

ERRATA

Page	Correction
8	Delete Fig. 5.5 . . . page 90a.
49	Change 0.060" fuel to 0.250" fuel.
66	Equation 4.12: insert minus sign in front of argument of exp.
74	Paragraph 1, line 4 and paragraph 3, line 2: change Eq. 4.4 to Eq. 4.5.
83	Equation 5.14: note nearly illegible factor of η following plus sign in numerator.
114	3rd line from bottom: omit subscript "A" on G(R, r).
116	5th line from bottom: change reference from (W5) to (W8).

DISTRIBUTION

MIT-2344-10 MITNE-81

AEC Research and Development Report

UC-34 Physics

1. USAEC, New York Operations Office, Library

2-4. USAEC, Reactor Physics Branch, Division of Reactor Development and Technology

5. USAEC, New York Patents Office, Brookhaven National Lab.

6. USAEC, Cambridge Branch, New York Operations Office, Research Contracts Division

7. USAEC, Division of Reactor Development and Technology

8. USAEC, HWOCR Branch

9. USAEC, Water Projects Branch

10. USAEC, Core Design Branch

11. USAEC, Division of Naval Reactors

12. Advisory Committee on Reactor Physics (E. R. Cohen)

13. ACRP (G. Dessauer)

14. ACRP (R. Fluharty)

15. ACRP (E. Gaerttner)

16. ACRP (R. Ehrlich)

17. ACRP (F. C. Maienschein)

18. ACRP (J. Chernick)

19. ACRP (R. Avery)

20. ACRP (M. Nelkin)

21. ACRP (F. Dawson)

22. ACRP (G. Hansen)

23. ACRP (W. B. Loewenstein)

24. ACRP (L. W. Nordheim)

25. ACRP (T. M. Snyder)

26. ACRP (R. Bayard)

27-29. D. T. I. E., Oak Ridge, for Standard Distribution

30-100. Internal Distribution

101. Combustion Engineering (S. Visner)

102. Brookhaven National Laboratories (H. Kouts)